IN-VITRO AND *IN-SILICO* COMPUTATIONAL MODELLING OF THE CANNABINOID TYPE 1 AND SEROTONIN 2A CLASS A G PROTEIN – COUPLED RECEPTORS

A Thesis Submitted to the
College of Graduate and Postdoctoral Studies
In Partial Fulfilment of the Requirements
For the Degree of Doctor of Philosophy
In the Department of Pharmacy and Nutrition
University of Saskatchewan
Saskatoon Canada

By

Asher Leib Brandt

Permission to use

In presenting this thesis in partial fulfillment of the requirements for a Postgraduate degree from the University of Saskatchewan, I agree that the Libraries of this University may make it freely available for inspection. I further agree that permission for copying of this thesis in any manner, in whole or in part, for scholarly purposes may be granted by the professor or professors who supervised my thesis work or, in their absence, by the Head of the Department or the Dean of the College in which my thesis work was done. It is understood that any copying or publication or use of this thesis/dissertation or parts thereof for financial gain shall not be allowed without my written permission. It is also understood that due recognition shall be given to me and to the University of Saskatchewan in any scholarly use which may be made of any material in my thesis/dissertation.

DISCLAIMER

Reference in this thesis to any specific commercial products, process, or service by trade name, trademark, manufacturer, or otherwise, does not constitute or imply its endorsement, recommendation, or favoring by the University of Saskatchewan. The views and opinions of the author expressed herein do not state or reflect those of the University of Saskatchewan and shall not be used for advertising or product endorsement purposes.

Requests for permission to copy or to make other uses of materials in this thesis in whole or part should be addressed to:

Head of the College of Pharmacy and Nutrition
107 Wiggins Road, Saskatoon SK
University of Saskatchewan
Saskatoon, Saskatchewan, S7N 5E5, Canada

OR

Dean
College of Graduate and Postdoctoral Studies
University of Saskatchewan
116 Thorvaldson Building, 110 Science Place
Saskatoon, Saskatchewan, S7N 5C9, Canada

TABLE OF CONTENTS

List of Figures

List of Tables

List of Equations

List of Abbreviations

2-AG	2-Arachidonylglycerol
5-HT_{2A}R	Serotonin 2A Receptor
AI	Artificial Intelligence
AC	Adenylate Cyclase
AUC	Area Under the Curve
AEA	Anandamide
cAMP	Cyclic Adenosine Monophosphate
CB1R	Type 1 Cannabinoid Receptor
CB2R	Type 2 Cannabinoid Receptor
CI	Confidence Interval
CNR1	Human Type 1 Cannabinoid Receptor Gene
CNS	Central Nervous System
CPU	Central Processing Unit
DAG	Diacylglycerol
DMSO	Dimethyl sulfoxide
E_{max}	The Maximum Effect
EC_{50}	Half Maximal Effective Concentration
ECL	Extracellular Loop
ECS	Endocannabinoid System
ER	Endoplasmic Reticulum
EDTA	Ethylenediaminetetraacetic acid
FDA	Food and Drug Administration
GPCR	G-Protein Coupled Receptor
GPU	Graphics Processing Unit
ICL	Intracellular Loop
LSD	Lysergic Acid Diethylamide
MMGBSA	Molecular Mechanics/Generalised-Born Surface Area
NAM	Negative Allosteric Modulator

PAM	Positive Allosteric Modulator
PBS	Phosphate Buffered Saline
PDB	Protein Data Bank
PNS	Peripheral Nervous System
PTSD	Post Traumatic Stress Disorder
SCRA	Synthetic Cannabinoid Receptor Agonists
SAR	Structure Activity Relationship
THC	Δ9 -Tetrahydrocannabinol
TM	Transmembrane
TMH	Transmembrane Helix
WT	Wild-type
NBOMe	N-Methoxybenzyl
GAT	Ganesh A. Thakur, referring to any compounds followed by a number code for allosteric ligands synthesized by Ganesh A. Thakur

Abstract

G protein-coupled receptors (GPCRs) represent one of the most important families of drug targets. Approximately 700 drugs target GPCR's, which accounts for 35% of FDA approved drugs. The type 1 cannabinoid receptor (CB1R), type 2 cannabinoid receptor (CB2R), and serotonin 2a receptor (5-HT_{2A}R) are 3 GPCRs being intensively studied as new therapeutic targets. These receptors are involved in pain, depression, anxiety, memory impairment, nausea and body temperature. Due to the vast spectrum of conditions these receptors modulate, development of novel drugs to target these receptors is paramount. Specifically, the studies outlined in this thesis explored the structure activity relationship between ligands that bind CB1R, CB2R and 5-HT_{2A}R using both *in silico* and *in vitro* methods. *In vitro* methods were utilized to determine whether novel ligands bound to the receptor using radioligand binding to measure affinity and functional assays to determine whether ligands activated receptor-dependent signaling cascades such as G protein-dependent inhibition of cAMP accumulation and recruitment of βarrestin2. Computational *in silico* methods were then explored to determine if the *in vitro* data could be supported. With these *in silico* methods the precise site(s) of ligand-GPCR interaction could be mapped down to the amino acid residue for precision structure-activity determination. From this interaction a computational proxy for binding affinity was used to measure the strength of the interaction. Looking forward, data compiled in these studies can now be applied to the high-throughput design and assessment of novel CB1R, CB2R, and 5-HT_{2A}R ligands and potential therapeutics.

Acknowledgements

I am extremely grateful for an experience I had with LSD at the age of 19-years old with my dear friend Andrew. During this experience I had the realization that small molecules can drastically change our perception of reality and was inspired to learn more about pharmacology. My local University had a bio-chemistry program and during my studies I learned that molecules and the receptors they bind to are 3-dimensional and somehow this interaction can change the "normal" mode of reality we interact with daily. I really fell in love with organic chemistry and biochemistry during this time. The study of psychedelics continues to be the driving force and inspiration for my lifelong curiosity in science.

To Dr. Robert B. Laprairie: You have let me combine my interest in chemistry with your knowledge of pharmacology to discover the beautiful world of computational molecular pharmacology. Without your continued support I likely would not have found this niche research area. I will always remember the day you taught me how to use AutoDock Vina in your office which changed my life. I could not have asked for a more compassionate kind human being to be my mentor. The University of Saskatchewan and your trainees are extremely lucky to have you.

To Dow. P Hurst: I will be forever grateful for the training in *in silico* molecular modelling you taught me during my stay at the University of North Carolina Greensboro.

To my wife Sloan and son Jasper: Jasper although you are only an infant now, I am so excited to see what you become. I will likely tell you bedtime stories about the ligand and the receptor instead of the tortoise and the hair.

CHAPTER 1
Introduction

Contribution Statement

The contents of this chapter are an expanded version of the previously published review article and book chapter "Computer modeling of allosteric modulators at G protein-coupled receptors".[1] The entirety of the publication was written by Asher L. Brandt with guidance from Dr. Robert B. Laprairie. The present chapter was adapter and expanded to encompass the scope of the thesis.

1.1 G Protein-Coupled Receptors

G protein-coupled receptors (GPCRs) represent the largest protein family encoded by the human genome.[2] Activated GPCRs transduce extracellular signals which in turn control key physiological effects.[3] The endogenous ligands that activate GPCRs include odors, photons, hormones and neurotransmitters.[4] Due to the ubiquitous nature of GPCRs they play a role in many diseases such as obesity, depression, cancer, type 2 diabetes, Alzheimer's and Parkinson's.[5] For this reason, approximately 35% of FDA-approved drugs target GPCRs.[6] The human genome encodes approximately 800 GPCRs, which are subdivided into 6 classes; class A (Rhodopsin-like), class B (Secretin receptor family), class C (Metabotropic glutamate), class D (Fungal mating pheromone receptors), class E (Cyclic AMP receptors) and class F (Frizzled/Smoothed).[7] GPCRs consist of 7 transmembrane (TM) helices connected via 3 extracellular (ECL) and 3 intracellular loops (ICL), a disulfide bridge between ECL2 and TM3 and a cytoplasmic C-terminus containing an α-helix (helix 8) parallel to the cell membrane (**Figure *1-1***).[8] Ligands such as peptide hormones bind to the extracellular domain and trigger intracellular signaling cascades which mediate the functions of the GPCR.[9]

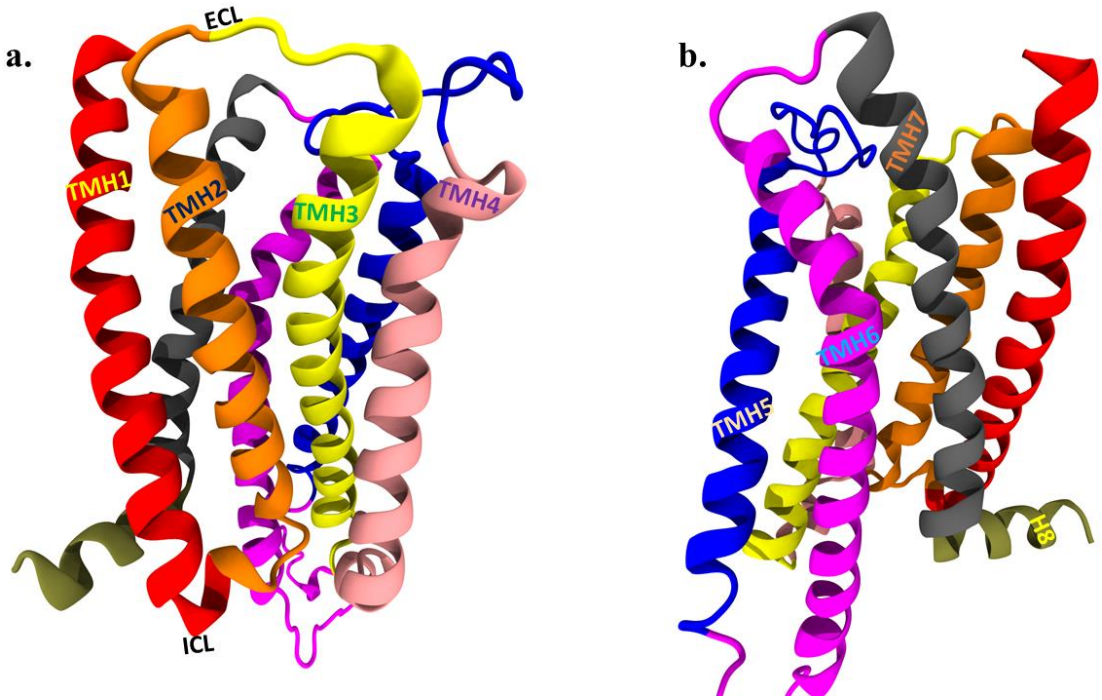

Figure 1-1. GPCR Structure. (a) Visualization of a GPCR. The perspective here is looking at the side of the GPCR from within the plasma membrane with a slight angle looking down from the extracellular surface. A defining feature of all GPCRs is having 7-Transmembrane helices. Transmembrane helices are: I red, II orange, III green, IV pink, V blue, VI purple, and VII grey. (b) Visualization of (a) rotated 180º.

1.2 GPCR Intra-Cellular Signaling Cascades

G proteins are a group of membrane resident proteins that recognize activated GPCRs and relay their messages allowing the bound ligand to produce a cellular effect.[10] There are four main families of G proteins; G_s, G_i, G_q and $G_{12/13}$.[11] While a G_S G protein stimulates the activation of adenylate cyclase (AC) and thus the production of cAMP, a G_i G protein inhibits the production of AC and thus the production of cAMP.[12] AC is a membrane bound enzyme activated by G_s and inhibited by G_i.[13] When activated, AC catalyzes the conversion of adenosine triphosphate (ATP) to cyclic adenosine monophosphate (cAMP).[14] cAMP activates cAMP-dependent protein kinases, and these kinases cause phosphorylation of certain enzymes specific to the agonist that bound to the receptor [15]. In the phospholipase C pathway, when the agonist binds to the receptor it activates a G_q protein.[16] Activated G_q protein then activates phospholipase.[17] This enzyme catalyzes the cleavage of phosphatidylinositol bi-phosphate into Diacylglycerol (DAG) and Inositol triphosphate (IP3).[18] IP3 receptor which is a ligand calcium channel is located on the membrane of the ER.[19] Binding of IP3 with its receptor causes release of Ca^{2+} ions into the cytoplasm.[20] Thus, the main goal of IP3 is to increase the cytosolic calcium ion concentration.[21] Phosphorylation is an important factor in GPCR activation because, after phosphorylation occurs, scaffold proteins known as βarrestins bind to the phosphorylated GPCR to deactivate the receptor and allow for internalization and recycling.[22] CB1R is predominantly G_i-coupled, whereas 5-HT_{2a}R is predominantly G_q-coupled.[23,24] Although both GPCRs are capable of engaging alternate signaling pathways such as $G_{12/13}$, G_i- and G_q-dependent signaling remain the best-characterized and therefore most-amenable to high through-put screening. Consequently, G protein-dependent CB1R signaling can be measured by a decrease in the accumulation of cAMP, while 5-HT_{2A}R can be measured by an increase in Ca^{2+} release from the endoplasmic reticulum.[25] Because both

receptors interact with βarrestins we can also measure a given ligand's activity via an increase in βarrestin recruitment to the intracellular face of the receptor. Routinely used high-throughput *in vitro* assays have been developed to readily measure secondary messenger pathways including cAMP and Ca^{2+} or protein-protein interactions such as βarrestin recruitment that we can use to quantify ligand potency, efficacy, and cooperativity.

Although these intracellular signaling cascades are initiated upon a ligand binding to a GPCR, the activation is not equal and depends on which particular ligand binds, often referred to as ligand bias.[26] The 2 major pathways of focus within the field of GPCR pharmacology are the G protein and the βarrestin pathway (***Figure 1-2***).[27] In some cases, these pathways are activated equally in which case the compound is called an unbiased agonist. As an example, the 5-HT_{2A}R agonists lysergic acid diethylamide (LSD) and ergotamine activate βarrestin2 recruitment with greater potency and efficacy than G_q and are therefore considered to be βarrestin2 biased agonists.[28,29]

An important consideration in GPCR pharmacology also pertains to the site at which a ligand binds to the GPCR. The conserved endogenous ligand of any GPCR always binds to a site called the orthosteric binding site.[30] For CB1R this is 2-arachidonlyglycerol (2-AG) and non-orthosteric binding sites on GPCRs are referred to as allosteric binding sites.[31] The most notable allosteric ligand amongst all GPCRs is cholesterol.[32] Allosteric ligands have received much investigation in the past 15 years because they offer several *potential* advantages over orthosteric ligands, including greater receptor subtype selectivity because allosteric sites are less evolutionary-conserved than orthosteric sites; and limited dependence, tolerance, or abuse liability because the ligands may only be active in the presence of the endogenous orthosteric compound.[33] These ligands have the ability to promote endogenous receptor activation, but not direct activation compared to an orthosteric ligand.[34] Allosteric modulators may be positive allosteric modulators

(PAMs) or negative allosteric modulators (NAMs).[35] A PAM may enhance the affinity, potency, and/or efficacy of the primary ligand whereas a NAM may reduce the affinity, potency, and/or efficacy of the primary ligand.[36]

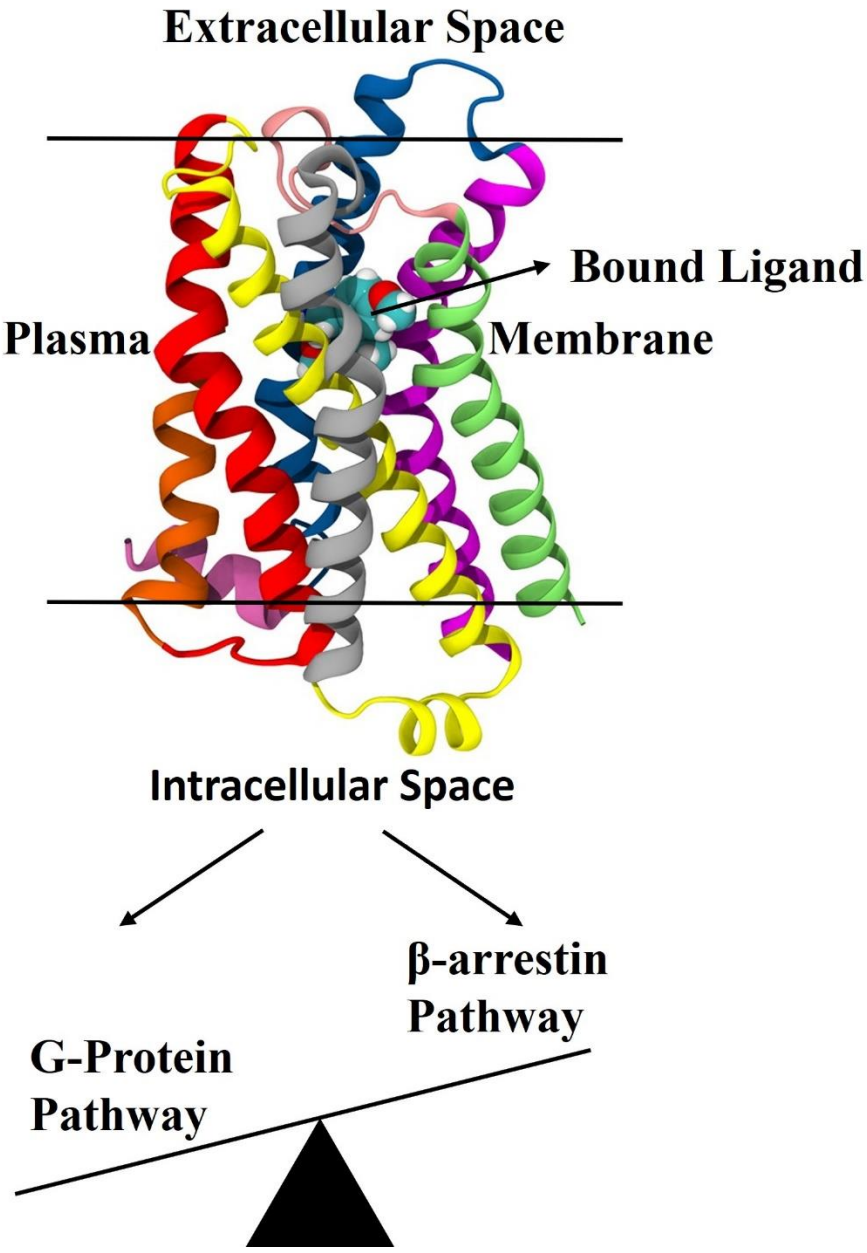

Figure 1-2. Ligand Bias. Upon ligand binding intracellular cascades are activated of which the G protein and βarrestin pathways are the best-characterized. Because these pathways are typically activated unequally one pathway will predominate similar to 2 people of different weights on a seesaw. The predominance of one pathway relative to another is often described as ligand bias.

1.3 Allosteric Site on GPCRs as FDA approved Drugs

Although there are 6 classes of GPCRs, we will only focus on class A GPCRs because the receptor's of focus in these studies - CB1R, CB2R, and 5-HT_{2A}R - are all class A. Allosteric sites on class A GPCRs are well documented. The major reason for this is that they have vast potential in terms of drug development. There are currently a few that are approved medications: ticagrelor, the anti-thrombosis medication that targets the P2Y purinoceptor 12 (P2Y12R) receptor; maraviroc an HIV medication that targets the CCR5 chemokine receptor; and plerixafor used during bone marrow transplants which targets the CXCR4 chemokine receptor. The binding of an allosteric modulator to its separate site from the orthosteric endogenous ligand results in a conformational change in shape to the orthosteric site which will affect this site in one of 3 ways: PAMs increase the affinity, potency, and/or efficacy of the orthosteric ligand; NAMs decrease the affinity, potency and/or efficacy of the orthosteric ligand; or silent allosteric modulator (SAM) causes no change in the affinity or efficacy of the orthosteric ligand.[37,38,39,40]

1.4 Cannabinoid Receptor Type 1

The type 1 cannabinoid receptor (CB1R) is a class A GPCR encoded by the *CNR1* gene in humans.[41] Specifically, CB1R is expressed in the peripheral nervous system (PNS) and central nervous system (CNS) of mammals and is involved in neuromodulatory processes.[41] Although CB1R is expressed in both the CNS and PNS it has higher concentrations in the CNS specifically within the hippocampus, basal ganglia, cerebellum, neocortex and spine.[41] Within these systems CB1R is found on pre-synaptic axon terminals of both glutamatergic and GABAergic neurons where activation of the receptor by endogenous cannabinoids limits further synaptic transmission from the pre-synaptic neuron.[42] Under the current model, the endogenous cannabinoids 2-arachodinylgylcerol (2-AG) and anandamide (AEA) are synthesized from membrane associated

lipid precursors on demand in response to physiological stimuli such as membrane depolarization in the post-synaptic neuron and travel in a retrograde manner to the pre-synaptic neuron to facilitate this CB1R-mediated and stimulus-dependent suppression of neurotransmitter release.[43] In mammals CB1R orthosteric activation by exogenous cannabinoids such as Δ^9-tetrahydrocannabinol (THC) and CP55,940 lead to decreased movement, anti-nociception and a decrease in body temperature accompanied by intoxication.[44] On the other hand, the endocannabinoid AEA does not produce intoxication but rather reduces pain, anxiety and stress.[45]

CB1R is comprised of 472 amino acids and there are 8 published crystal structures for the receptor available on the protein data bank.[46,47,48,49,50,51,48,52] In their inactive states, both CB1R and CB2R contain a salt bridge between D6.30 and R3.50.[53] Upon agonist binding, receptor activation occurs via a conformational rearrangement of W6.48 and F3.36 which consequently breaks the salt bridge.[53] This salt bridge is thought to keep both CB1R and CB2R in their inactive states and the breaking of this lock is hypothesized to activate the receptor putting it in an agonist conformation. In terms of critical residues in the orthosteric binding pocket, mutagenesis studies have shown that S383$^{7.39}$A mutation drastically reduces (50 – 100 fold) the affinity of both AM4056 and HU210.[54] This is due to the loss of a H-bond when the serine is mutated to an alanine. This residue is conserved in CB2R; thus this H-bond appear to be critical for activity in both receptors.

CB1R has gained much interest within the past few years because it is the receptor that mediates the intoxicating effects of THC from the *Cannabis sativa* plant. Beyond THC, *Cannabis sativa* may produce upwards of 500 other phytocannabinoids of which approximately 120 have been identified.[55] The discovery of naturally-occurring plant cannabinoids and the development of novel synthetic cannabinoids that target CB1R both represent important pursuits for novel therapeutics

in the contexts of pain, psychiatric conditions, neurodegenerative diseases, and metabolic disorders.

1.5 Cannabinoid Receptor Type 2

Similarly, the type 2 cannabinoid receptor (CB2R) is a class A GPCR encoded by the *CNR2* gene in humans.[56] CB2R is located in the PNS specifically immune cells. While activation of CB1R typically leads to intoxication, activation of CB2R inhibits proinflammatory cytokine production and subsequent release of anti-inflammatory cytokines.[57] The CB2R agonist GW842166x has been shown to produce neuroprotective effects in the 6-OHDA mouse model of Parkinson's disease.[58] CB2R is comprised of 360 amino acids and 4 solved crystal structures exist on the Protein Data Bank (PDB).[50,59,60,61] Due to quite similar sequence homology of CB1R and CB2R especially in the orthosteric binding site, developing selective CB2R ligands remains a challenge.

1.6 Psychedelics and the Serotonin 2a Receptor (5-HT_{2A}R)

Serotonin binds to 14 different serotonin receptors in order to mediate its biological effects.[62] Of these 14 receptors, the 5-HT_{2A}R has been under heavy investigation recently for its potential as a molecular target to treat post-traumatic stress disorder (PTSD) and depression.[63] Specifically, this applies to 5-HT_{2A}R agonists that are colloquially referred to as psychedelics including LSD, mescaline, and psilocybin.[64] 5-HT_{2A}R is found in high levels in the CNS specifically cortex, caudate nucleus, nucleus accumbens, locus coeruleus, olfactory tubercle, and hippocampus.[65] It was discovered in 1998 by Franz Vollenweider that 5-HT_{2A}R is the key site for psychedelics' mechanism of action.[66]

The first 5-HT_{2A}R crystal structure to be solved with a psychedelic bound was published in 2020 which showed LSD bound to 5-HT_{2A}R (***Figure 1-3***).[29] The structure elucidated the presence of a salt bridge between the protonated amine on LSD and a negatively charged oxygen atom on

D155$^{3.32}$, a common interaction that appears in all 5-HT$_{2A}$R active compounds.[29] The indole hydrogen also forms a H-bond with S242$^{5.46}$.[29] This H-bond likely occurs amongst other psychedelics with an indole scaffold such as psilocin and the endogenous ligand serotonin. This is supported by mutagenesis studies that show mutation S242$^{5.46}$A mutation leads to a drastic decrease in LSD and other psychedelics tryptamines binding affinity.[67,68] Unfortunately, these data have become a controversial topic as a recent crystal structure published with psilocin and serotonin do not include an interaction at S242.[5.46,69,70] Of note, data from the earlier study are supported by in vitro pharmacological evidence whereas the more recent 2022 data are not.[70] The final notable interaction that came from the 2020 study was the L229^{ECL2} forming hydrophobic interactions with the diethylamide moiety of LSD. The authors provide compelling *in vitro* data that correlate the interaction between LSD and L229^{ECL2} with the long residence time of LSD at the receptor.[29,71] L229^{ECL2} functions as a lid above the LSD binding site of 5-HT$_{2A}$R making it difficult for LSD to dissociate from the receptor.[29,71] Mutation of L229^{ECL2} to alanine results in a 10-fold increase in the rate of LSD's dissociation from 5-HT$_{2A}$R.[29,71] In contrast, the endogenous ligand, serotonin, does not interact with L229^{ECL2} and therefore has a much briefer residence time at the receptor as shown through functional *in vitro* and computational experiments.[29,68,71] Based on their *in vitro* and computational data, the authors hypothesize that ligand residence time at 5-HT$_{2A}$R correlates with βarrestin2 recruitment and some of the psychotropic effects of LSD.[29,71] Consequently, the data support a direct through line from ligand structure-activity relationships to ligand bias and drug safety. Studies such as Wacker et al. 2020[29] are compelling examples of how insights into GPCR structure-activity relationships can be developed using a combination of crystallographic data, *in vitro* and computational modelling.

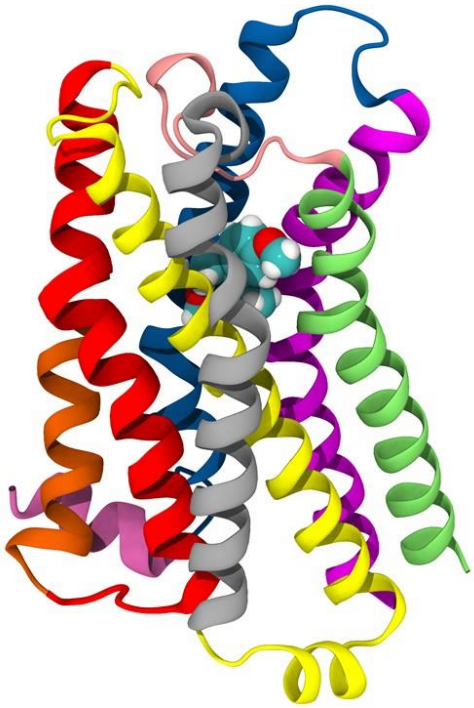

Figure 1-3. 5-HT$_{2A}$R Crystal Structure with LSD bound PDB ID: GWGT. In this view of 5-HT$_{2A}$R LSD is shown as the blue, white and red spheres in the center as VDW. Transmembrane helices are: I orange, II red, III yellow, IV grey, V green, VI purple, and VII blue. LSD is stabilized via a salt bridge with D155$^{3.32}$ and a H-bond with S242$^{5.46}$.

1.7 Computational Modelling of G protein-coupled receptors

Computational modelling in pharmacology refers to the use of computers coupled with mathematical modelling and quantum mechanics [specifically central processing units (CPUs) and graphics processing units (GPUs)] to uncover how biomolecules interact with one another.[72] With computational modelling one can generate on a computer how both protein-protein interactions occur as well as ligand-protein interactions. This is especially useful in understanding interactions (H-bond, Salt Bridge, Hydrophobic, π-π, Cation- π) between amino acids on the protein and functional groups on a ligand necessary for biological activity of a ligand-receptor complex. This is used for making future predictions about whether or not a ligand with a known structure will bind to and activate a protein before having to run an *in vitro* experiment.

For this dissertation, the goal of computational modelling is to (1) create a 3D model of how a given ligand binds to a receptor and (2) use this information to support *in vitro* data. The use of computational modelling in GPCR drug discovery began roughly in 2007, when the human β 2-adrenergic receptor structure was solved via x-ray diffraction.[73] Seven years earlier in 2000 the structure of a mammalian GPCR, bovine rhodopsin was solved.[74] As of August 5^{th,} 2022, 788 GPCR structures have been solved for 136 different receptors. Early-stage computational work focused on creating ligands that bound to the orthosteric binding pocket, which is where each GPCRs respective endogenous ligand binds. Although this method works well for solving the crystal structure of a GPCR, it does not work well for therapeutic ligand design. This is due to the highly conserved nature of a GPCRs orthosteric site, which makes developing selective ligands extremely difficult.[40] In addition, because orthosteric agonists bind the same sites as endogenous ligands, all physiological signals from a GPCR are superseded by exogenous orthosteric agonists.[75] Moreover, accumulating data demonstrate exogeneous orthosteric agonists have a higher potential

to produce intoxication, receptor desensitization, tolerance and dependence than allosteric ligands.[76] Ligands that bind to allosteric sites have become much more attractive targets for drug discovery for this reason. A growing number of researchers have solved GPCR structures with allosteric modulators bound using both cryo-EM and X-ray crystallography. This in turn has allowed for the discovery of (1) more allosteric sties on GPCRs, and (2) the development of allosteric modulators with higher selectivity. However, allosteric sites can be problematic to probe or assess by cryo-EM and crystallography because allosteric ligands tend to have lower affinity at allosteric sites, which are often "superficial" or sit on the surfaces of a protein, or because allosteric sites may overlap with of modulators of the receptor, such as cholesterol that could themselves be considered allosteric. Given the number of GPCR structures solved to date, computer modelling has become a growing field in drug discovery and pharmacology. It has also highlighted the considerable similarity of GPCR structure and highly conserved nature of a number of TMH residues which has required scientists to use the Ballesteros-Weinstein nomenclature system for naming specific residues (***Figure 1-4***).

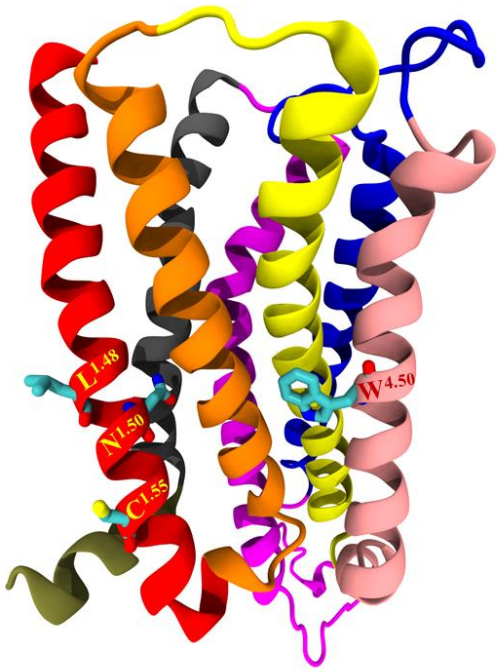

Figure 1-4. Ballesteros-Weinstein Numbering System. The numbering scheme by Ballesteros-Weinstein is a method for numbering amino acid positions in GPCRs. In each of the 7-TMH's the most conserved residue is denoted 50. While in TMH1 (red) this is Asparagine (N) on TMH4 (pink) this is Tryptophan (W). In this case these amino acids are denoted at $N^{1.50}$ and $W^{4.50}$. Any amino acid going in the direction of the N-terminus is treated as the negative direction whereas the C-terminus being the positive direction. For example, the cysteine residue is denoted at $C^{1.55}$ because it is 5 amino acids closer to the C-terminus than $N^{1.50}$ whereas $L^{1.48}$ is 2 positions closer to the N-terminus than $N^{1.50}$.

1.7.1 *In silico* Modelling of CB1R allosteric ligands

Within this thesis, development of allosteric ligands is focused of CB1R. CB1R is a key mediator in the endocannabinoid system which has 2 endogenous agonists: AEA and 2-AG. With growing number of constituencies decriminalizing or legalizing cannabis globally, research concerning CB1R and cannabinoids has grown. THC is the psychoactive and intoxicating compound present in cannabis and is known to be a partial agonist that binds the orthosteric sites of CB1R and CB2R. Targeting CB1R has applications in treating pain, movement disorders, epilepsy and obesity.[77] Because direct-acting orthosteric agonists of CB1R produce intoxication, the development of allosteric modulators at CB1R may provide the most promise. In terms of the orthosteric binding site there are 6 crystal structures that show the binding site in high resolution. Despite this little *in silico* work has been conducted as CB1R orthosteric ligands are intoxicating thus are not sought after as therapeutic agents but rather tool compounds for studying the receptor. However, using these crystal structures mutagenesis studies have shown that S383$^{7.39}$A mutation drastically reduced (50 – 100 fold) the affinity of both AM4056 and HU210 (CB1R orthosteric agonists).[54] The only CB1R allosteric modulator to have a known solved binding site is the CB1R NAM ORG27569 (PDB 6KQI).[47] Although ORG27569 significantly increases binding affinity of CP55,940 (a synthetic CB1R orthosteric agonist) at CB1R and decreases the binding affinity of rimonabant (a CB1R inverse agonist) it decreases the efficacy of CP55,940 in G protein-mediated coupling and therefore is functionally considered a NAM.[78] The ORG27569 isothiocyanate analog GAT100 has been shown to be a more potent and efficacious CB1R NAM than ORG27569 for βarrestin1 recruitment, PLCβ3 and ERK1/2 phosphorylation, cAMP accumulation, and CB1R internalization in HEK293A cells overexpressing CB1R and in Neuro2a and STHdh$^{Q7/Q7}$ cells endogenously expressing CB1R.[79] The rationale for making the isothiocyanate derivative was to

form a covalent bond on CB1R which was found to occur at C382$^{7.38}$.[80] PDB ID 6KQI shows us that ORG27569 binds to an extrahelical site on the inner leaflet of the membrane. Most of the contacts interact with TM4 however the ligand extends along a lipid-facing hydrophobic surface to additionally contact TM2.[47] This binding site overlaps with the cholesterol binding site on multiple GPCRs including CB1R.[48] Upon ORG27569 binding CB1R adopts an inactive conformation such that TM6 packs against TM3 and TM5.[47] This causes a blockage of the G protein-interacting residues observed in the crystal structure of CB1 with the G_i complex.[51] This observation is consistent with experiments that show ORG27569 diminishes G_i coupling in the presence of an agonist.[78]

Another allosteric modulator of CB1R that holds potential in understanding the function of allosteric sites is the racemic compound GAT211 and its purified enantiomers (R)-GAT228 and (S)-GAT229.[81] GAT211 has been shown to be a selective CB1R allosteric agonist-PAM (i.e. ago-PAM) because it displays both PAM and agonist activity in HEK293A cells expressing CB1R.[82] By purifying GAT211 into its respective enantiomers it was found that the allosteric agonist activity resided with the *R*-enantiomer GAT228, whereas the PAM activity resided with the *S*-enantiomer GAT229.[81] In binding experiments, GAT211 enhances the binding of the orthosteric agonist [^{3}H]CP55,940 and reduces the binding of orthosteric inverse agonist rimonabant.[82] Being that neither GAT211 nor its enantiomers competed for binding with [^{3}H]CP55,940 it is unlikely that the agonist nature of GAT211 and GAT228 is the result of their binding to the orthosteric site. Using a computational modelling-based approach known as forced-biased MMC simulated annealing that GAT228 and GAT229 have distinct binding sites on CB1R (***Figure 1-5***).[83] GAT228 binds in the IC TMH1-2-4 exosite.[83] The 2 oxygens on the NO_2 form a dual H-bond with 2 hydrogens on R148^{IC1} and another H-bond exist between the hydrogen on the indole and a nitrogen

atom on H154$^{2.41}$.[83] Face-to-face aromatic stacking was observed between the indole ring phenyl substituent and F237$^{4.46}$ and a T-shaped aromatic stack was observed between the phenyl ring attached to the stereocenter and W2.41$^{4.50}$.[83] This binding site promotes agonism via a conformation change in F237$^{4.46}$ into a γ1 g+ → trans state causing the breaking of the R3.50/D6.30 ionic lock which in turn appears to activate CB1R.[83] GAT229 binds to the EC TMH2-3-ECL1 binding stie.[83] The indole hydrogen forms an H-bond with D176$^{2.63}$ and another H-bond was observed between the NO_2 group and Y172$^{2.59}$.[83] A cation-π interaction was observed between the indole ring of GAT229 and R182^{ECL1}.[83] The indole ring phenyl ring substituent was observed to have an off-set parallel aromatic stack with Y172$^{2.59}$.[83] GAT229 alone can not break the ionic lock that activates CB1R and thus alone is not an agonist, but because it stabilizes an orthosteric agonist when bound it acts as a PAM.

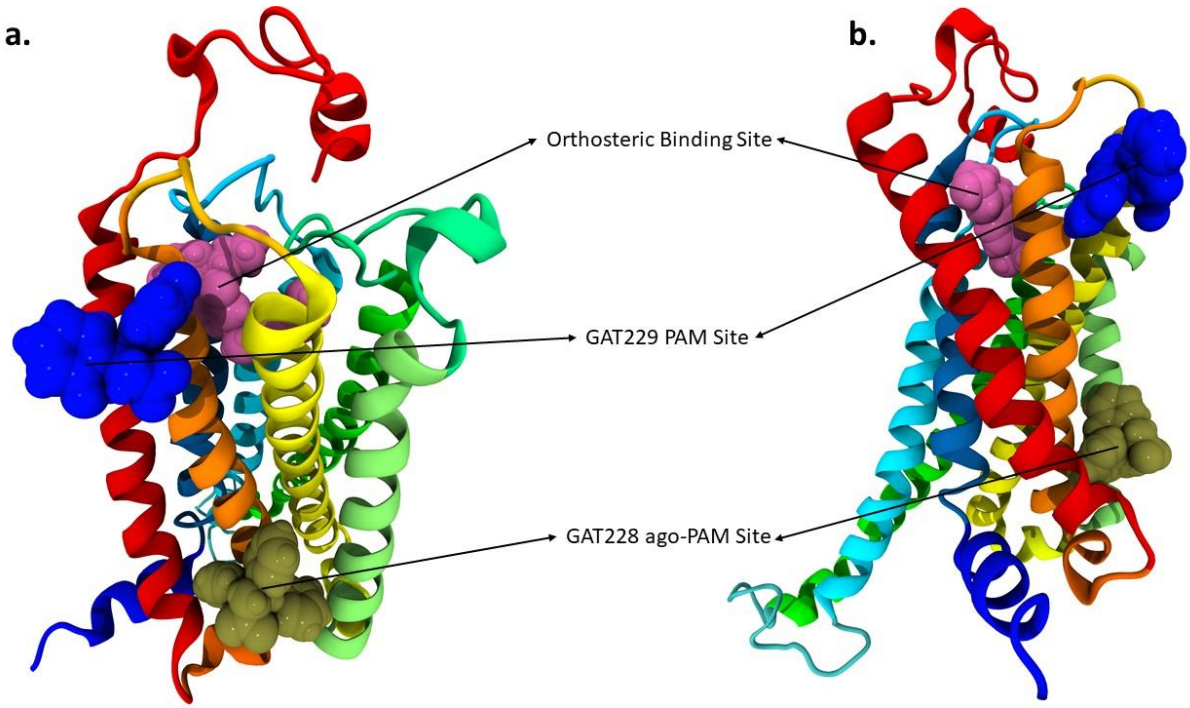

Figure 1-5. CB1R with three different binding sites shown. In these views of CB1R the orthosteric site is shown in magenta, an identified PAM site in blue, and another identified ago-PAM site in tan. Transmembrane helices are: I red, II orange, III yellow, IV light green, V green, VI cyan, and VII blue.

1.8 Objectives of This Research

GPCRs continue to be among the leading class of protein targets for drug development. At the leading edge of this area is a need to understand previously poorly-characterized GPCRs that are the primary targets for controlled and prohibited substances, namely cannabinoids, and psychedelics. As the control status, legality, and medical access to cannabis and psychedelics continue to shift research is desperately needed to understand the potential harms and therapeutic utility of cannabinoids and psychedelics. In addition, the opportunity to develop allosteric ligands that target the cannabinoid receptor in particular may represent a means to bypass the undesirable effects of orthosteric ligands.

The long-term hypothesis of this research is that the cannabinoid and serotonin receptors are tractable therapeutic targets for the development of drugs for unmet clinical needs including pain, epilepsy, and anxiety. To this end, the overall objective of this research is to advance knowledge of these receptors' fundamental structure-activity relationships through the use of *in vitro* and *in silico* computer modelling assays performed on CB1R, CB2R, and 5-HT_{2A}R. The aims of this research were to understand (1) The SAR between compounds that separately bind CB1R, CB2R and 5-HT_{2A}R; (2) How this SAR can be used to elucidate biased agonism at CB1R, CB2R and 5-HT_{2A}R; and (3) How computational methodologies can be employed to explain pharmacological properties of these compounds.

Each chapter in this thesis represents work already published or under peer review. Although methodologies and approaches overlap between each individual study all methods have been included in order to illustrate key differences in technique and approach. Chapter 2 shows that enantiomerically separated compounds display a difference in pharmacology and binding sites on CB1R. Chapter 3 builds upon chapter 2 and shows that computational modelling can be used to

optimize ligands that bind to the CB1R ago-PAM site. Chapter 4 characterizes select synthetic cannabinoid receptor agonists at CB1R and CB2R. Chapter 5 characterizes NBOMe compounds at 5-HT_{2A}R looking at the relationship in vitro and in silico of changing methoxy groups on the phenethylamine ring. Lastly chapter 6 summarizes the research provided and looks at philosophical considerations regarding this research.

CHAPTER 2

Pharmacological Evaluation of Enantiomerically Separated Positive Allosteric Modulators of Cannabinoid 1 Receptor, GAT591 and GAT593

Copyright statement

This chapter is in review for publication. The manuscript has been modified to meet formatting requirements.

Contribution statement

The manuscript used as the basis for this chapter was written by me – Asher Brandt – with guidance from Dr. Robert B. Laprairie. *In silico* and *in vitro* data were collected and analyzed by myself with technical assistance from Dr. Robert B. Laprairie and Dow P. Hurst (University of North Carolina, Greensboro). GTPγS experiments were performed in the laboratory of Dr. Roger Pertwee (University of Aberdeen) and analyzed by Asher Brandt and Dr. Robert B. Laprairie. *In vivo* experiments were performed with the assistance of Ayat Zagzoog (University of Saskatchewan).

2.1 Introduction

The endogenous cannabinoid system (ECS) is composed of endogenous ligands (e.g. anandamide [AEA] and 2-arachidonoylglycerol [2-AG]), anabolic and catabolic enzymes, and receptors (the predominant receptors being the type 1 and 2 cannabinoid receptors [CB1R, CB2R]). [84,85] The ECS is ubiquitous in the human body.[86] Both CB1R and CB2R are class A G protein-coupled receptors (GPCRs).[87] CB1R is most-abundant in the brain and central nervous system (CNS) whereas CB2R is most-abundant in cells of the immune system.[88] The primary role of CB1R is to regulate mood, diet, sleep and pain sensation whereas CB2R regulates immune responses.[89] Both receptors are activated by the endogenous ligands AEA and 2-AG.[90] Due to the ubiquitous nature of CB1R and CB2R, the ECS is considered a potential target for a wide array of diseases, but CB1R in particular is considered a target for the treatment of pain and neurological disorders such as epilepsy, Huntington's disease, and glaucoma.[91]

The intoxicating effects of *Cannabis* represent a major limitation to its use as medicine. The intoxicating effects of *Cannabis* are due to Δ^9-tetrahydrocannabinol (THC) binding to the orthosteric site of CB1R. It is hypothesized that the intoxicating properties of CB1R activation could be avoided if a drug bound to the allosteric site of the receptor. Allosteric modulators may be positive allosteric modulators (PAMs), negative allosteric modulators (NAMs), or silent allosteric modulators.[92] A PAM enhances the effect of the primary ligand, a NAM reduces the effect of the primary ligand, and a silent allosteric ligand does not affect the pharmacology of the orthosteric ligand.[36] The first described CB1R allosteric modulator was Org27569, which drove the development of indole sulfonamides as potent CB1R NAMs.[93]

In an earlier study published by the Laprairie lab[94], we reported on the pharmacology of racemic CB1R allosteric modulators GAT591 and GAT593 (***Figure 2-1***), wherein we observed these

ligands have both allosteric-agonist and positive allosteric modulator (ago-PAM) properties. We found that GAT591 and GAT593 act at allosteric sites due to their ability to enhance the binding of [^{3}H]CP55,940 at CB1R and at the same time modulate the receptor in absence of an orthosteric ligand.[91]

Biased agonism describes the ability of a ligand to preferentially activate one signalling pathway compared to another; [92,36] for example G protein- versus βarrestin-mediated signaling.[93] Previous work has shown that the racemic mixtures GAT591 and GAT593 displayed bias towards $G_{i/o}$ signaling as compared to βarrestin, which is correlated with improved cell viability.[91] Additional studies from our group support the idea that G protein bias of PAMs is correlated with improved outcomes in rodent models of Huntington's disease, pain, and absence epilepsy [95,96,81]; whereas βarrestin bias may be correlated with reduced cell viability and increased pathology in animal models of absence epilepsy and Huntington's disease.[81,97] One of the challenges in developing ligands for GPCRs is biased agonism.[92] To further understand the molecular mechanism(s) of action and probe for potential enantiospecific interactions, we separated the enantiomers, determined their absolute stereochemistry and conducted a biochemical characterization using cAMP and βarrestin2 assays to determine their allosteric-agonist and PAM activity. Previously we observed the distinct pharmacology between the enantiomers of (±)-GAT211, where (*R*)-GAT228 was an allosteric-agonist, (*S*)-GAT229 showed pure PAM activity at CB1R.[95] In this study we observed that the enantiomers of GAT591 and GAT593 display unique *in vitro* and *in vivo* effects that are likely to be associated with their unique modes of binding to CB1R.

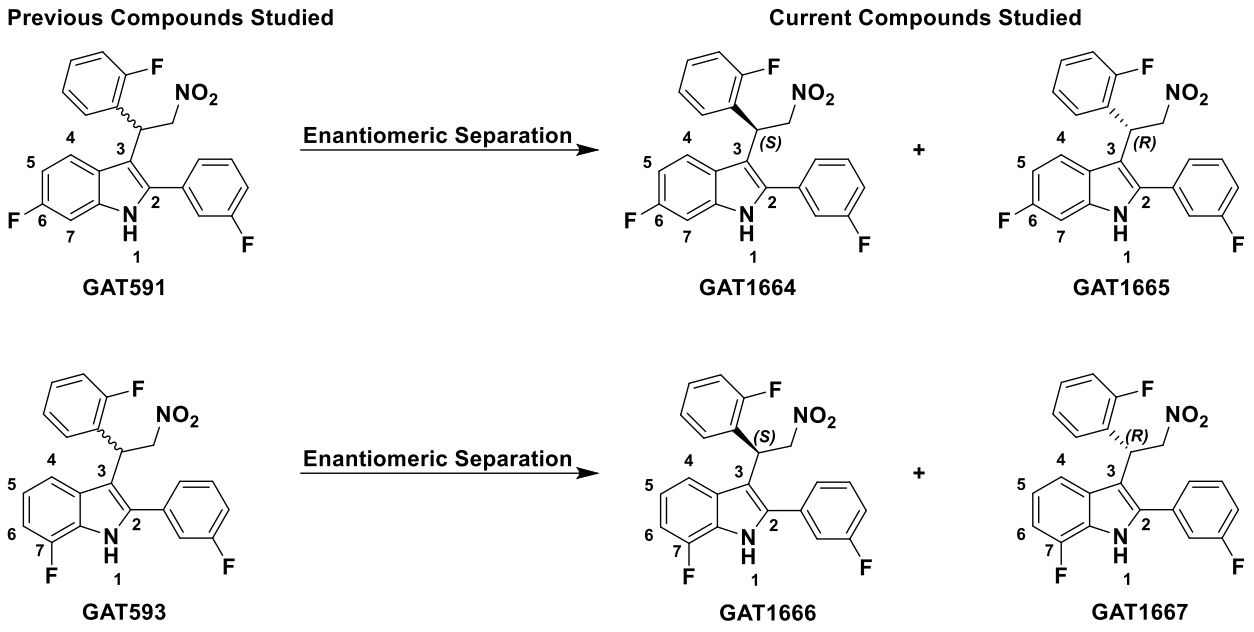

Figure 2-1. GAT591 previously studied was separated out into its respective enantiomers (GAT1664 and GAT1665) and GAT593 was separated out into its respective enantiomers (GAT1666 and GAT1667). The difference between GAT1664 and GAT1665 vs GAT1666 and GAT1667 is the position of the fluorine.

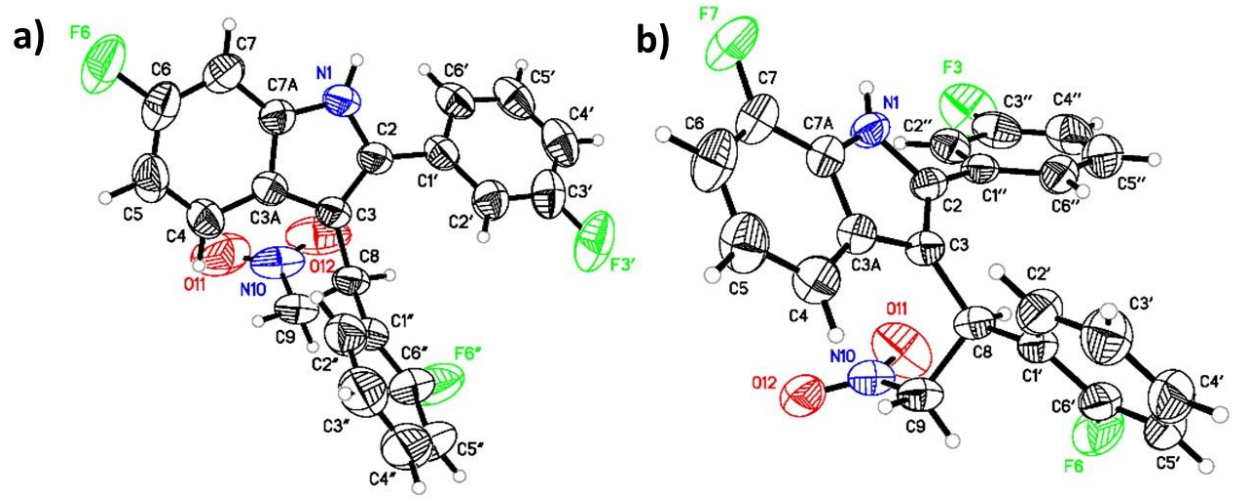

Figure 2-2. ORTEP diagram of (+)-GAT1664 (a, CCDC no. 2086717) and (+)-GAT1666 (b, CCDC no. 2086718)

2.2 Experimental Section

2.2.1 *In vitro* evaluation

Compounds used. Unless otherwise noted, all reagents and chemicals were purchased from Sigma-Aldrich (Mississauga, ON). CP55,940 and THC were purchased from Cayman (Ann Arbor, MI) and Sigma-Aldrich, respectively. All other tested compounds were obtained from Dr. Ganesh Thakur, Northeastern University. All compounds were initially dissolved in DMSO and diluted in a 10% DMSO solution in PBS. Compounds were added directly to cell culture at the time and concentrations indicated at a final concentration of 0.1% DMSO.

Cell culture. HitHunter (cAMP) and PathHunter (βarrestin2) CHO-K1 cells stably-expressing human CB1R (CB1R) from DiscoveRx (Eurofins, Freemont, CA) were maintained at 37°C, 5% CO_2 in DMEM/F-12 containing 10% FBS and 1% penicillin/streptomycin. Cell media was changed approximately every 48 h and cell passage number was maintained below 35. In addition, 0.5% geneticin was used for CHO-K1 CB1R HitHunter cAMP cells and 1% geneticin and 0.5% hygromycin b was used for CHO-K1 CB1R PathHunter βarrestin2 cells.

HitHunter cAMP assay. cAMP inhibition was performed in the presence of 10 µM forskolin (FSK) using the DiscoveRx HitHunter assay in CHO-K1 CB1R cells. Cells (160,000 cells/well in 96 well plates) were incubated overnight in Opti-MEM (Invitrogen) containing 1% FBS at 37°C and 5% CO_2. Opti-MEM media was removed and replaced with cell assay buffer (DiscoveRx) and then cells were simultaneously treated with 10 µM FSK and experimental compounds (0.10 nM - 10 µM) for 90 min. cAMP antibody solution and working detection solutions were the added according to the manufactures protocol (DiscoveRx), and cells were incubated for 60 min at room temperature. cAMP solution A was added according to the manufacturer's protocol (DiscoveRx) and cells were incubated for an additional 60 minutes at room temperature before

chemiluminescence was measured on a Cytation5 plate reader (top read, gain 200, integration time 10 sec). Data are presented as percent maximal CP55,940-dependent inhibition of cAMP accumulation.

PathHunter βarrestin2 assay. βarrestin2 recruitment was determined using the CB1R CHO-K1 cell PathHunter assay (DiscoveRx). Cells (160,000 cells/well in 96 well plates) were incubated overnight in Opti-MEM (Invitrogen) containing 1% FBS at 37°C and 5% CO_2. Cells were then simultaneously treated with experimental compounds (0.10 nM - 10 µM) for 90 min. Detection solution was the added to cells according to the manufacturer's protocol (DiscoveRx), and cells were incubated for 60 minutes at room temperature. Chemiluminescence was measured on a Cytation5 plate reader (top read, gain 200, integration time 10 sec). Data are presented as percent maximal CP55,940-dependent stimulation or fold over vehicle.

[^{3}H]CP55,940 radioligand displacement assay. Previous studies have shown that CB1R PAMs enhance orthosteric agonist binding (e.g. CP55,940).[98] Radioligand binding assays were carried out with 1 nM [^{3}H]CP55,940 in Tris buffer (75 mM Tris-HCl, 12.5 mM $MgCl_2$, 1 mM EDTA, 1% BSA, pH 7.4) with a total assay volume of 200 µL. The assay began with the addition of transfected CB1R CHO-K1 cell membranes (25 µg protein per well). The assays were left to equilibrate at room temperature for 2 h before vacuum filtration using a Millipore Sigma 12-well sampling manifold and filter paper that had been soaked in wash buffer. Each reaction well was washed 3 times with a 2 mL aliquot of Tris-binding buffer. The filters were removed then submerged in 5 mL of scintillation fluid (Ultima Gold F, PerkinElmer, Woodbridge ON). Radioactivity was quantified by liquid scintillation spectrometry. Specific binding was defined as the difference between binding that occurred in the presence and in the absence of 1 µM unlabeled or CP55,940. Data are presented as percent [^{3}H]CP55,940 bound.

[^{35}S]GTPγS assay: This assay was conducted in the laboratory of Dr. Roger Pertwee as described in previous reports.[95] To summarize, the assay was completed in the presence of [^{35}S]GTPγS (0.1 nM), GDP (30 μM), GTPγS (30 μM) using membranes derived from CHO-K1 cells (1 mg/mL) overexpressing CB1R. Assay buffer consisted of 50 mM Tris, 10 mM $MgCl_2$, 100 mM NaCl, 0.2 mM EDTA and 1 mM DTT at pH 7.4. Membranes were incubated at 30°C for 90 min in a total volume of 500 mL. Reactions were ended by the addition of ice-cold wash buffer (50 mM Tris and 1 mg/mL BSA, pH 7.4) followed by rapid filtration under vacuum through pre-soaked Whatman GF/B glass-fibre filters in a 24-well sampling manifold (Brandel Cell Harvester; Brandel Inc, Gaithersburg, MD, USA). Reaction wells were washed six times with a 1.2 mL aliquot of Tris-binding buffer. Filters were subsequently oven-dried for 60 min and placed in 3 mL of scintillation fluid (Ultima Gold XR, PerkinElmer). Bound radioactivity was determined by liquid scintillation counting. Basal [^{35}S]GTPγS binding was determined in the presence of 20 mM GDP without any compounds present. Non-specific binding was determined in the presence of 10 mM GTPγS.

2.2.2 *In vivo* evaluation

Triad assessment in mice. Male C57BL/6 mice (Charles River, Senneville, QC) between 4 and 7 months of age were used for these studies. Animals were group housed at the Laboratory Animal Services Unit (LASU) at the University of Saskatchewan (3-5 animals/cage) with a standard 12:12 light-dark cycle, ad libitum access to food and water, and environmental enrichment. Mice were randomly assigned to receive either vehicle or 0.1, 1, 3 or 10 mg/kg compound as indicated in figure legends (n = 5 – 6 mice/treatment group). Compounds administered intraperitoneally (i.p.) were prepared in vehicle [ethanol and cremaphor in saline (1:1:18)]. Catalepsy was assessed in the bar holding assay 5 min after drug administration. Mice were placed so that their forepaws clasped

a 0.7 cm ring clamp positioned 4.5 cm above the surface of the testing space.[99] The length of time the ring was held was recorded in seconds. The trial ended if the mouse turned its head or body or made 3 consecutive escape attempts to a maximum of 60 sec. Body temperature was measured by rectal thermometer 15 min after drug administration. Anti-nociceptive effects were measured in the warm water (52±2°C) tail-flick test 20 min after drug administration. Response in this case was defined by the removal of the tail from the warm water, with a maximal response time of 20 sec. Catalepsy and tail flick data are presented as percent maximum possible effect (MPE). Compounds were administered at the doses indicated. Experimenters were blinded to treatment for all behavioral assessments and analyses. Animals were purchased, rather than bred, to reduce animal numbers. In all cases, experiments were performed with the approval of the University Animal Care Committee (UACC) at the University of Saskatchewan and are in keeping with the guidelines of the Canadian Council on Animal Care (CCAC) and the ARRIVE guidelines.[100]

2.2.3 *In silico* evaluation

Molecular docking. A conformational analysis was performed on GAT1664, GAT1665, GAT1666 and GAT1667 using Spartan '18 V1.4.5.[101] Molecular mechanics were applied to each rotamer to obtain a local minimum.[101] After duplicates were eliminated, HF/6-31G* was applied to the remaining rotamers to obtain the global minimum energy conformation.[101]

CB1R model: The CB1R model has been described in detail[83], but in brief: The CB1R model used in this study was based on the CB1R activated state crystal structure (PDB-ID: 5XRA) and the cryo-EM CB1R/Gi bound structure (PDB-ID: 6N4B). Structures were prepared with the Protein Preparation protocol[102], mutations in the 5XRA structure were returned to wild-type (WT), and both models were inspected for close contacts and crystal packing effects. Modification of the 5XRA structure to create the CB1R model involved calculating low free energy conformations for

TMH2/7 to accommodate mutation data for S383$^{7.39}$, F2.61, F2.64 [54,103]. In addition, because of loop compression in the 5XRA structure, the IC1 loop from the 6N4B Gi bound structure was used in the model. TMH4 in the 5XRA CB1R R* structure has tight crystal contacts on its IC end with TMH1 of another bundle because of antiparallel packing. For this reason, the conformation of TMH4 in the 6N4B Gi bound structure was used in the model. Modeller was used to remodel the EC3 loop (D6.58 to T7.33) and allow K(373) to interact with D2.63, consistent with mutation results.[104,105] Modeller was also used to extend and model the N-terminus to S(88) with inclusion of the C(98) to C(107) disulfide bridge.[106,107] The receptor/ligand complex was energy minimized in Prime.[102] The Prime implicit membrane functionality was employed. Hydrophilic residues facing the binding crevice and within the low dielectric region of the implicit membrane were excluded from the low dielectric via exclusion spheres placed on each residue. The Generalized Born/Surface Area (GB/SA) continuum solvation model for water was used with the dielectric set to 80 outside of the implicit membrane region and 2 within. A truncated Newton conjugate gradient minimization was performed using the OPLS3e force field for one iteration up to a maximum of 1000 steps and with a 0.1 kcal/mol gradient endpoint. Constraints of 1 kcal/mol were placed on the C-alpha atoms of residues R3.50, Y5.58, L6.33, and Y7.53 to prevent the intracellular opening present in the R* structures from closing during the minimization.

MMC calculations: Confirmation of the binding site by Metropolis Monte Carlo calculations had been published previously on fragments of GAT228/229.[83] We repeated these calculations on identically designed fragments from GAT591/593 and found similar results. *Docking*: Once the two sites were confirmed, the structures of GAT1664-7 were docked in the intracellular TMH1/2/4 site with H2.41, F4.46, and W4.50 used as direct interaction sites. GAT1664 and GAT1666 were docked in the TM2/3/ECL1 site with Y2.59 and D2.63 as direct interaction sites. In addition, after

extensive previously published molecular dynamics calculations on unfluorinated versions of the GAT compounds (GAT1600-3), R(148) was modeled to interact directly with the carbonyl oxygens of the last turn of TMH1 and not the nitro group within the compounds.[108] The receptor/ligand complexes were energy minimized in Prime.[102] The Prime implicit membrane functionality was employed. Hydrophilic residues facing the binding crevice and within the low dielectric region of the implicit membrane were excluded from the low dielectric via exclusion spheres placed on each residue. The Generalized Born/Surface Area (GB/SA) continuum solvation model for water was used with the dielectric set to 80 outside of the implicit membrane region and 1 within. A truncated Newton conjugate gradient minimization was performed using the OPLS3e force field for 1 iteration, up to a maximum of 1000 steps and with a 0.1 kcal/mol gradient endpoint. Constraints of 1 kcal/mol placed on the c-alpha atoms of residues R3.50, Y5.58, L6.33, and Y7.53 were set to prevent the intracellular opening from closing during the minimization. The resulting docks were refined with the Induced Fit protocol.[102] The Glide box size was set to 12 Å3 centered on the ligand and the SP docking algorithm employed. Residues within 5 Å of the docked ligand were included in the Prime refinement stage, except in the case of the TM2/3 PAM site where S2.60 and K3.28 were excluded based on mutation data.[54,109] The implicit membrane previously used during the initial Prime minimization was employed here as well.

MMGBSA analysis: Each of the GAT1664-7 ligand receptor complexes were evaluated via MMGBSA. This was the scoring function used to evaluate each complex and not glide scores. This method is used to estimate the relative binding affinities for a list of ligands (reported in kcal/mol). As the MMGBSA binding energies are approximate free energies of binding, a more negative value indicated stronger binding. For this computation the VSGB solvation model was employed while the chosen force field OPLS4 was used.

2.2.4 Statistical Analysis

Data related to EC_{50} and E_{max} in **Figure *2-3*** and ***Figure 2-5*** were obtained with nonlinear regression models (4-parameter model, GraphPad Prism 9.0, San Diego, CA). Results were calculated as percent response relative to the reference agonist CP55,940 (**Figure *2-3***), percent [^{3}H]CP55,940 bound (***Figure 2-5a***), or percent stimulation above baseline (***Figure 2-5b,c*).** Significance was determined by non-overlapping 95% C.I. or by one-way ANOVA followed by Bonferroni's post-hoc test. $p < 0.05$ was considered significant. In order to estimate bias, concentration-response curves were globally fit to the operational model (Eq. 2-1; Prism).[110] In the operational model, E is efficacy, E_{max} is the maximum response, [A] is agonist concentration, n is the Hill Slope, τ is the transducer constant (*i.e.*, the inverse of the fraction of receptors that must be occupied to achieve a half-maximal response), and K_A is the estimated agonist affinity.[111] *To* best fit data, the transduction coefficient $\log(\tau/K_A)$ (*i.e.* logR), n, and E_{Max} were shared and $\log K_A$ was constrained between 0 and -15. In cases where a compound did not achieve a clear plateau in the concentration-response, E_{max} was set to the maximum response observed and EC_{50} was set to 10,000 nM. Relative agonist activity compared to a reference agonist (CP55,940) was calculated as show in Eq. 2-2.[111] ΔlogR values were compared for test compounds between assays measuring inhibition of cAMP and βarrestin2 recruitment to determine bias factor ($\Delta\Delta$logR) (Eq. 2-3).[112] Data related to ***Figure 2-6*** was analyzed via a two-way mixed ANOVA. This was implemented to analyze the main effect of drug treatments and main effects of groups as well as interaction between drug treatments and group. Bonferroni's post-hoc test was performed for all pairwise comparisons. GraphPad Prism 9.0 was used to analyze *in vivo* data and $p < 0.05$ was considered to be statistically significant. Data are expressed as mean ± SEM of at least 6 independent experiments.

$$E = \frac{E_{max}[A]^n \tau^n}{[A]^n \tau^n + ([A] + K_A)^n} \quad \text{Eq. 2-1}$$

$$\Delta log R = log(\tau/K_A)_{Testcompound} - log(\tau/K_A)_{Refcompound} \quad \text{Eq. 2-2}$$

$$logbias = \Delta\Delta log R = \Delta\Delta log\ (\tau/K_A)_{R1-R2} = \Delta log(\tau/K_A)_{R1} - \Delta log(\tau/K_A)_{R2} \quad \text{Eq. 2-3}$$

2.3 Results and Discussion

2.3.1 Synthesis, chiral separation and absolute stereochemistry determination

GAT591 and GAT593 were synthesized on a multigram scale in the laboratory of Dr. Ganesh Thakur (Northeastern University) using our previously published method.[95] Both enantiomers of each compound were separated in high optical purity (>99%) using superfluid chiral HPLC (for details see ***Supplementary Info 2.5*)**. The absolute stereochemistry of (+)-GAT1664 and (+)-GAT1666 was determined by single-crystal X-ray diffraction technique (***Figure 2-2***) and was found to be "S" for both of these enantiomers (Figure 2-2). Based on this study, we can predict the absolute stereochemistry of each opposite enantiomers, (-)-GAT1665 and (-)-GAT1667 as "R" (***Figure 2-1*** and ***Figure 2-2***)

2.3.2 *In vitro* evaluation

Our *in vitro* study explored CB1R-dependent modulation of cAMP inhibition and βarrestin2 recruitment in CHO-K1 cells stably-expressing CB1R with or without CP55,940. Inhibition of cAMP accumulation is $G_{i/o}$-protein mediated whereas recruitment of βarrestin2 is G protein independent.[113] In a previous paper, GAT591 and GAT593 displayed mixed agonist and PAM (i.e. ago-PAM) activity.[95] The compounds GAT591 and GAT593 contain a 50:50 racemic mixture of both *R* and *S* enantiomers. In this paper each enantiomer was investigated to determine which enantiomer had agonist activity and which had the PAM activity, as we previously observed these

properties to be enantiomerically distinct in the compounds GAT211, GAT228, and GAT229.[82] Separating GAT591 and GAT593 into their respective enantiomers gave GAT1664, GAT1665, GAT1666 and GAT1667 (***Figure 2-1***).

All enantiomers displayed G protein-mediated agonist activity at CB1R as shown by their ability to inhibit cAMP in the absence of an orthosteric agonist (**Figure *2-3a***). Similarly, all 4 compounds displayed activity consistent with positive allosteric modulation of CB1R in the presence of the orthosteric agonist CP55,940 in the cAMP assay (**Figure *2-3d*)**. Comparing **Figure *2-3a*** to **Figure *2-3d***, the studied GAT compounds were more efficacious as PAMs but display allosteric agonist activity. As an agonist, GAT1666 displayed the greatest efficacy, and GAT1667 displayed the greatest efficacy at inhibiting cAMP as a PAM. All enantiomers displayed low nanomolar potency as agonists with no statistical difference among the compounds (**Figure *2-3***). Both *R*-enantiomers (GAT1665 and GAT1667) displayed greater PAM potency and efficacy than the *S*-enantiomers (GAT1664 and GAT1666), with GAT1667 being the most-potent and efficacious (**Figure *2-3d***). These observations are in keeping with our earlier findings with the parent racemic ligands wherein PAM activity is predominantly attributable to GAT229, which shares the same spatial orientation as GAT1665 and GAT1667, and agonist activity is predominantly attributable to GAT228, which shares the same spatial orientation as GAT1664 and GAT1666.[82]

Both GAT1665 and GAT1667 recruited βarrestin2 as low-potency agonists and PAMs at CB1R (**Figure *2-3e***). GAT1664 did not recruit βarrestin2 to CB1R while GAT1666 displayed a weak ability to do so as an agonist (**Figure *2-3b,e***). This suggest that as agonists, GAT1665 and GAT1667 (the *R*-enantiomers) recruit βarrestin2.

From these data, bias (ΔΔlogR) was estimated between cAMP inhibition and βarrestin2 recruitment (**Figure *2-3c,f***). In instances where E_{max} for βarrestin2 was not reached as shown by a

clear plateau in data, E_{max} was set to the maximum response observed and EC_{50} was set to 10,000 nM to provide some estimate of bias. As an agonist, GAT1664 displayed no activity for βarrestin2 recruitment and calculations of ΔΔlogR are therefore not possible for this compound which appears to heavily favour G protein-dependent inhibition of cAMP (**Figure *2-3c***). GAT1666 displayed signaling bias towards cAMP inhibition ***(*Figure *2-3c***). GAT1665 did not display significant signaling bias although its potency and efficacy generally favored cAMP inhibition (**Figure *2-3***). GAT1667 did display signaling bias for the inhibition of cAMP as an agonist (**Figure *2-3***). As PAMs, GAT1664 and GAT1666 displayed no activity in the βarrestin2 recruitment assay and therefore calculations of ΔΔlogR are not possible (**Figure *2-3f***). GAT1665 and GAT1667 displayed signaling bias towards cAMP inhibition relative to βarrestin2 recruitment (**Figure *2-3f***). The parent compound GAT229 shares the same spatial orientation as GAT1665 and GAT1667 and is also a cAMP inhibition-biased PAM.[82] Therefore, these data confirm previous observations that this scaffold's spatial orientation promotes G protein-biased PAM activity and extends earlier reports to demonstrate increased potency and efficacy of fluorine-substituted ligands as compared to parent compounds.[82]

a.

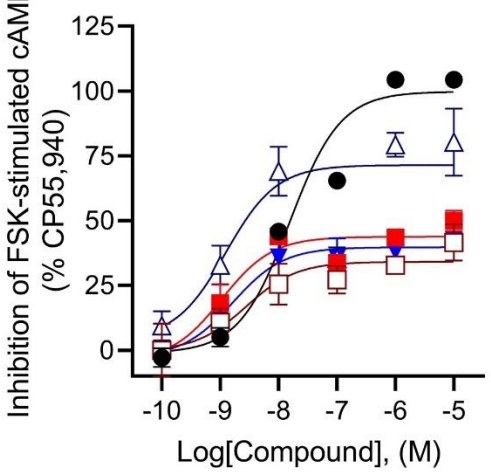

	EC_{50} (nM) 95% C.I.	E_{max} ± S.E.M.
CP55,940	15 (10 - 24)	100 ± 2.4
GAT1664	2.8 (0.11 - 12)	34 ± 4.5*
GAT1665	1.1 (0.15 - 6.5)*	44 ± 4.6*
GAT1666	1.3 (0.18 - 8.0)	71 ± 5.7
GAT1667	1.7 (0.13 - 14)	40 ± 4.6*

b.

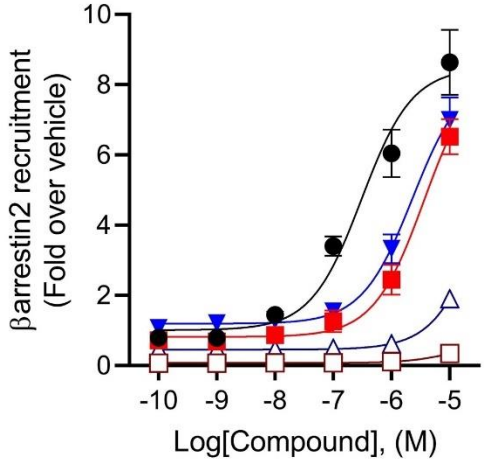

	EC_{50} (nM) 95% C.I.	E_{max} ± S.E.M.
CP55,940	310 (120 - 810)	8.5 ± 0.52
GAT1664	> 10,000	0.93 ± 0.37
GAT1665	> 10,000	6.5 ± 0.97
GAT1666	> 10,000	1.9 ± 0.03
GAT1667	> 10,000	7.0 ± 0.68

c.

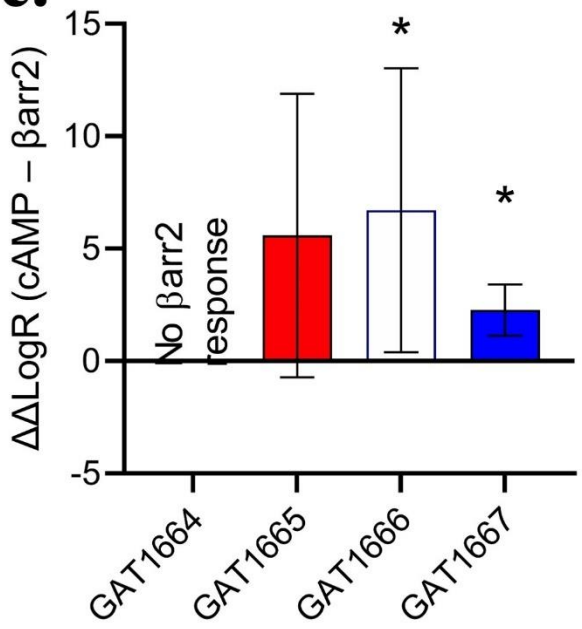

d.

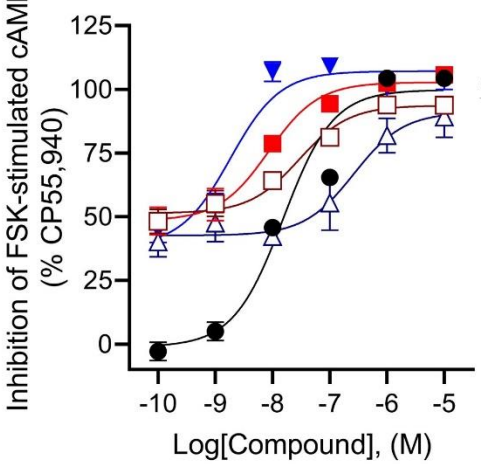

	EC_{50} (nM) 95% C.I.	E_{max} ± S.E.M.
CP55,940	15 (10 - 24)	100 ± 2.4
100 nM CP55,940 + Compound		
GAT1664	29 (12 - 70)	94 ± 2.3
GAT1665	8.6 (4.1 - 18)	102 ± 2.4
GAT1666	270 (59 - 350)*	91 ± 7.3
GAT1667	1.8 (1.1 - 3.0)*	107 ± 2.2

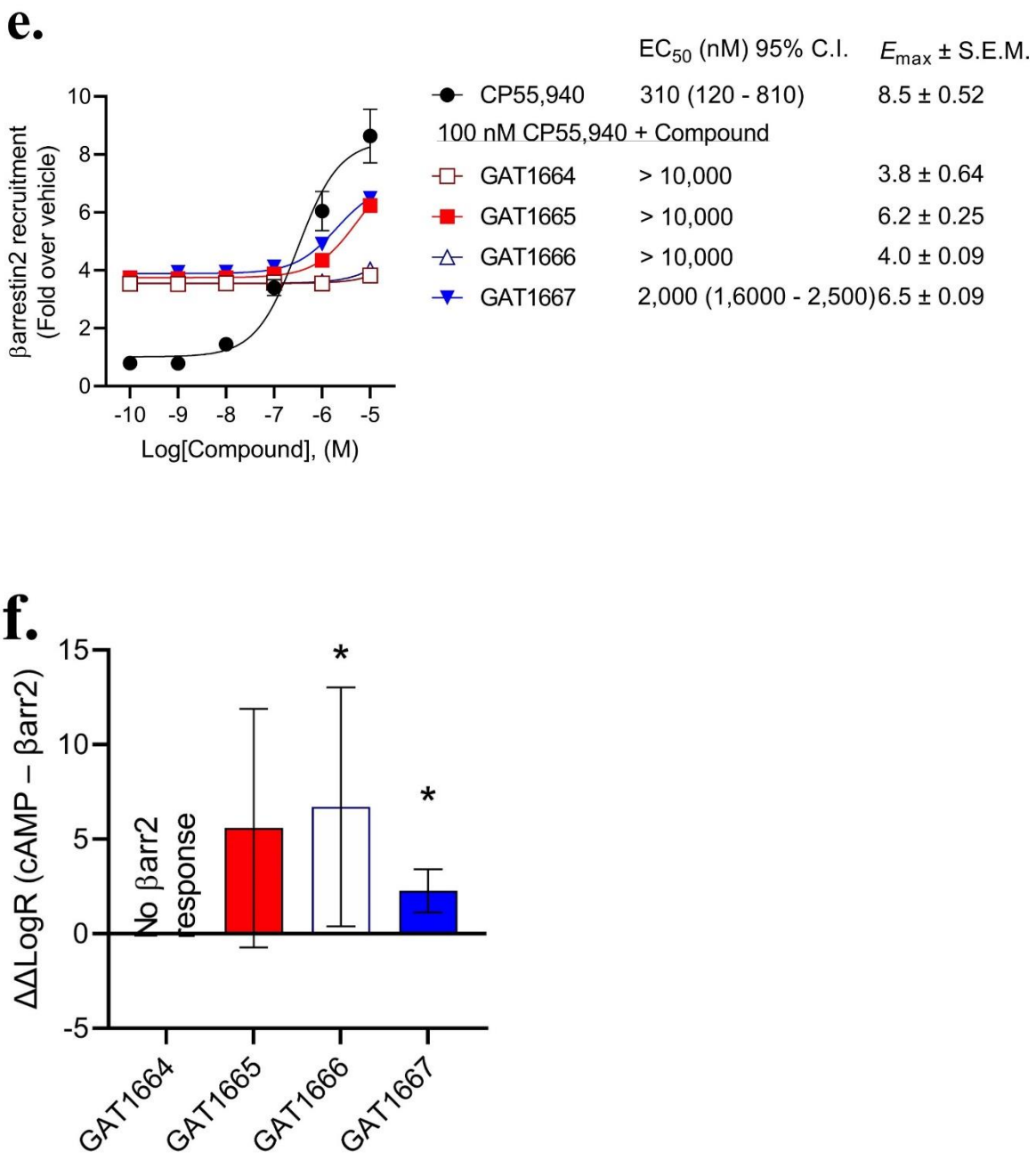

Figure 2-3. Assessment of GAT1664, GAT1665. GAT1666, and GAT1667 signaling. CB1R CHO-K1 were treated with 0.10 nM – 10 µM GAT compounds ± 100 nM CP55,940. (**a**) cAMP inhibition of GAT compounds as agonists, (**b**) βarrestin2 recruitment of GAT compounds as agonists, (**d**) cAMP inhibition of GAT compounds as PAMs in the presence of 100 nM CP55,940, and (**e**) βarrestin2 recruitment of GAT compounds as PAMs in the presence of 100 nM CP55,940. (**a,b,d,e**) cAMP inhibition and βarrestin2 recruitment data are expressed as % CP55,940 max. Data were fit to a nonlinear regression (4-parameter model, GraphPad v. 9.0) to determine EC_{50} and E_{max}. Data are mean ± SEM (E_{max}) or 95% CI (EC_{50}); n = 4 - 12 independent experiments

performed in triplicate. *p < 0.05 compared to CP55,940 as determined by one-way ANOVA followed by Bonferroni's post-hoc test or non-overlapping 95% CI. (**c,f**) Concentration-response data were fit to the operational model of Black and Leff (1983) (GraphPad v. 9.0). Data are mean with 95% CI. *p < 0.05 compared to 0 as determined by non-overlapping 95% CI; n = 4 - 6 (**c**) Agonist bias [ΔΔlogR (cAMP – βarrestin2)] between cAMP inhibition and βarrestin2 recruitment. (**f**) PAM bias [ΔΔlogR (cAMP – βarrestin2)] between cAMP inhibition and βarrestin2 recruitment.

In the previous set of experiments, we determined the agonist and PAM activity of compounds in the βarrestin2 recruitment assay was attributed to the *R*-enantiomers GAT1665 and GAT1667 while the *S*-enantiomers showed little (GAT1666) to no (GAT1664) agonist or PAM activity in the βarrestin2 recruitment assay. Due to this, we sought to understand whether these agonist effects could be reversed using the inverse agonist SR141716A. Co-treatment of CHO-K1 CB1R cells with 1 μM GAT1665 or GAT1667 and increasing concentrations of SR141716A resulted in an SR141716A concentration-dependent decrease in βarrestin2 recruitment (***Figure 2-4***). Therefore, the orthosteric inverse agonist SR141716A was able to prevent the agonist activity of the 2 putative allosteric ligands, suggesting an overlap in either the physical binding sites of these ligands or their functional interactions within the receptor or both.

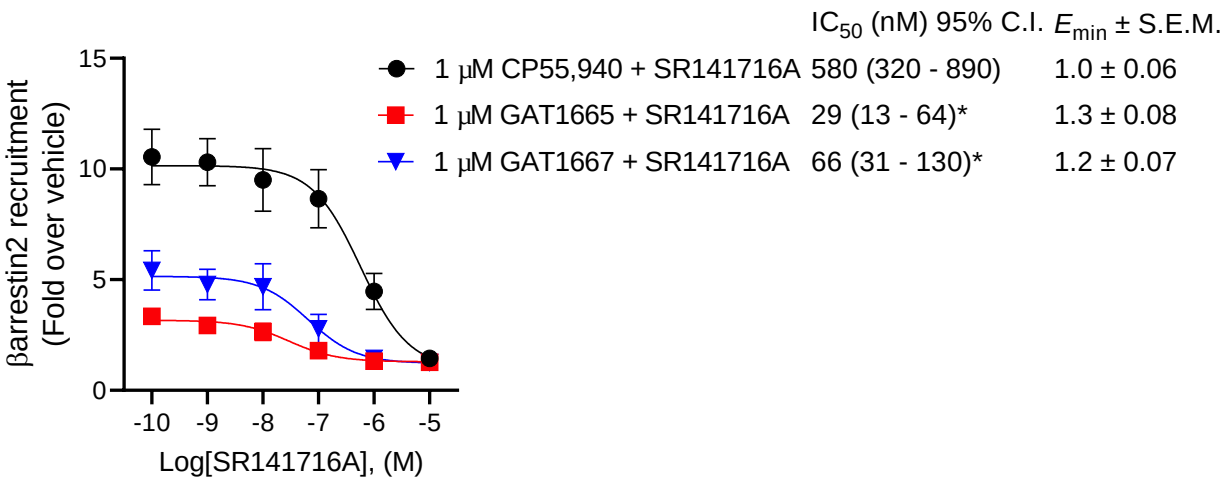

Figure 2-4. CB1R CHO-K1 cells were treated with 0.10 nM – 10 µM SR141716A + 1 µM CP55,940, GAT1665, or GAT1667. Data are expressed as fold over the vehicle. Data were fit to a nonlinear regression (4-parameter model, GraphPad v. 9.0) to determine EC_{50} and E_{max}. Data are mean ± SEM (E_{max}) or 95% CI (EC_{50}); n ≥ 6 independent experiments performed in triplicate. *p < 0.05 compared to CP55,940 as determined by one-way ANOVA followed by Bonferroni's post-hoc test or non-overlapping 95% CI.

Next, we sought to assess the ability of these compounds to modulate orthosteric agonist binding to CB1R. All enantiomers studied augmented [^{3}H]CP55,940 binding, consistent with their proposed PAM activity, with the *R*-enantiomers GAT1665 and to a greater extent GAT1667 increasing [^{3}H]CP55,940 binding (***Figure 2-5***). GAT1667 displayed the highest affinity among the enantiomers tested (K_D = 28 [15 – 52] nM). Enantiomers were also tested for their ability to promote G protein coupling in the GTPγS assay (***Figure 2-5b,c***). All of the enantiomers tested increased G protein coupling alone (i.e. in the absence of the orthosteric agonist CP55,940) with the *R*-enantiomers GAT1665 and GAT1667 being more potent than the *S*-enantiomers and GAT1667 in particular displaying the greatest potency (EC_{50} = 8.0 [3.4 – 17] nM) (***Figure 2-5b***). GAT1666 displayed a lower efficacy than other compounds tested (***Figure 2-5b***). When 1 μM of each enantiomer was tested in the presence of CP55,940 each enantiomer augmented G protein coupling in the presence of 1 and 10 nM, consistent with positive allosteric modulation (***Figure 2-5c***). The stimulatory activity of these enantiomers at 1 μM ablated the concentration-response curve for these experiments; however no difference in maximum effect was observed. Consistent with earlier observations, GAT1667 produced the largest increase in G protein coupling among the enantiomers tested here (***Figure 2-5c***). Therefore, all enantiomers tested were able to enhance CP55,940 binding and stimulate G protein coupling alone or in the presence of CP55,940, which is consistent with their activity as ago-PAMs. Between the enantiomers tested, GAT1667 consistently displayed the greatest potency and efficacy.

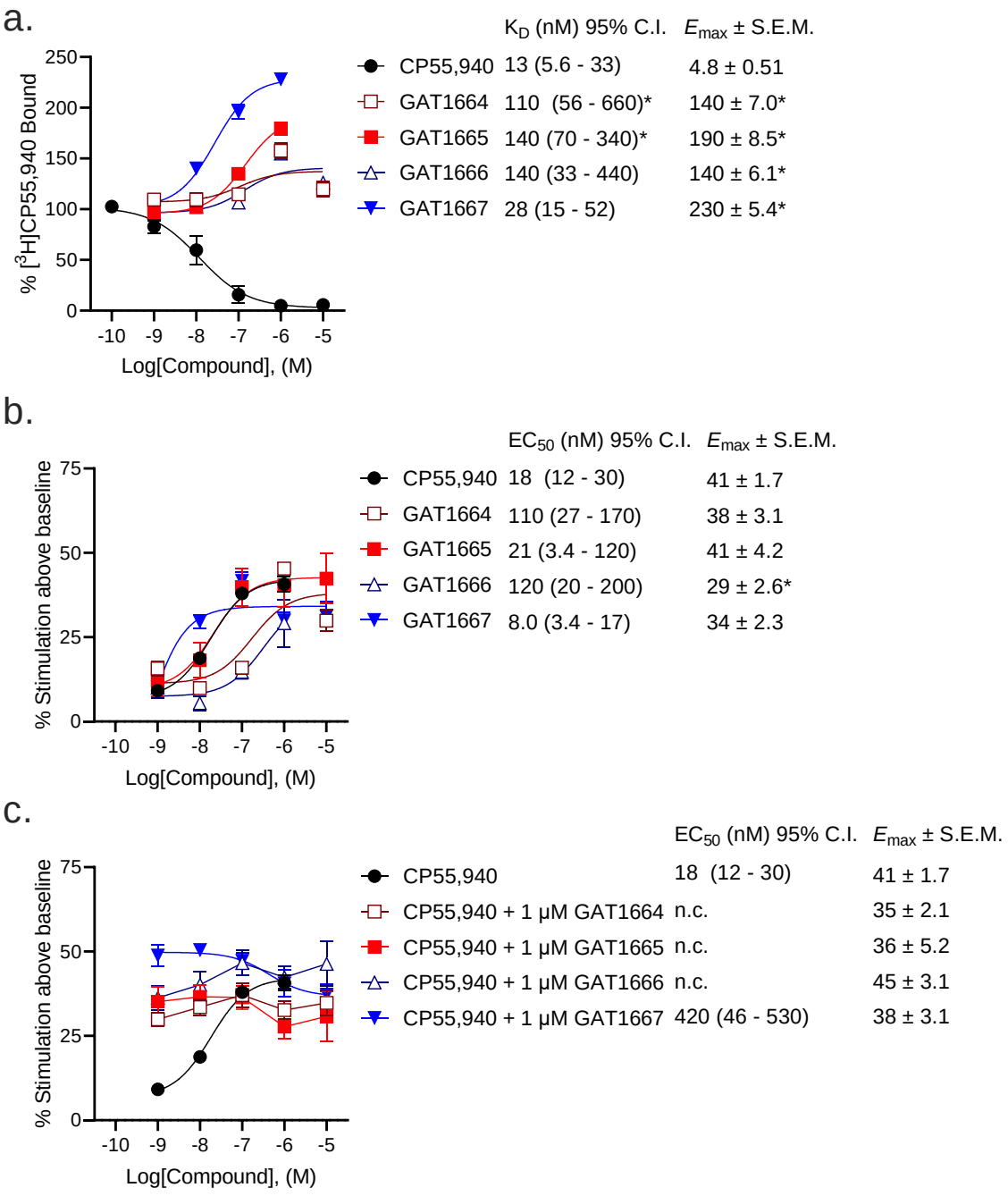

Figure 2-5. (a) Radioligand binding of 1 nM [^{3}H]CP55,940 and (b,c) G protein binding of [^{35}S]GTPgS to membranes from CB1R CHO-K1 cells. CB1R CHO-K1 cells were treated with 0.10 nM – 10 µM compounds in the presence 1 nM [^{3}H]CP55,940 (**a**) or 1.0 nM [^{35}S]GTPγS (**b**). Data are expressed as % radioligand bound (**a**) or % stimulation above baseline (i.e. vehicle) levels (**b,c**). Data were fit to a nonlinear regression (4-parameter model, GraphPad v. 9.0) to determine K_D, EC_{50}, and E_{max}. Data are mean ± SEM (E_{max}) or 95% CI (K_D, EC_{50}); n ≥ 6 independent experiments. *p < 0.05 compared to CP55,940 as determined by one-way ANOVA followed by Bonferroni's post-hoc test or non-overlapping 95% CI.

2.3.3 *In vivo* evaluation

All enantiomers were evaluated in male C57BL/6 mice using a triad of outcomes consisting of catalepsy, body temperature, and nociception. Previous studies have shown that the racemic GAT591 and GAT593 did not produce catalepsy or hypothermia at 0.1, 1, 3, or 10 mg/kg (i.p.) compared to vehicle [95]. Both GAT591 and GAT593 however did produce a dose-dependent anti-nociceptive effect in the tail flick assay that was significant relative to vehicle at 3 and 10 mg/kg.[95] In this study we evaluated all separated optically pure enantiomers in a triad assay. When tested alone, GAT1664, GAT1665, GAT1666 and GAT1667 did not produce catalepsy, hypothermia, or anti-nociceptive effects at 0.1, 1, 3, or 10 mg/kg i.p. compared to vehicle (***Figure 2-6a-c***). We also tested these enantiomers as PAMs by co-administering a sub-threshold dose of 1 mg/kg THC with each GAT compound. It was found that GAT1665 and GAT1667 displayed significant cataleptic, hypothermic, and anti-nociceptive effects at 3 and 10 mg/kg i.p. compared to vehicle (***Figure 2-6d-f***). Therefore, GAT1664, GAT1665, GAT1666, and GAT1667 do not alter physiology in normal, otherwise healthy adult mice as agonists, but GAT1665 and GAT1667 are able to augment THC's effects as PAMs when administered once. For comparison, the racemic parent compounds, GAT591 and GAT593, do dispaly nociception *in vivo*.[95,82]

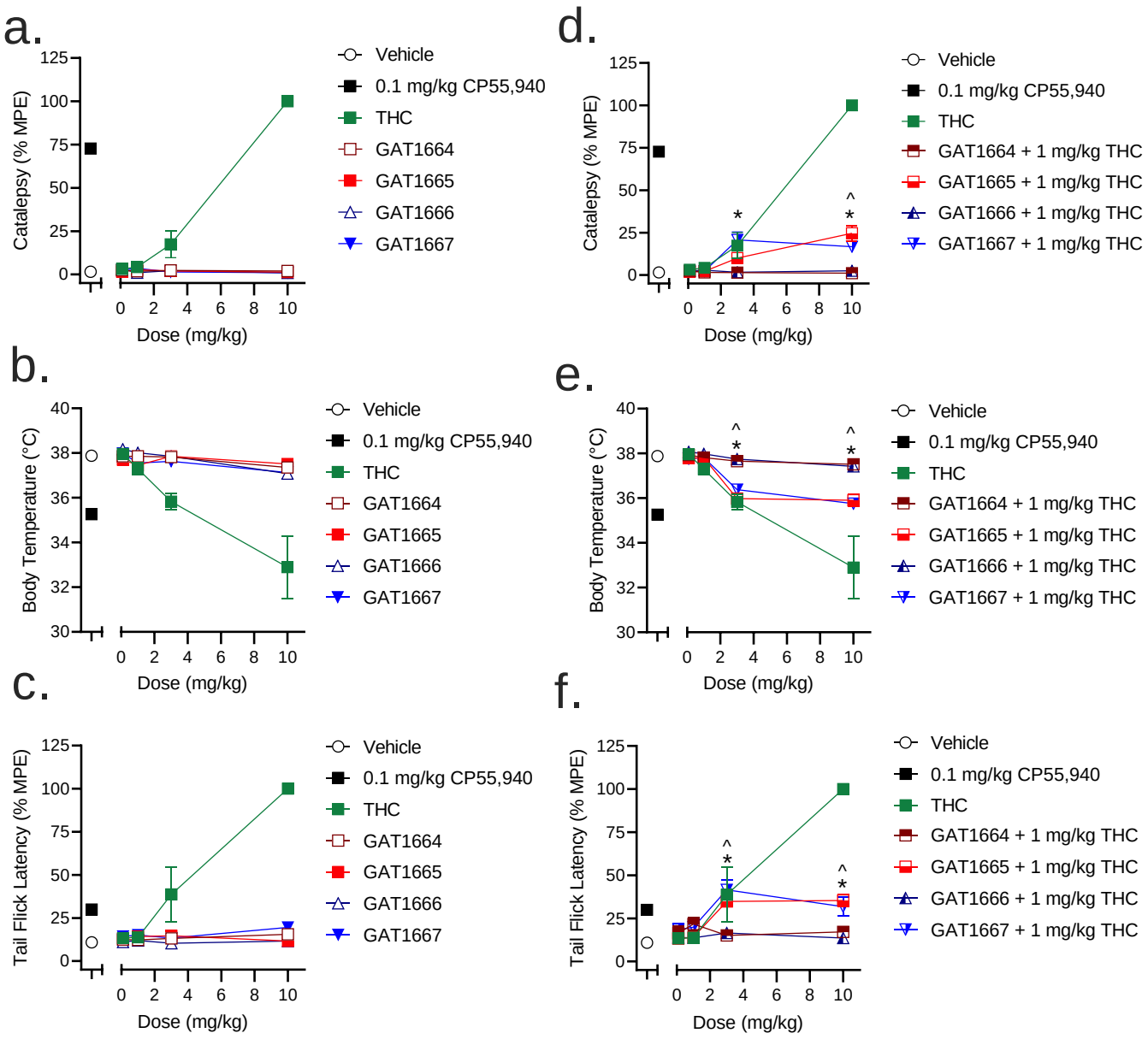

Figure 2-6. *In vivo* effects of GAT1664, GAT1665, GAT1666 and GAT1667 in male C57BL/6 mice. C57BL/6 mice were administered compounds either alone (**a**,**b**,**c**) or co-administered with 1 mg/kg THC (**d**,**e**,**f**) to assess catalepsy, hypothermia and nociception. Doses used were 0.1 – 10 mg/kg compound or volume-matched vehicle control (1:1:18 ethanol/cremaphor/saline) and assessment of catalepsy (% MPE 60 sec) **(a)**, body temperature (**b)**, and nociception in the tail flick assay (% MPE 20 sec) (**c)** were performed; n = 5-6/group; data are mean ± SEM. ^p < 0.05 for GAT1665 compared to vehicle; *p < 0.05 for GAT1667 compared to vehicle as determined by two-way ANOVA followed by Bonferroni's post-hoc test.

2.3.4 In silico studies

Compounds were docked to a modelled structure of CB1R to determine their putative binding sites within the receptor. GAT1664 and GAT1666 bound to an allosteric site on CB1R proximal to the intracellular face of the receptor in tan (***Figure 2-7***). An H-bond exists between the indole hydrogen in white and the nitrogen atom in blue (H – N distance 1.96 Å) on $H154^{2.41}$ (***Figure 2-7a***). One of the fluorobenzyl groups on GAT has a face-to-face π-π interaction with $F237^{4.46}$ (4.03Å) while the other fluorobenzyl has a T-shaped π-π interaction with each ring on $W241^{4.50}$ (4.96Å to the 6 – membered ring; 5.09Å to the 5 – membered ring) (***Figure 2-8***). Upon binding to CB1R the conformation of the *ortho*-fluorobenzyl substituent on GAT1664 rotates 90°. The conformational cost for this rotation is 2.35 kcal/mol (***Table 2-1***). GAT1666 has the same binding pose, thus the binding energy was measured to look at the relative affinity. GAT1666 is more stable than GAT1664 by 2.31 kcal/mol (ΔG GAT1666 - ΔG GAT1664) which suggests that it has a higher affinity to the allosteric site of CB1R shown in tan (***Figure 2-7***). This can be attributed to changing the fluorine on the 6^{th} position of the indole (GAT1664) to the 7^{th} position on the indole (GAT1666). The binding of a compound to this site may allow it to act as an agonist by promoting the X1 = g+ → trans conformation of residue F4.46, facilitating breaking of the R3.50/D6.30 ionic lock which has been shown to activate CB1R (***Figure 2-7*** and ***Figure 2-8***).[83]

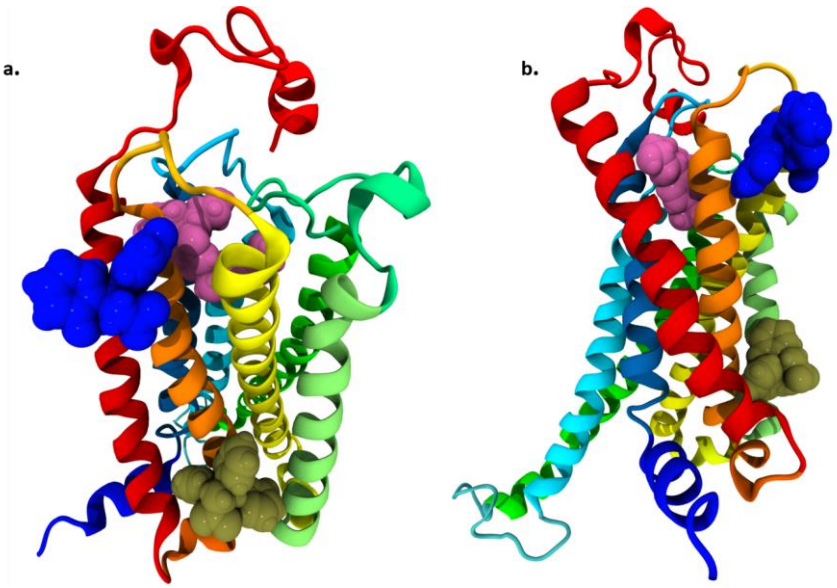

Figure 2-7. CB1R with three different binding sites shown. In these views of CB1R the orthosteric site is shown in magenta, an identified PAM site in blue, and another identified ago-PAM site in tan. Transmembrane helices are: I red, II orange, III yellow, IV light green, V green, VI cyan, and VII blue. (**a**) is a visualization of CB1R looking down on the extracellular surface. (**b**) is a visualization of CB1R looking across at the transmembrane domains.

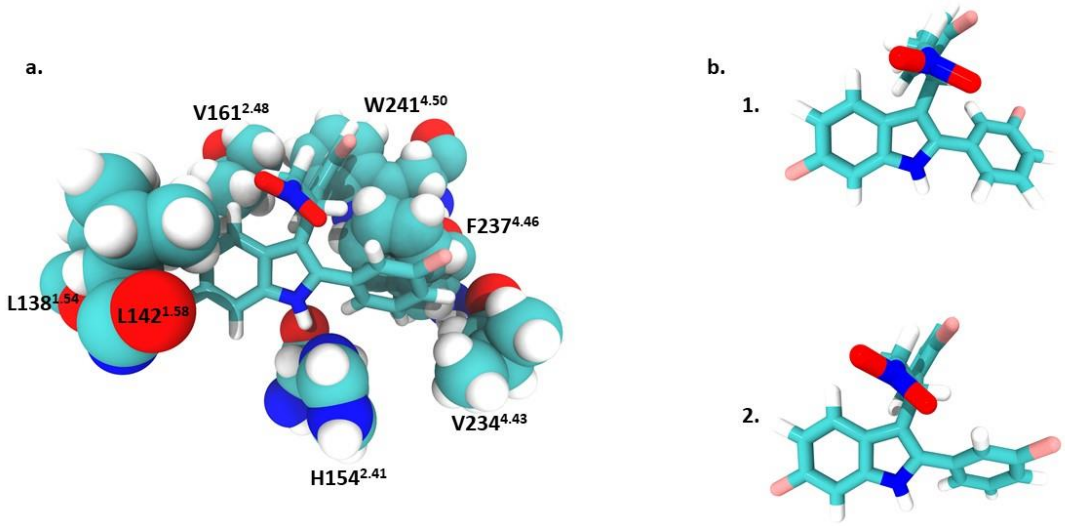

Figure 2-8. GAT1664 binds to an allosteric agonist site. (**a**) Main interactions between GAT1664 and the amino acid residues in the binding pocket. The conformation of GAT1664 (**b1**) before it binds to CB1R and then the conformation of GAT1664 (**b2**) after it binds to CB1R.

Table 2-1. The conformational cost of GAT compounds is displayed as well as the relative affinity represented by binding energy.

Compound	Conformational cost (kcal/mol)	ΔG (kcal/mol)
GAT1664	2.35	-69.68
GAT1665	3.27	-60.77
GAT1666	2.48	-71.99
GAT1667	3.60	-64.55

GAT1665 and GAT1667 bind to a distinct allosteric site on CB1R relative to GAT1664 and GAT1666 (***Figure 2-7*** and ***Figure 2-9***). The NO_2 group on GAT1665 has a H-bond between 1 of the oxygens shown in red and a hydrogen atom on $Y172^{2.59}$ (O – H distance 2.17Å) (***Figure 2-9***). Another H-bond exists between the indole hydrogen in white and an oxygen atom in red on $D176^{2.63}$ (H – O distance 2.29Å) (***Figure 2-9***). A cation-π interaction exists between $R182^{ECL1}$ and each ring on the indole on GAT1665 (six – membered ring centroid on indole to NH_2^+ on $R182^{ECL1}$ distance 3.59Å; five – membered ring centroid on indole to NH_2^+ on $R182^{ECL1}$ distance 3.66Å) (***Figure 2-9***). One of the fluorobenzyl groups on GAT has a face-to-face π-π interaction with $Y172^{2.59}$ (4.05Å) (***Figure 2-9***). Upon binding to CB1R the conformation of the NO_2 rotates in order to H-bond with $Y172^{2.59}$ (***Table 2-1***). The conformational cost for this rotation is 3.27 kcal/mol. If we compare the binding energy of GAT1665 and GAT1667 it is apparent that GAT1667 is more stable than GAT1665 bound to the PAM site by 4.78 kcal/mol (ΔG GAT1667 - ΔG GAT1665). This can be attributed to changing the fluorine on the 6^{th} position of the indole (GAT1665) to the 7^{th} position on the indole (GAT1667). The previously characterized compound GAT229 also binds to this site and lacks intrinsic activity thus both these compounds alone can not induce the active state of CB1R and thus are PAMs. The *R*-enantiomers (GAT1665 and

GAT1667) undergo a smaller conformational cost than the *S*-enantiomers (GAT1664 and GAT1666) upon binding to their respective sites on CB1R (***Table 2-1***). The *R*-enantiomers (GAT1665 and GAT1667) bind to the ago-PAM site (ΔG = -60.77 and -64.55 kcal/mol) significantly weaker than the *S*-enantiomers (GAT1664 and GAT1666) bind to the PAM site (-69.68 and 71.99 kcal/mol).

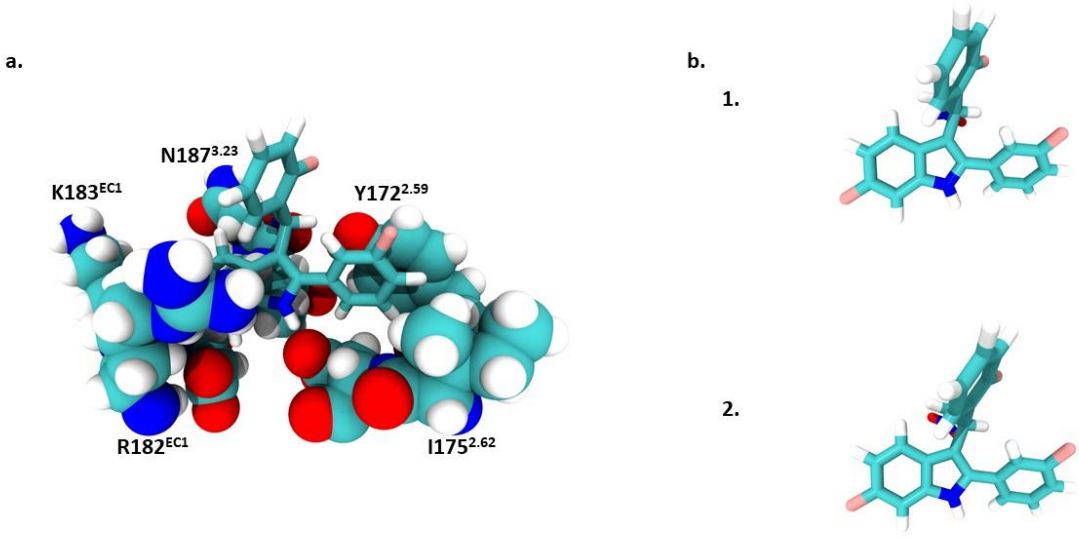

Figure 2-9. **GAT1665 binds to the PAM site in blue (Fig. 6).** (**a**) Main interactions between GAT1665 and the amino acid residues in the binding pocket. (**b**) The conformation of GAT1665 (**b1**) it binds to CB1R and then the conformation of GAT1665 (**b2**) after it binds to CB1R.

2.4 Conclusion

In summary, the purified enantiomers of GAT591 and GAT593 displayed unique pharmacology. The purified enantiomers GAT1664, GAT1665, GAT1666, and GAT1667 bound to CB1R in the low nM range and were shown to enhance binding of [^{3}H]CP55,940 at CB1R. Enhancing the binding of an orthosteric ligand is a characteristic of a PAM and these observations are consistent with all compounds operating in part via positive allostery.[39]

In addition to this, we demonstrated that these enantiomers activate CB1R-dependent inhibition of cAMP and βarrestin2 recruitment. All of the GAT compounds tested here did inhibit cAMP accumulation either as agonists or PAMs, with GAT1665 and GAT1667 displaying the greatest potency and efficacy as CB1R PAMs in the presence of 100 nM CP55,940. In the βarrestin2 assay GAT1665 and GAT1667 (*R*-enantiomers) acted as ago-PAM's while GAT1664 and GAT1666 (*S*-enantiomers) showed little to no activity as either an agonist or PAM. In the G protein coupling assay the *R*-enantiomers GAT1665 and GAT1667 also showed higher potency and efficacy than *S*-enantiomers as agonists and PAMs. As for the *in vivo* studies, no compounds tested produced catalepsy, hypothermia or antinociceptive effects at 0.1, 1, 3 or 10 mg/kg i.p. compared to vehicle as agonists, but GAT1665 and GAT1667 did potentiate the effects of THC as PAMs. These data are congruent with previous observations that CB1R ago-PAMs are inactive or minimally active *in vivo* in wild-type, otherwise healthy animals under non-pathological and acute conditions.[77] *In silico* studies revealed that GAT1664 and GAT1666 preferentially bind to a putative allosteric agonist site of CB1R near the intracellular face of the receptor between transmembrane helices I and IV; while GAT1665 and GAT1667 preferentially bind to a putative PAM site of CB1R on the extracellular receptor surface. Enantiomers may display low affinity to multiple allosteric sites, accounting for the allosteric agonist activity of GAT1665 and GAT1667. Collectively, these data

support retained, potent, G protein-biased, ago-PAM enantiomeric-specific activity at CB1R for the GAT211 ligand scaffold and demonstrate enhanced potency and efficacy of these ligands relative to the parent compound.[95,82] The absolute orientation of GAT1665 and GAT1667 is maintained relative to the previously-characterized CB1R PAM GAT229.[98] Moreover, recent data from the racemic mixtures of these enantiomers indicates fluorine addition improves both metabolic stability and blood brain barrier penetrance; with GAT593 – and therefore GAT1667 – being superior to GAT591.[95] Therefore, studies are now underway to assess the *in vivo* efficacy of GAT1667 in the contexts of absence epilepsy and pain during both acute and chronic treatment paradigms.

2.5 Supplementary Info

2.5.1 NMR Data

(+)-(*S)*-6-Fluoro-2-(3-fluorophenyl)-3-(1-(2-fluorophenyl)-2-nitroethyl)-1*H*-indole (GAT1664): ^{1}H NMR (400 MHz, DMSO-d_6): δ 11.66 (bs, 1H), 7.77 (dd, *J*= 5.3, 8.8 Hz, 1H), 7.67−7.57 (m, 2H), 7.39−7.25 (m, 4H), 7.18−7.89 (m, 3H), 6.85 (t, *J*= 8.7 Hz, 1H,), 5.59-5.53 (m, 2H), 5.43 (d, *J*= 8.4 Hz, 1H).; $[\alpha]_D^{24}$ = +70.80 (c 1 g/100 mL, MeOH); MS-ESI (*m/z*) 397 $[M + H]^+$.

(-)-(*R)*-6-Fluoro-2-(3-fluorophenyl)-3-(1-(2-fluorophenyl)-2-nitroethyl)-1*H*-indole (GAT1665): ^{1}H NMR (400 MHz, DMSO-d_6): δ 11.66 (bs, 1H), 7.77 (dd, *J*= 5.3, 8.8 Hz, 1H), 7.67−7.57 (m, 2H), 7.39−7.25 (m, 4H), 7.18−7.89 (m, 3H), 6.85 (t, *J*= 8.7 Hz, 1H,), 5.59-5.53 (m, 2H), 5.43 (d, *J*= 8.4 Hz, 1H).; $[\alpha]_D^{24}$ = -87.85 (c 1 g/100 mL, MeOH) ; MS-ESI (*m/z*) 397 $[M + H]^+$.

(+)-(*S)*-7-Fluoro-2-(3-fluorophenyl)-3-(1-(2-fluorophenyl)-2-nitroethyl)-1H-indole (GAT1666): ^{1}H NMR (400 MHz, DMSO-d_6): δ 11.96 (bs, 1H), 7.67-7.57 (m, 3H), 7.41−7.25 (m, 4H), 7.18−6.98 (m, 2H), 6.96 (d, *J*= 8.0 Hz, 1H,), 5.61-5.49 (m, 2H), 5.393 (t, *J*= 8.4 Hz, 1H).; $[\alpha]_D^{24}$ = +24.80 (c 1 g/100 mL, MeOH); MS-ESI (*m/z*) 397 $[M + H]^+$.

(-)-(*R)*-7-Fluoro-2-(3-fluorophenyl)-3-(1-(2-fluorophenyl)-2-nitroethyl)-1H-indole (GAT1667): ^{1}H NMR (400 MHz, DMSO-d_6): δ 11.96 (bs, 1H), 7.67-7.57 (m, 3H), 7.41−7.25 (m, 4H), 7.18−6.98 (m, 2H), 6.96 (d, *J*= 8.0 Hz, 1H,), 5.61-5.49 (m, 2H), 5.393 (t, *J*= 8.4 Hz, 1H).; $[\alpha]_D^{24}$ = -75.86 (c 1 g/100 mL, MeOH); MS-ESI (*m/z*) 397 $[M + H]^+$.

Elution	Injection
FlowRate : 3 ml/min	Column Name : Lux C4
Co-Solvent : 40%	Sample Name : LD7 : GAT591-Fraction-1-B551834
Co-Solvent Name : Methanol	Injected Volume : 2 µl
Outlet Pressure: 100 bar	Temperature : 35 °C

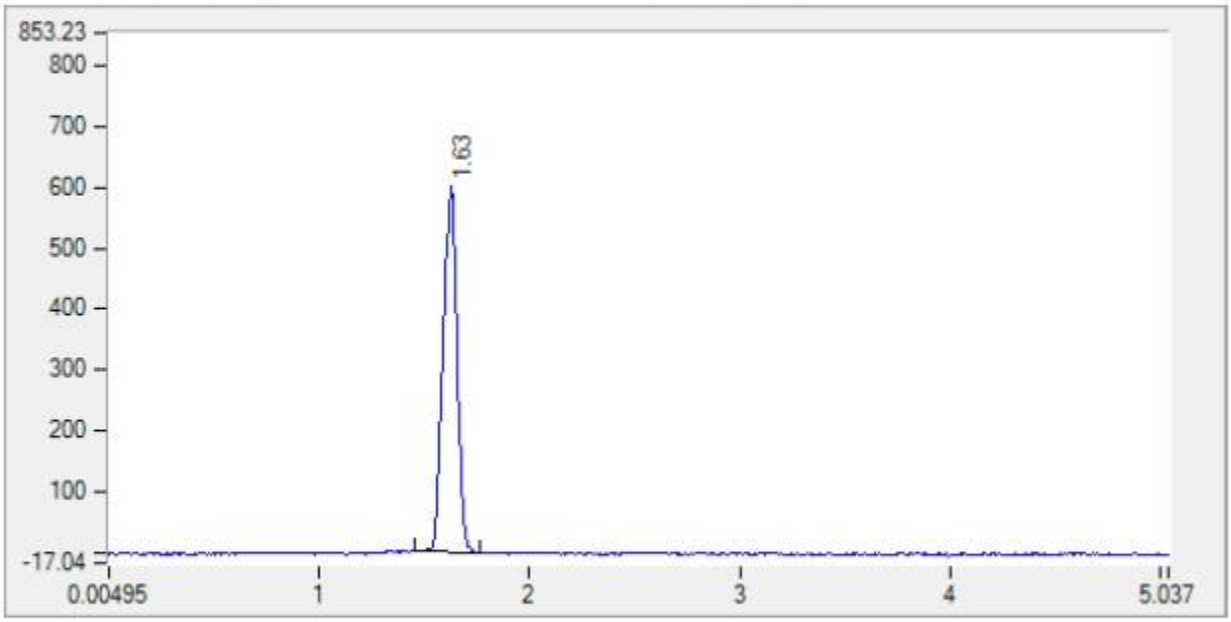

Results UV1

Sr.No.	RT	Area	Area %
1	1.63	2855.929	100.000

Figure 2-10. Preparative HPLC chromatogram for (+)-GAT1664

Elution	Injection
FlowRate : 3 ml/min	Column Name : Lux C4
Co-Solvent : 40%	Sample Name : LD8 : GAT591-Fraction-2-B551841
Co-Solvent Name : Methanol	Injected Volume : 2 µl
Outlet Pressure: 100 bar	Temperature : 35 °C

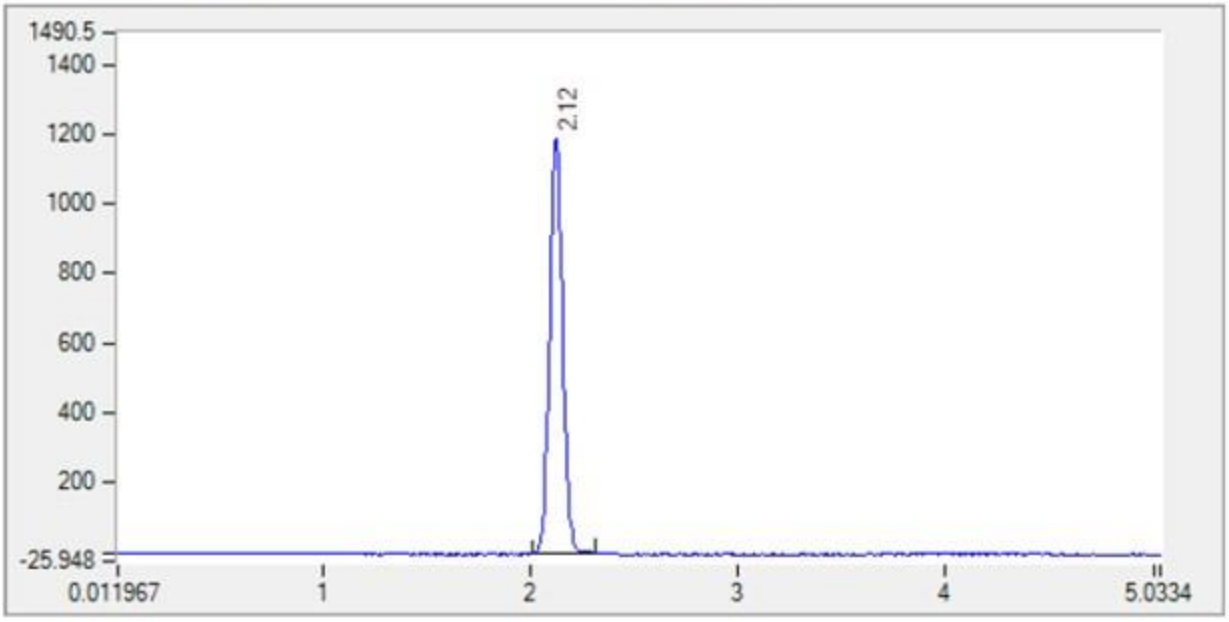

Results UV1			
Sr.No.	RT	Area	Area %
1	2.12	5164.687	100.000

Figure 2-11. Preparative HPLC chromatogram for (-)-GAT1665

Elution	Injection
FlowRate : 3 ml/min	Column Name : Lux C4
Co-Solvent : 40%	Sample Name : LE1 : GAT593-Fraction-1-B551844
Co-Solvent Name : Methanol	Injected Volume : 2 µl
Outlet Pressure: 100 bar	Temperature : 35 °C

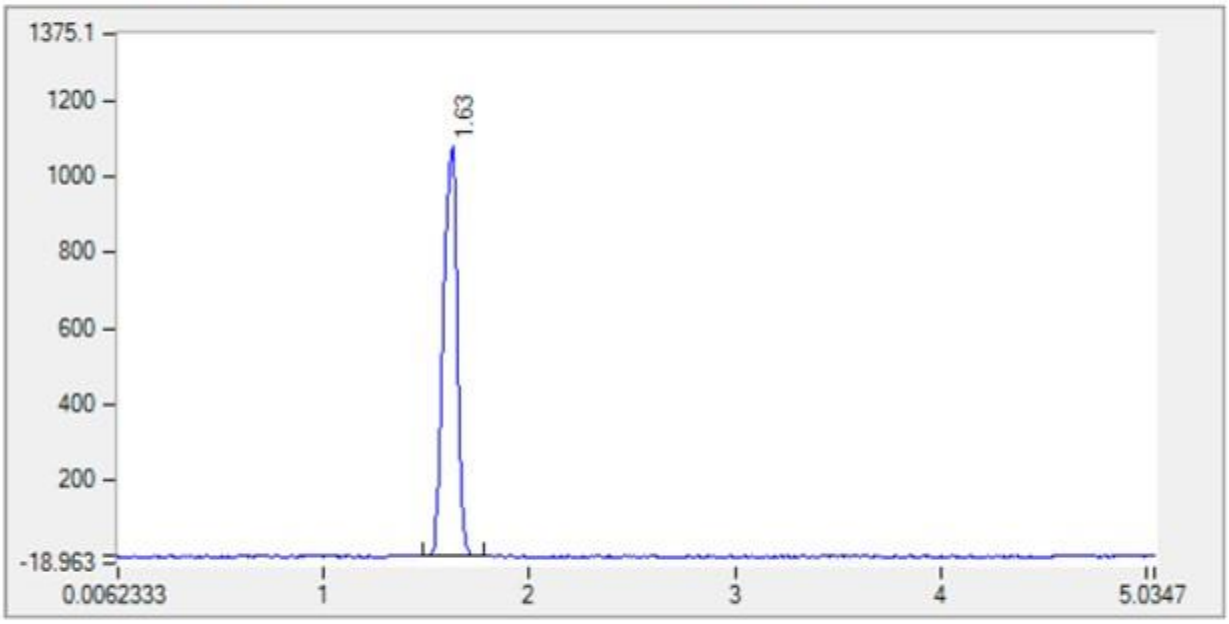

Results UV1

Sr.No.	RT	Area	Area %
1	1.63	4955.462	100.000

Figure 2-12. Preparative HPLC chromatogram for (+)-GAT1666

Elution	Injection
FlowRate : 3 ml/min	Column Name : Lux C4
Co-Solvent : 40%	Sample Name : LE2 : GAT593-Fraction-2-B551846
Co-Solvent Name : Methanol	Injected Volume : 2 µl
Outlet Pressure: 100 bar	Temperature : 35 °C

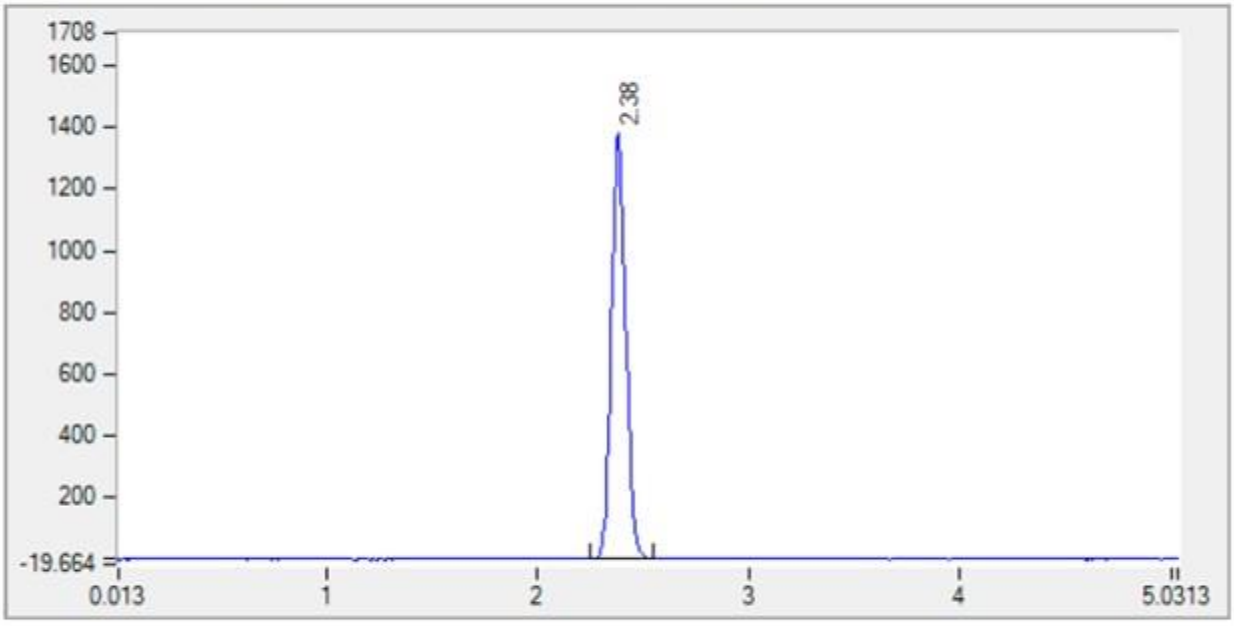

Results UV1

Sr.No.	RT	Area	Area %
1	2.38	6604.798	100.000

Figure 2-13. Preparative HPLC chromatogram for (-)-GAT1667

CHAPTER 3

In Silico Evaluation of Halogenated Bioisosteres at the Type 1 Cannabinoid Receptor Allosteric Agonist Site

Copyright statement

This chapter is in review for publication. The manuscript has been modified to meet formatting requirements.

Contribution statement

The manuscript used as the basis for this chapter was written with guidance from Dr. Robert B. Laprairie. *In silico* data were collected and analyzed by myself with technical assistance from Dr. Robert B. Laprairie, Dr. Christopher P. Phenix and Dr. Jane Alcorn.

3.1 Introduction

The type 1 cannabinoid receptor (CB1R) is a class A G protein-couped receptor (GPCR). GPCRs are the target of approximately 35% of approved drugs because they regulate numerous, diverse, physiological processes and have druggable sites that are accessible at the cell surface.[65] Specifically, CB1R has 3 identified ligand binding sites: (1) the orthosteric site where the endogenous ligands 2-arachidonoylglycerol (2-AG) and anandamide (AEA) bind; (2) an allosteric site located between transmembrane helix 2 (TMH2) and extracellular loop 1 (ECL1) where positive allosteric modulators (PAMs) such as GAT229 bind; and (3) an allosteric agonist-PAM (i.e. ago-PAM) site on the intracellular surface of the receptor between TMSs 1, 2, and 4 where compounds such as GAT228 bind (***Figure 1-5***).[83,114] Although CB1R orthosteric ligands have been used as tool compounds in understanding the function of CB1R, their use as therapeutics remains limited due to on-target interference with constitutive physiological signaling and resultant neurological effects.[115] In contrast to orthosteric ligands, allosteric ligands of CB1R are now being studied as a means of modulating CB1R signaling without the potential therapeutic limitations of tolerance, dependence, or intoxication.[116,117] True PAMs do not have an intrinsic agonist activity; instead, they modulate activity through a conformational shape change of the orthosteric binding pocket which alters the GPCRs signaling output.[118] Ago-PAMs *do* possess intrinsic agonist activity as they can activate GPCR signaling in the absence of an orthosteric ligand.[119] The ability of such compounds to act as agonists may be due to them occupying several binding sites in the absence of a bound agonist.[120] Using ago-PAMs with intrinsic activity may be attractive for treating diseases whose etiology involves decline or loss of endogenous neurotransmitters because such compounds augment the activity of the endogenous system, without producing tolerance or dependence effects, as we have seen previously in rodent models of pain.[82,116.117] We have

previously demonstrated that fluorinated and methyl-substituted derivatives of the ago-PAM GAT228 display efficacy in rodent models of pain and glaucoma.[96,108,82,116,117,120] Although these probe compounds display nanomolar potency, their limited solubility in aqueous environments (GAT228 cLogP 5.04) and metabolic stability (GAT228 human microsomal CL_{int} 81.2 µL/min/mg protein, $t_{1/2}$ 28.4 min) make them poor drug candidates.[121]

With several CB1R crystal structures now available, *in silico* modelling is an attractive means of drug discovery and optimization.[48] The advantage of running *in silico* modelling before synthesis and *in vitro* and *in vivo* experiments is to enable the rational design of improved ligands expected to bind to the desired site on the protein target. Moreover, *in silico* modeling allows for the rapid substitution of known sub-groups and testing to streamline subsequent syntheses. Quick and efficient program scripts are now widely available to conduct such studies with glide ligand docking through Maestro.[102] Such docking studies are referred to as Molecular Mechanics-Generalized Born Surface Area (MMGBSA) in silico studies.[122] Not only can the script dock a large library of ligands, but it also can dock hundreds of poses of each ligand and report ligand-receptor binding poses according to their estimated lowest energy conformers. Once the best pose has been selected, the ligand/receptor complex can undergo a minimization to capture the whole system (i.e., ligand bound to receptor) in its lowest energy state. One can further use the MMGBSA script to compare the relative binding affinity of a library of compounds. It is hoped that the advent and widespread use of these workflow will allow for rational drug design that is low cost and efficient. In the present study, we explored the generation and evaluation of bioisosteres for the GAT228 scaffold. Candidates with various bioisosteres were docked to the ago-PAM site of CB1R to determine what ligand substitutions were tolerated with respect to affinity at the CB1R ago-PAM site. From these studies we were able to identify 4 potential leads with improved drug-like

properties and CB1R ago-PAM affinity in silico compared to the parent compound, GAT228. These novel lead compounds with improved drug-like properties can now be synthesized and tested in rodent models of pain, glaucoma, and other neurodegenerative diseases where earlier derivatives demonstrated efficacy.

3.2 Materials and Methods

3.2.1 *In Silico* receptor preparation

Docking studies were conducted using the agonist bound human CB1R crystal structures PDB: 6N4B[51] and 5XR8.[48] Both 6N4B and 5XR8 are modified CB1R. 6N4B is a 3.0 Å structure of full-length CB1R having N-terminal FLAG and C-terminal hexahistidine tags in complex with human heterotrimeric Giβ1γ2.[51] 5XR8 is a 2.95 Å resolution structure truncated at amino acids 1-98, 307-331, and 415-472 with a flavodoxin insert at intracellular loop 3 (IC3).[48] Protein modelling before docking was done with SWISS-MODEL for which the UniProt ID: P215541 (CNR1_Human) was used along with PDB 6N4B[51] to build a model receptor. This receptor was then prepared in Maestro (v. 12.2) using that program's protein preparation wizard.[102] During preparation, the ionization of the protein structure was optimized using PROPKA at pH 7.0; and the space-filling of the protein structure and ligands were optimized minimized using OPLS-3e force field.[102] Amino acid position is described throughout this study according to the numbering convention of Ballesteros and Weinstein (***Figure 1-4***).[123]

3.2.2 Ligand Preparation

All compounds screened in this study were generated via bioisosteric replacement in Maestro (v. 12.2) using GAT228 as a template. Tautomer's were generated for each ligand and the dominant ionization state of acidic and basic functional groups were used assuming pH 7.0.

3.2.3 Receptor grid generation and molecular docking

The grid box for receptor-ligand interaction was defined by selecting the residues (R148, H2.41, F2.42, F4.46 and W4.50) that interact with GAT228 at the ago-PAM exosite (IC TMH1-2-4).[83] Standard precision docking was used with enhanced conformational sampling for each ligand to ensure an exhaustive search. [102] Compounds that did not have a dual H-bond with R148 and an H-bond with H2.41 as shown by glide scores were not considered and deleted because these interactions are thought to be critical to ago-PAM activity.[120,51] Energies of the remaining ligand-receptor complexes were minimized using Prime in the Schrödinger suite of programs[102] and the lipid membrane was set to a thickness of 31.2Å, as recommended and described for other class A GPCRs.[124] This minimization is necessary for further evaluation because although the ligand is docked with enhanced conformational sampling the receptor is fixed. Molecular mechanics generalized Borne surface area (MMGBSA) was used in Prime to predict the relative binding affinity of each ligand in CB1R.[114,116] MMGBSA uses 3 input files to calculate the binding free energy (ΔG_{bind}); ligand-receptor complex (E_{compex}), the free protein ($E_{protein}$) and the free ligand (E_{ligand}) where ΔG is calculated via the following equation:[125]

$$\Delta G_{bind} = E_{complex}\ (\text{minimized}) - [E_{ligand}\ (\text{minimized}) + E_{receptor}\ (\text{minimized})] \qquad \textbf{Eq. 3-1}$$

3.2.4 Physicochemical and Pharmacokinetic Properties Prediction

Table 3-1. Physicochemical and Pharmacokinetic Properties modeled in this study

Property or Descriptor	Description	Range or recommended values
Mol. WT.	Molecular weight of the molecule	130.0 – 725.0
QPlogBB	Predicted brain/blood barrier partition coefficient. Note: QikProp predictions are for orally delivered drugs.	-3 – 1.2
Donor HB	Estimated number of hydrogen bonds that would be donated by the solute to water molecules in an aqueous solution. Values are averages taken over a number of configurations so they can be a non-integer.	0.0 – 6.0
Acceptor HB	Estimated number of hydrogen bonds that would be accepted by the solute from water molecules in an aqueous solution. Values are averages taken over a number of configurations, so they ca be non-integer.	2.0 – 20.0
QPlog o/w	Predicted octanol/water coefficient	-2.0 – 6.5
Rule of Five	Number of violations of Lipinski's rule of five. The rules are mol_MW < 500, QPlog o/w < 5, donor HB ≤ 5, acceptor HB ≤ 10. Compounds that satisfy these rules are considered drug-like.	Maximum is 4
% Human Oral Absorption	Predicted human oral absorption on 0 to 100% scale. The prediction is based on a quantitative multiple linear regression model.	>80% is high. <25% is poor

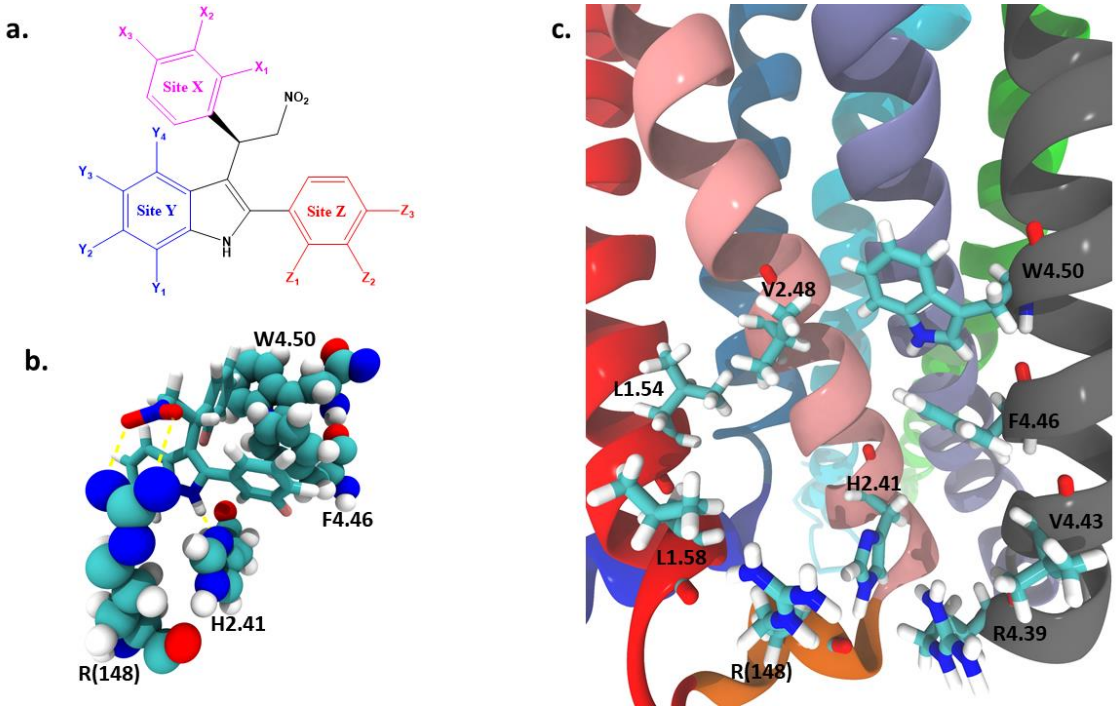

Figure 3-1. (a) The GAT228 scaffold has 3 sites represented by site X site Y and site Z. While sites X and Z have 3 positions that can be halogenated, site Y has 4 which gives a total of 36 isomers for each halogen. (b) The GAT228 scaffold has a dual H-bond with R(148), H-bond with H1.54 and an aromatic stack with both W4.50 and F4.46. In this representation the residues are displayed in their Van der Waal radii representation. (c) The GAT228 scaffold binds to the ago-PAM site of CB1R and interacts with residues on TMH1, 2 and 4.

3.3 Results and Discussion

3.3.1 GAT228 Isomers Effect on MMGBSA (ΔG)

In the first part of the study, we evaluated the effect of a halogen substitutions on each position of X, Y, and Z on the GAT228 scaffold (***Figure 3-1a***). Because position Y has 4 possible substitutions for a halogen whereas positions X and Z have 3, due to sigma bond rotation of the phenyl ring, we evaluated 36 constitutional isomers for each halogen totaling 144 unique ligands. The rationale for studying all 4 halogens (fluorine, chlorine, bromine, and iodine) was to determine the effects that both bond length and atomic radius have on relative binding affinity. In addition, halogen substitution on the aromatic rings – primarily with fluorine or chlorine – was expected to alter the electron density and affect π-π stacking interactions between ligand and receptor aromatic rings. Given that GAT228 is comprised of unmodified phenyl rings and has been experimentally shown to bind to the ago-PAM site with high affinity, this compound was used as a control providing a benchmark ΔG value for comparison that was calculated to be -65.24 kcal/mol (***Figure 3-2***). Previous *in vitro* studies have shown that 2 GAT228 derivatives that each have 3 fluorine substitutions – GAT1665 and GAT1667 – both bind to and activate CB1R, but interestingly a significant increase in ΔG was only observed for GAT1667 (ΔG GAT1667 = -70.88 kcal/mol) when compared to GAT228, but not GAT1665 (ΔG GAT1665 = -65.74 kcal/mol) (***Figure 3-2***).[95] For 20/36 fluorinated analogs, ΔG was less than -65.24 kcal/mol indicating a greater relative binding affinity at CB1R. Four fluorine analogs displayed a ΔG less than -70.00 kcal/mol. When all 36 fluorine isomers were docked, 16/36 did not meet the requirement of a dual H-bond with R148 and an H-bond with H2.41 and thus were not considered (***Figure 3-2***).[83] For the remaining 20 ligands that did dock correctly, a significant increase in relative binding affinity was observed as shown by a lower ΔG. To further evaluate how much space is available to accommodate larger

substituents on each ring inside the CB1R ago-PAM site, 36 brominated analogs were docked. Eighteen of 36 ligands did not dock to the CB1R ago-PAM site, and for the remaining 18 ligands that did bind the ΔG was greater than that of the chlorinated analogs indicating a decrease in binding affinity. This suggests that the chlorinated analogs display the greatest relative binding affinity. Lastly, 36 of the iodinated analogs were docked to the CB1R ago-PAM site and 27/36 ligands did not dock to the targeted ago-PAM site. The remaining 9 ligands showed weaker relative binding affinity than the brominated analogs. Overall, this suggests that to optimize relative binding affinity the aromatic rings within the GAT228 scaffold are best-substituted with chlorine atoms to minimize the binding energy between CB1R and the ligand within the modelingCB1R ago-PAM site.

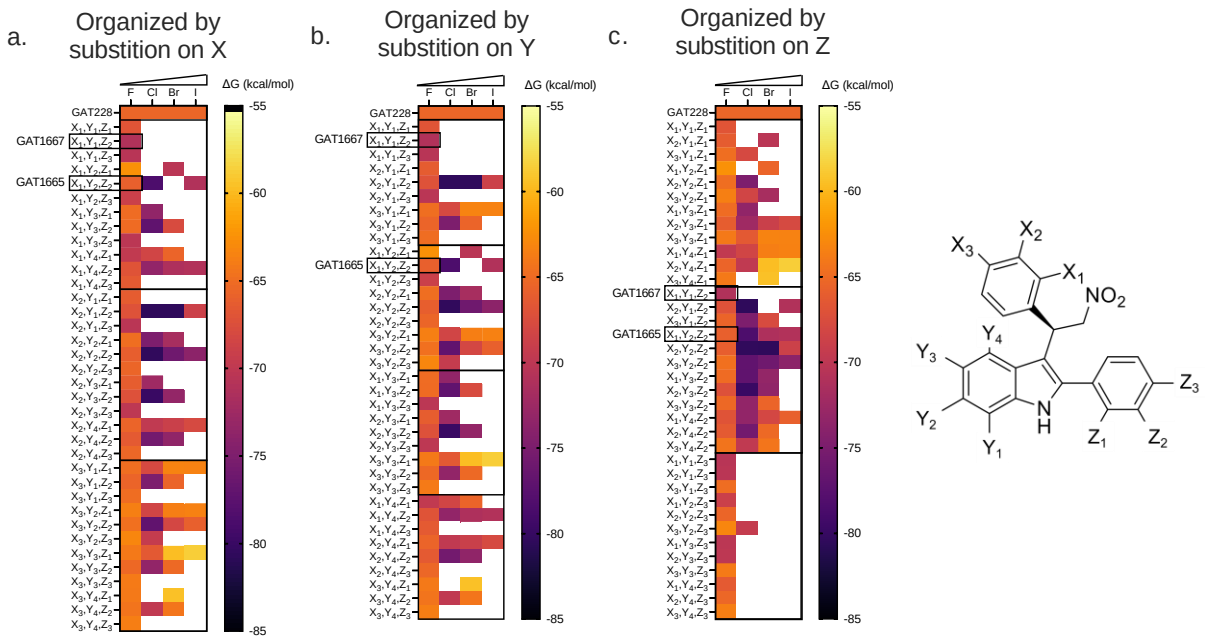

Figure 3-2. The MMGBSA values were plotted in GraphPad Prism (v.9.1.1) and displayed as a heatmap. The heat map spans from -55 kcal/mol (light yellow) to -85 kcal/mol (dark purple). Because there are 3 sites that underwent substitution each graph contains identical data that are re-organized by each site to show how each site is affected by specific substitutions of a H with a halogen atom. Areas on the graphs that are white represent compounds that did not have a dual H-bond with R148 and an H-bond with H2.41 (***Figure 3-1b***).

Upon further examination of the CB1R ago-PAM site it was observed that an arginine residue R(4.39) lies near near site Y of the GAT228 scaffold. Since arginine is an H-bond donor and is near site Y of the GAT228 scaffold, we hypothesized that the introduction of a H-bond acceptor placed at the correct position of site Y could lead to a new H-bond and increase the relative binding affinity (***Figure 3-1b***). To evaluate this design strategy, a nitro group (NO_2) was placed on positions 1, 2, or 3 of site Y and docked to the ago-PAM site of CB1R.[126,127] Interestingly, analogs with the NO_2 group at positions 1 and 3 did not form this H-bond with R4.39 presumably because the NO_2 group was too far away. In contrast, those derivatives with NO_2 at position 2 formed a dual H-bond with R4.39. While the control compound GAT228 had a ΔG of -65.24 kcal/mol, the NO_2 derivative at position 2 of site Y had a ΔG of -71.70 kcal/mol, which is likely attributable to the NO_2 group. Eight fluorinated analogs of the NO_2 derivative were also docked to the ago-PAM site of CB1R with 6/8 showing greater relative binding affinity than GAT228 or the NO_2-substituted GAT228 analog (***Figure 3-3***). This same approach was executed for 8 of the chlorinated analogs and only 3 docked to the CB1R ago-PAM site; with 2 analogs having increased binding affinity over the fluorinated analogs (***Figure 3-3***). The addition of the dual H-bond with R4.39 slightly changes the binding pose in such a way that when chlorines are added little room is available in the binding pocket, which leads to unfavorable steric clashing. We then created a series of 8 NO_2-fluorinated or -chlorinated compounds on site X and Z. It was observed that a combination of fluorine and chlorine increased ΔG relative to GAT228 but performed worse than the fluorine substitution. Overall, in this set of compounds studied fluorine substitution performed the best when a NO_2 group was placed on position 2 of site Y.

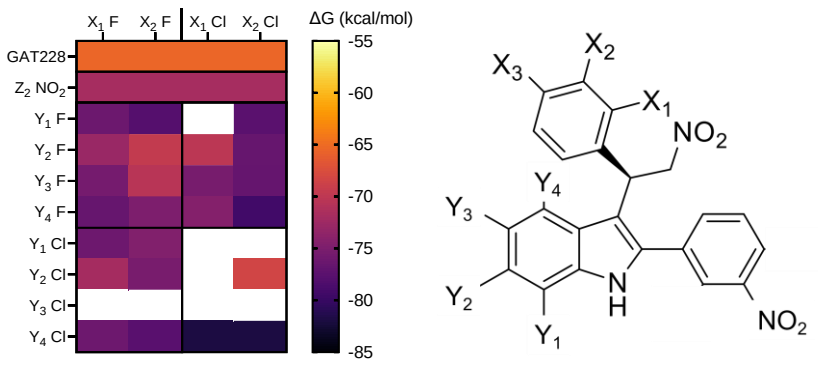

Figure 3-3. MMGBSA values were plotted using GraphPad Prism (v.9.1.1) and displayed as a heatmap. The heat map spans from -55 kcal/mol (light yellow) to -85 kcal/mol (dark purple). For this series of ligands Z_2 was set as a NO_2 to form the H-bond with R4.39 while sites X and Y were set to evaluate different derivatives bearing fluorine and chlorine. Blank spots are representative of compound that did not dock in the correct pose (***Figure 3-1*b**).

We then looked at the effects of replacing the ring at site X with a series of pyridine derivatives. It was found that the optimal position for the nitrogen in the pyridine ring was para to the R substituent (***Figure 3-4*****a**), which was 2.25 kcal/mol more stable than the fluorinated GAT228 control (GAT1665). Placing the nitrogen at any other position within the ring led to reduced binding affinity compared to the control compound. This was further tested with a series of pyrimidine derivatives. Although the 1,2 and 4,5 analogs bound to the site with higher affinity, all performed worse than the control, GAT1665. The phenyl ring at site X was also changed to several other 5 membered thiazole and thiophene rings (***Figure 3-4*****b)**. The compounds of this class that performed the best were the thiazole substituted compounds where 2/3 of them showed higher relative binding affinity than the control. This systematic approach was also applied to site Y. All but 1 of the pyridine derivatives at this site performed worse than the control whereas for the pyrimidine derivatives 4/6 performed better than the control. Substitution of site Z with thiophene **(*Figure 3-4*c**) was well tolerated but performed worse than the control. Overall, this suggest that changing site X or Z to a heterocyclic functional group does not seem to cause drastic changes to relative binding affinity.

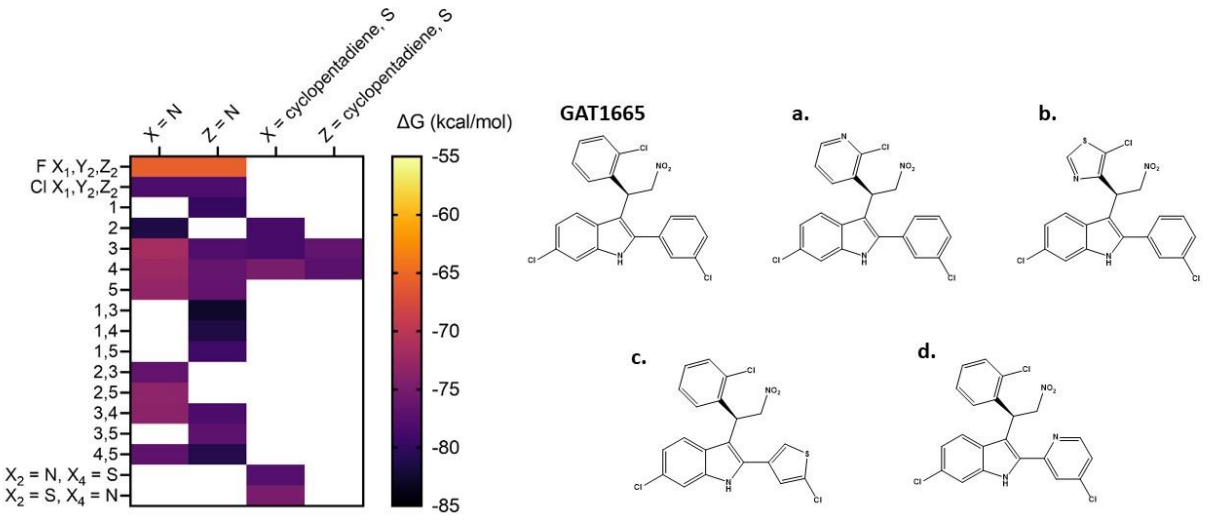

Figure 3-4. MMGBSA values were plotted in GraphPad Prism (v.9.1.1) and displayed as a heatmap. The heat map spans from -55 kcal/mol (light yellow) to -85 kcal/mol (dark purple). For this series of ligands, calculations were performed on a series of both pyridine and cyclopentadiene derivatives.

3.3.2 GAT228 Isomers Differ in their Physicochemical and Pharmacokinetic Properties

Although MMGBSA is a validated tool for predicting the relative binding affinity of a ligand/receptor complex, these measurements are representative of the pharmacodynamics of the ligand only. In order to further evaluate each analog to assist in identifying potential therapeutic candidates, we predicted the PK properties of each ligand using the QikProp module in Maestro. For the halogenated GAT228 compounds, each analog broke at least 1 of Lipinski's rules having an *n*-octanol-water partition coefficient (K_{OW}) > 5. (***Table 3-2*** – ***Table 3-7***). However, 11 compounds from ***Table 3-6*** and 4 compounds from ***Table 3-7*** display a $K_{ow} < 5$ thus making these more attractive candidates as lead compounds. Select compounds also had a molecular weight > 500 Da. From this perspective the fluorinated and chlorinated derivatives were better candidates that could potentially be used as a drug-like molecules compared to the brominated and iodinated derivatives. Notably, all fluorinated and chlorinated analogs are predicted to have 100% oral absorption whereas the brominated and iodinated derivatives do not. Because the structures of the halogenated derivatives are quite similar, the number of H-bond acceptors is 2 and donors are 1. As discussed above, the H-bond donor is the hydrogen on the indole while the H-bond acceptors are the 2 oxygens on the NO_2 group. For all the halogenated GAT228 derivatives, the predicted blood/brain barrier partition coefficient (QPlogBB) fell within the reference range. For ligands in ***Table 3-6*** NO_2 substitution at site Z reduces the bioavailability of ligands in ***Table 3-2*** and ***Table 3-3*** by approximately 12%. For the last set of compounds where the ring at site X or Z was replaced with pyridine and cyclopentadiene rings all but 4 of the compounds broke 1 Lipinski rule being QPlog o/w but were still within the recommended range. All of these 25 compounds except for 2 displayed human oral absorption greater than 80% (***Table 3-7***)

3.3.3 Selecting Lead Compounds

A lead compound in this case should display greater relative binding affinity than GAT228, break none of Lipinski's rules and be able to cross the blood-brain barrier. In terms of the blood-brain barrier metric (QPlogBB) larger negative values are indicative of limited accessibility into the blood brain barrier by passive diffusion and will likely become concentrated in the periphery.[128] Even though the compounds in ***Table 3-6*** 6 are still within the accepted range of QPlogBB, the added NO_2 group limits their ability to cross the blood-brain barrier via passive diffusion thus these compounds would not be considered lead candidates. The fluorinated, chlorinated, brominated, and iodinated compounds in ***Table 3-2*** – ***Table 3-5*** break at least one of Lipinsk'si rules and these compounds can be disregarded. Of the fluorinated and chlorinated compounds in ***Table 3-2*** and ***Table 3-3***, 3 disobey QPlog o/w rules, the brominated and iodinated compounds in ***Table 3-4*** and ***Table 3-5*** break the molecular mass rule (i.e. mass > 500 kDa). With all of these factors considered, only 4 compounds from ***Table 3-7*** satisfy all criteria and are considered lead candidates ***(Figure 5***). While GAT228 breaks one of Lipinski's rules, compounds '**a'** – '**d**' do not. All of these compounds have a significantly better MMGBSA than GAT228. Overall compound C shows the greatest promise as it theoretically crosses the blood-brain barrier better than GAT228 when the QPlogBB values are compared. However, in an *in vivo* or *in vitro* setting these slight differences might be negligible and or non-translatable and thus future *in vitro* assessment of compounds '**a'** – '**d**' would test the reliability of these modeling softwares and their utility in the advancement of novel CB1R ligands.

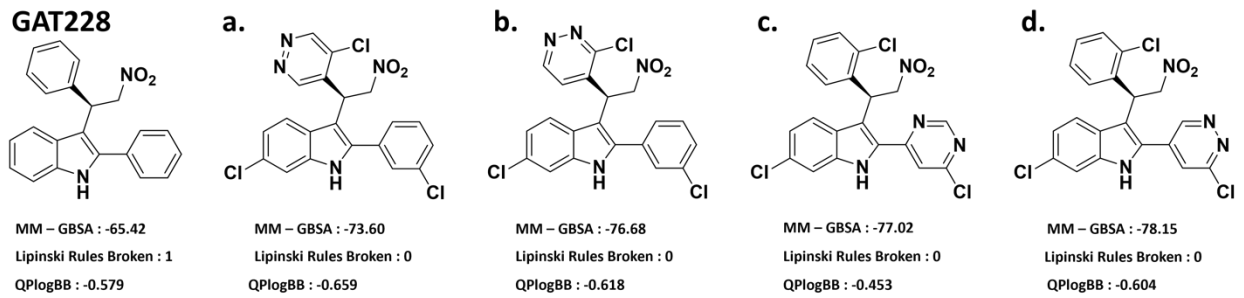

Figure 3-5. Four lead compounds were selected of the 202 compounds analyzed based on modeled MMGBSA and PK data.

3.4 Conclusion

Herein, we report the use of computational methods to identify lead compounds, based on derivatives of the GAT scaffold, predicted to bind to the CB1R ago-PAM site as potential drug candidates. This was achieved by combining MMGBSA calculations to identify compounds that have greater relative affinity towards CB1R than GAT228 along with predictions of physicochemical and PK parameters. In general, we determined that the addition of chlorine atoms onto the phenyl rings as well as introduction of a pyridine ring into the GAT228 scaffold led to improved binding affinity. Subsequent studies are required to synthetize the lead compounds identified here followed by experiments, *in vitro* and *in vivo*, to determine their potency, efficacy and PK properties. Ultimately it is hoped that the technologies incorporated into the present study can be implemented to expedite CB1R drug discovery specifically – and GPCR drug discovery generally – while also avoiding costly *in vitro* experimentation and unnecessary animal usage for *in vivo* studies.

3.5 Supplementary Info

Table 3-2. ADME analysis of Fluorinated Substituted GAT228 Compounds

Compound	Mol. WT.	QPlogBB	Donor HB	Accept HB	QPlog o/w	Rule Of Five	% Human Oral Absorption	MM-GBSA (kkal/mol)
Reference	130 – 725	-3.0 – 1.2	0 – 6.0	2.0 – 20.0	-2.0 – 6.5	4 is Max	>80% is high	n/a
GAT228	342.396	-0.579	1	2	5.215	1	100	-65.24
X_1 =F, Y_1 = F, Z_1 = F	396.368	-0.331	1.000	2.000	5.453	1	100.000	-66.73
X_1 =F, Y_1 = F, Z_2 = F	396.368	-0.288	1.000	2.000	5.605	1	100.000	-70.88
X_1 =F, Y_1 = F, Z_3 = F	396.368	-0.286	1.000	2.000	5.609	1	100.000	-70.29
X_2 =F, Y_1 = F, Z_1 = F	396.368	-0.252	1.000	2.000	5.654	1	100.000	-66.06
X_2 =F, Y_1 = F, Z_2 = F	396.368	-0.238	1.000	2.000	5.682	1	100.000	-66.99
X_2 =F, Y_1 = F, Z_3 = F	396.368	-0.141	1.000	2.000	5.769	1	100.000	-70.09
X_3 =F, Y_1 = F, Z_1 = F	396.368	-0.253	1.000	2.000	5.652	1	100.000	-64.65
X_3 =F, Y_1 = F, Z_2 = F	396.368	-0.244	1.000	2.000	5.693	1	100.000	-65.43
X_3 =F, Y_1 = F, Z_3 = F	396.368	-0.245	1.000	2.000	5.692	1	100.000	-64.75
X_1 =F, Y_2 = F, Z_1 = F	396.368	-0.306	1.000	2.000	5.551	1	100.000	-66.27
X_1 =F, Y_2 = F, Z_2 = F	396.368	-0.321	1.000	2.000	5.584	1	100.000	-65.74
X_1 =F, Y_2 = F, Z_3 = F	396.368	-0.307	1.000	2.000	5.578	1	100.000	-68.77
X_2 =F, Y_2 = F, Z_1 = F	396.368	-0.268	1.000	2.000	5.65	1	100.000	-64.69
X_2 =F, Y_2 = F, Z_2 = F	396.368	-0.262	1.000	2.000	5.686	1	100.000	-65.86
X_2 =F, Y_2 = F, Z_3 = F	396.368	-0.261	1.000	2.000	5.667	1	100.000	-65.34
X_3 =F, Y_2 = F, Z_1 = F	396.368	-0.276	1.000	2.000	5.589	1	100.000	-63.44
X_3 =F, Y_2 = F, Z_2 = F	396.368	-0.26	1.000	2.000	5.67	1	100.000	-64.48
X_3 =F, Y_2 = F, Z_3 = F	396.368	-0.27	1.000	2.000	5.769	1	100.000	-62.95
X_1 =F, Y_3 = F, Z_1 = F	396.368	-0.313	1.000	2.000	5.57	1	100.000	-64.78
X_1 =F, Y_3 = F, Z_2 = F	396.368	-0.326	1.000	2.000	5.597	1	100.000	-64.85
X_1 =F, Y_3 = F, Z_3 = F	396.368	-0.301	1.000	2.000	5.584	1	100.000	-70.01

X_2 =F, Y_3 = F, Z_1 = F	396.368	-0.177	1.000	2.000	5.656	1	100.000	-66.05
X_2 =F, Y_3 = F, Z_2 = F	396.368	-0.259	1.000	2.000	5.682	1	100.000	-67.01
X_2 =F, Y_3 = F, Z_3 = F	396.368	-0.274	1.000	2.000	5.704	1	100.000	-69.91
X_3 =F, Y_3 = F, Z_1 = F	396.368	-0.218	1.000	2.000	5.641	1	100.000	-63.92
X_3 =F, Y_3 = F, Z_2 = F	396.368	-0.249	1.000	2.000	5.649	1	100.000	-65.06
X_3 =F, Y_3 = F, Z_3 = F	396.368	-0.261	1.000	2.000	5.693	1	100.000	-63.79
X_1 =F, Y_4 = F, Z_1 = F	396.368	-0.349	1.000	2.000	5.283	1	100.000	-69.50
X_1 =F, Y_4 = F, Z_2 = F	396.368	-0.33	1.000	2.000	5.429	1	100.000	-66.79
X_1 =F, Y_4 = F, Z_3 = F	396.368	-0.324	1.000	2.000	5.407	1	100.000	-66.28
X_2 =F, Y_4 = F, Z_1 = F	396.368	-0.457	1.000	2.000	5.998	1	100.000	-65.38
X_2 =F, Y_4 = F, Z_2 = F	396.368	-0.353	1.000	2.000	5.699	1	100.000	-66.29
X_2 =F, Y_4 = F, Z_3 = F	396.368	-0.361	1.000	2.000	5.667	1	100.000	-65.22
X_3 =F, Y_4 = F, Z_1 = F	396.368	-0.354	1.000	2.000	5.631	1	100.000	-63.84
X_3 =F, Y_4 = F, Z_2 = F	396.368	-0.328	1.000	2.000	5.541	1	100.000	-64.25
X_3 =F, Y_4 = F, Z_3 = F	396.368	-0.334	1.000	2.000	5.553	1	100.000	-63.49

Table 3-3. ADME analysis of Chlorinated Substituted GAT228 Compounds

Compound	Mol. WT.	QPlogBB	Donor HB	Accept HB	QPlog o/w	Rule of five	% Human Oral Abosorptio	MM-GBSA (kkal/mol)
Reference	130 – 725	-3.0 – 1.2	0 – 6.0	2.0 – 20.0	-2.0 – 6.5	4 is Max	>80% is high	n/a
GAT228	342.396	-0.579	1	2	5.215	1	100	-65.24
X_1 = Cl, Y_1 = Cl, Z_1 = Cl	445.732	-0.134	1	2	6.297	1	100	
X_1 = Cl, Y_1 = Cl, Z_2 = Cl	445.732	-0.091	1	2	6.368	1	100	
X_1 = Cl, Y_1 = Cl, Z_3 = Cl	445.732	-0.079	1	2	6.355	1	100	
X_2 = Cl, Y_1 = Cl, Z_1 = Cl	445.732	-0.075	1	2	6.439	1	100	
X_2 = Cl, Y_1 = Cl, Z_2 = Cl	445.732	-0.06	1	2	6.449	1	100	-80.31
X_2 = Cl, Y_1 = Cl, Z_3 = Cl	445.732	-0.071	1	2	6.41	1	100	
X_3 = Cl, Y_1 = Cl, Z_1 = Cl	445.732	-0.07	1	2	6.459	1	100	-67.78
X_3 = Cl, Y_1 = Cl, Z_2 = Cl	445.732	-0.077	1	2	6.459	1	100	-74.67
X_3 = Cl, Y_1 = Cl, Z_3 = Cl	445.732	-0.118	1	2	6.241	1	100	
X_1 = Cl, Y_2 = Cl, Z_1 = Cl	445.732	-0.155	1	2	6.347	1	100	
X_1 = Cl, Y_2 = Cl, Z_2 = Cl	445.732	-0.155	1	2	6.354	1	100	-78.19
X_1 = Cl, Y_2 = Cl, Z_3 = Cl	445.732	-0.128	1	2	6.305	1	100	
X_2 = Cl, Y_2 = Cl, Z_1 = Cl	445.732	-0.124	1	2	6.379	1	100	-74.76
X_2 = Cl, Y_2 = Cl, Z_2 = Cl	445.732	-0.121	1	2	6.407	1	100	-80.23
X_2 = Cl, Y_2 = Cl, Z_3 = Cl	445.732	-0.118	1	2	6.295	1	100	
X_3 = Cl, Y_2 = Cl, Z_1 = Cl	445.732	-0.121	1	2	6.419	1	100	-68.26
X_3 = Cl, Y_2 = Cl, Z_2 = Cl	445.732	-0.122	1	2	6.422	1	100	-76.80
X_3 = Cl, Y_2 = Cl, Z_3 = Cl	445.732	-0.165	1	2	6.143	1	100	-69.26
X_1 = Cl, Y_3 = Cl, Z_1 = Cl	445.732	-0.185	1	2	6.268	1	100	-73.21
X_1 = Cl, Y_3 = Cl, Z_2 = Cl	445.732	-0.148	1	2	6.369	1	100	-76.84
X_1 = Cl, Y_3 = Cl, Z_3 = Cl	445.732	-0.127	1	2	6.335	1	100	
X_2 = Cl, Y_3 = Cl, Z_1 = Cl	445.732	-0.127	1	2	6.401	1	100	-72.21
X_2 = Cl, Y_3 = Cl, Z_2 = Cl	445.732	-0.155	1	2	6.4	1	100	-79.63

X_2 = Cl, Y_3 = Cl, Z_3 = Cl	445.732	-0.107	1	2	6.379	1	100	
X_3 = Cl, Y_3 = Cl, Z_1 = Cl	445.732	-0.123	1	2	6.433	1	100	-66.32
X_3 = Cl, Y_3 = Cl, Z_2 = Cl	445.732	-0.139	1	2	6.496	1	100	-73.14
X_3 = Cl, Y_3 = Cl, Z_3 = Cl	445.732	-0.271	1	2	6.226	1	100	
X_1 = Cl, Y_4 = Cl, Z_1 = Cl	445.732	-0.21	1	2	6.265	1	100	-68.23
X_1 = Cl, Y_4 = Cl, Z_2 = Cl	445.732	-0.156	1	2	6.187	1	100	-73.13
X_1 = Cl, Y_4 = Cl, Z_3 = Cl	445.732	-0.193	1	2	6.132	1	100	
X_2 = Cl, Y_4 = Cl, Z_1 = Cl	445.732	-0.148	1	2	6.22	1	100	-69.59
X_2 = Cl, Y_4 = Cl, Z_2 = Cl	445.732	-0.306	1	2	6.21	1	100	-75.42
X_2 = Cl, Y_4 = Cl, Z_3 = Cl	445.732	-0.223	1	2	6.309	1	100	
X_3 = Cl, Y_4 = Cl, Z_1 = Cl	445.732	-0.232	1	2	6.394	1	100	
X_3 = Cl, Y_4 = Cl, Z_2 = Cl	445.732	-0.218	1	2	6.407	1	100	-69.69
X_3 = Cl, Y_4 = Cl, Z_3 = Cl	445.732	-0.134	1	2	6.297	1	100	

Table 3-4. ADME analysis of Brominated Substituted GAT228 Compounds

Compound	Mol. WT.	QPlogBB	Donor HB	Acceptor HB	QPlog o/w	Rule of 5	% Human Oral Absorption	MM-GBSA (kkal/mol)
Reference	130 – 725	-3.0 – 1.2	0 – 6.0	2.0 – 20.0	-2.0 – 6.5	4 is Max	>80% is high	n/a
GAT228	342.396	-0.579	1	2	5.215	1	100	-65.24
X_1 = Br, Y_1 = Br, Z_1 = Br	579.085	-0.059	1	2	6.461	2	95.575	
X_1 = Br, Y_1 = Br, Z_2 = Br	579.085	-0.054	1	2	6.573	2	95.791	
X_1 = Br, Y_1 = Br, Z_3 = Br	579.085	-0.055	1	2	6.579	2	95.849	
X_2 = Br, Y_1 = Br, Z_1 = Br	579.085	-0.065	1	2	6.438	2	95.321	
X_2 = Br, Y_1 = Br, Z_2 = Br	579.085	-0.028	1	2	6.652	2	95.768	-80.31
X_2 = Br, Y_1 = Br, Z_3 = Br	579.085	-0.049	1	2	6.651	2	95.762	
X_3 = Br, Y_1 = Br, Z_1 = Br	579.085	-0.113	1	2	6.939	2	100	-63.22
X_3 = Br, Y_1 = Br, Z_2 = Br	579.085	-0.046	1	2	6.667	2	95.718	-65.41
X_3 = Br, Y_1 = Br, Z_3 = Br	579.085	0.078	1	2	6.746	2	100	
X_1 = Br, Y_2 = Br, Z_1 = Br	579.085	-0.204	1	2	6.054	2	92.204	-70.10
X_1 = Br, Y_2 = Br, Z_2 = Br	579.085	-0.095	1	2	6.517	2	94.499	
X_1 = Br, Y_2 = Br, Z_3 = Br	579.085	-0.146	1	2	6.403	2	93.835	
X_2 = Br, Y_2 = Br, Z_1 = Br	579.085	-0.11	1	2	6.576	2	94.362	-71.56
X_2 = Br, Y_2 = Br, Z_2 = Br	579.085	-0.107	1	2	6.622	2	94.562	-75.76
X_2 = Br, Y_2 = Br, Z_3 = Br	579.085	-0.213	1	2	7.101	2	100	
X_3 = Br, Y_2 = Br, Z_1 = Br	579.085	-0.101	1	2	6.642	2	94.596	-63.50
X_3 = Br, Y_2 = Br, Z_2 = Br	579.085	-0.148	1	2	6.667	2	93.982	-67.95
X_3 = Br, Y_2 = Br, Z_3 = Br	579.085	-0.129	1	2	6.237	2	93.898	
X_1 = Br, Y_3 = Br, Z_1 = Br	579.085	-0.124	1	2	6.482	2	94.119	
X_1 = Br, Y_3 = Br, Z_2 = Br	579.085	-0.169	1	2	6.322	2	93.034	-67.63
X_1 = Br, Y_3 = Br, Z_3 = Br	579.085	-0.11	1	2	6.53	2	94.484	
X_2 = Br, Y_3 = Br, Z_1 = Br	579.085	-0.121	1	2	6.508	2	93.646	

X_2 = Br, Y_3 = Br, Z_2 = Br	579.085	-0.135	1	2	6.622	2	94.048	-73.08
X_2 = Br, Y_3 = Br, Z_3 = Br	579.085	-0.122	1	2	6.54	2	94.271	
X_3 = Br, Y_3 = Br, Z_1 = Br	579.085	-0.099	1	2	6.68	2	94.733	-59.51
X_3 = Br, Y_3 = Br, Z_2 = Br	579.085	-0.103	1	2	6.666	2	94.878	-65.01
X_3 = Br, Y_3 = Br, Z_3 = Br	579.085	-0.236	1	2	5.816	2	91.337	
X_1 = Br, Y_4 = Br, Z_1 = Br	579.085	-0.182	1	2	6.148	2	92.767	-65.38
X_1 = Br, Y_4 = Br, Z_2 = Br	579.085	-0.18	1	2	6.168	2	92.97	-71.11
X_1 = Br, Y_4 = Br, Z_3 = Br	579.085	-0.264	1	2	6.616	2	95.139	
X_2 = Br, Y_4 = Br, Z_1 = Br	579.085	-0.21	1	2	6.405	2	92.955	-68.83
X_2 = Br, Y_4 = Br, Z_2 = Br	579.085	-0.201	1	2	6.335	2	92.568	-73.30
X_2 = Br, Y_4 = Br, Z_3 = Br	579.085	-0.12	1	2	6.179	2	93.664	
X_3 = Br, Y_4 = Br, Z_1 = Br	579.085	-0.216	1	2	6.406	2	91.68	-59.32
X_3 = Br, Y_4 = Br, Z_2 = Br	579.085	-0.179	1	2	6.361	2	92.862	-64.13
X_3 = Br, Y_4 = Br, Z_3 = Br	579.085	-0.182	1	2	6.531	2	93.84	

Table 3-5. ADME analysis of Iodinated Substituted GAT228 Compounds

Compound	Mol. WT.	QPlogBB	Donor HB	Acceptor HB	QPlog o/w	Rule of 5	% Human Oral Absorption	MM-GBSA (kkal/mol)
Reference	130 – 725	-3.0 – 1.2	0 – 6.0	2.0 – 20.0	-2.0 – 6.5	4 is Max	>80% is high	n/a
GAT228	342.396	-0.579	1	2	5.215	1	100	-65.24
X_1 = I, Y_1 = I, Z_1 = I	720.086	-0.182	1	2	6.531	2	93.84	
X_1 = I, Y_1 = I, Z_2 = I	720.086	-0.127	1	2	7.326	2	100	
X_1 = I, Y_1 = I, Z_3 = I	720.086	0.043	1	2	6.77	2	100	
X_2 = I, Y_1 = I, Z_1 = I	720.086	-0.028	1	2	6.806	2	100	
X_2 = I, Y_1 = I, Z_2 = I	720.086	-0.012	1	2	6.804	2	96.603	-68.74
X_2 = I, Y_1 = I, Z_3 = I	720.086	-0.172	1	2	6.819	2	94.598	
X_3 = I, Y_1 = I, Z_1 = I	720.086	-0.091	1	2	6.766	2	95.788	-63.25
X_3 = I, Y_1 = I, Z_2 = I	720.086	-0.134	1	2	6.675	2	95.15	
X_3 = I, Y_1 = I, Z_3 = I	720.086	-0.047	1	2	6.851	2	96.286	
X_1 = I, Y_2 = I, Z_1 = I	720.086	-0.008	1	2	6.829	2	96.749	
X_1 = I, Y_2 = I, Z_2 = I	720.086	-0.024	1	2	6.818	2	100	-70.88
X_1 = I, Y_2 = I, Z_3 = I	720.086	-0.085	1	2	6.785	2	95.9	
X_2 = I, Y_2 = I, Z_1 = I	720.086	-0.066	1	2	6.783	2	95.421	
X_2 = I, Y_2 = I, Z_2 = I	720.086	-0.237	1	2	6.777	2	93.362	-73.59
X_2 = I, Y_2 = I, Z_3 = I	720.086	-0.178	1	2	6.693	2	93.449	
X_3 = I, Y_2 = I, Z_1 = I	720.086	-0.087	1	2	6.773	2	95.854	-63.30
X_3 = I, Y_2 = I, Z_2 = I	720.086	-0.064	1	2	6.785	2	95.442	-65.73
X_3 = I, Y_2 = I, Z_3 = I	720.086	-0.082	1	2	6.879	2	95.899	
X_1 = I, Y_3 = I, Z_1 = I	720.086	-0.147	1	2	6.958	2	96.81	
X_1 = I, Y_3 = I, Z_2 = I	720.086	-0.199	1	2	7.288	2	100	
X_1 = I, Y_3 = I, Z_3 = I	720.086	-0.178	1	2	7.255	2	100	
X_2 = I, Y_3 = I, Z_1 = I	720.086	-0.087	1	2	6.769	2	95.829	
X_2 = I, Y_3 = I, Z_2 = I	720.086	-0.083	1	2	6.827	2	95.593	

$X_2 = I, Y_3 = I, Z_3 = I$	720.086	-0.081	1	2	6.819	2	95.51	
$X_3 = I, Y_3 = I, Z_1 = I$	720.086	-0.081	1	2	6.774	2	95.887	-58.51
$X_3 = I, Y_3 = I, Z_2 = I$	720.086	-0.085	1	2	6.868	2	95.834	
$X_3 = I, Y_3 = I, Z_3 = I$	720.086	-0.092	1	2	6.863	2	95.765	
$X_1 = I, Y_4 = I, Z_1 = I$	720.086	-0.143	1	2	6.395	2	93.732	
$X_1 = I, Y_4 = I, Z_2 = I$	720.086	-0.037	1	2	6.526	2	95.929	-70.73
$X_1 = I, Y_4 = I, Z_3 = I$	720.086	-0.037	1	2	6.548	2	96.002	
$X_2 = I, Y_4 = I, Z_1 = I$	720.086	-0.245	1	2	6.535	2	92.511	-67.76
$X_2 = I, Y_4 = I, Z_2 = I$	720.086	-0.066	1	2	6.71	2	95.755	
$X_2 = I, Y_4 = I, Z_3 = I$	720.086	-0.02	1	2	6.709	2	95.994	
$X_3 = I, Y_4 = I, Z_1 = I$	720.086	-0.239	1	2	6.526	2	92.462	
$X_3 = I, Y_4 = I, Z_2 = I$	720.086	-0.067	1	2	6.706	2	95.712	
$X_3 = I, Y_4 = I, Z_3 = I$	720.086	-0.059	1	2	6.713	2	95.772	

Table 3-6. ADME analysis of Nitro Substituted GAT228 Compounds

Compound	Mol. WT.	QPlogBB	Donor HB	Acceptor HB	QPlog o/w	Rule of 5	% Human Oral Absorption	MM-GBSA (kkal/mol)
Reference	130 – 725	-3.0 – 1.2	0 – 6.0	2.0 – 20.0	-2.0 – 6.5	4 is Max	>80% is high	
GAT228	342.396	-0.579	1	2.00	5.215	1	100	-65.24
$Z_2 = NO_2$ (Control)	387.394	-1.732	1.00	3.00	4.237	0	88.432	-71.70
$X_1 = F, Y_1 = F, Z_2 = NO_2$	423.375	-1.379	1.00	3.00	4.958	0	92.389	-75.97
$X_2 = F, Y_1 = F, Z_2 = NO_2$	423.375	-1.186	1.00	3.00	4.829	0	95.558	-77.65
$X_1 = F, Y_2 = F, Z_2 = NO_2$	423.375	-1.533	1.00	3.00	4.980	0	94.228	-72.59
$X_2 = F, Y_2 = F, Z_2 = NO_2$	423.375	-1.236	1.00	3.00	4.746	0	95.122	-69.47
$X_1 = F, Y_3 = F, Z_2 = NO_2$	423.375	-1.511	1.00	3.00	4.776	0	92.568	-75.34
$X_2 = F, Y_3 = F, Z_2 = NO_2$	423.375	-1.376	1.00	3.00	4.722	0	93.431	-70.29
$X_1 = F, Y_4 = F, Z_2 = NO_2$	423.375	-1.301	1.00	3.00	4.508	0	93.505	-76.47
$X_2 = F, Y_4 = F, Z_2 = NO_2$	423.375	-1.337	1.00	3.00	4.643	0	94.177	-74.66
$X_1 = Cl, Y_1 = Cl, Z_2 = NO_2$	456.284	-1.355	1.00	3.00	5.410	1	85.143	
$X_2 = Cl, Y_1 = Cl, Z_2 = NO_2$	456.284	-1.104	1.00	3.00	5.252	1	85.986	
$X_1 = Cl, Y_2 = Cl, Z_2 = NO_2$	456.284	-1.454	1.00	3.00	5.391	1	83.685	
$X_2 = Cl, Y_2 = Cl, Z_2 = NO_2$	456.284	-1.136	1.00	3.00	5.234	1	85.352	-68.27
$X_1 = Cl, Y_3 = Cl, Z_2 = NO_2$	456.284	-1.442	1.00	3.00	5.415	1	84.004	
$X_2 = Cl, Y_3 = Cl, Z_2 = NO_2$	456.284	-1.112	1.00	3.00	5.172	1	84.981	
$X_1 = Cl, Y_4 = Cl, Z_2 = NO_2$	456.284	-1.442	1.00	3.00	5.224	1	83.282	-81.65
$X_2 = Cl, Y_4 = Cl, Z_2 = NO_2$	456.284	-1.451	1.00	3.00	5.393	1	83.381	-81.69
$X_1 = Cl, Y_1 = F, Z_2 = NO_2$	439.830	-1.243	1.00	3.00	5.061	1	84.774	
$X_1 = F, Y_1 = Cl, Z_2 = NO_2$	439.830	-1.062	1.00	3.00	5.231	1	88.370	-75.89
$X_1 = F, Y_2 = Cl, Z_2 = NO_2$	439.830	-1.248	1.00	3.00	5.188	1	85.629	-71.72
$X_1 = Cl, Y_2 = F, Z_2 = NO_2$	439.830	-1.251	1.00	3.00	5.095	1	84.605	-70.04
$X_1 = Cl, Y_3 = F, Z_2 = NO_2$	439.830	-1.204	1.00	3.00	5.106	1	85.189	-75.15
$X_1 = F, Y_3 = Cl, Z_2 = NO_2$	439.830	-1.181	1.00	3.00	5.100	1	86.231	

X_1 = F, Y_4 = Cl, Z_2 = NO_2	439.830	-1.339	1.00	3.00	4.910	0	96.167	-75.93
X_1 = Cl, Y_4 = F, Z_2 = NO_2	439.830	-1.289	1.00	3.00	4.984	0	100.000	-74.23
X_2 = Cl, Y_1 = F, Z_2 = NO_2	439.830	-1.328	1.00	3.00	5.195	1	84.206	-77.25
X_2 = F, Y_1 = Cl, Z_2 = NO_2	439.830	-1.073	1.00	3.00	5.277	1	88.119	-74.40
X_2 = F, Y_2 = Cl, Z_2 = NO_2	439.830	-1.206	1.00	3.00	5.252	1	86.215	-75.08
X_2 = Cl, Y_2 = F, Z_2 = NO_2	439.830	-1.351	1.00	3.00	5.182	1	83.766	-76.36
X_2 = Cl, Y_3 = F, Z_2 = NO_2	439.830	-1.143	1.00	3.00	5.267	1	86.956	-76.43
X_2 = F, Y_3 = Cl, Z_2 = NO_2	439.830	-1.148	1.00	3.00	5.255	1	86.819	
X_2 = F, Y_4 = Cl, Z_2 = NO_2	439.830	-1.287	1.00	3.00	5.022	1	83.612	-77.38
X_2 = Cl, Y_4 = F, Z_2 = NO_2	439.830	-1.369	1.00	3.00	5.513	1	83.847	-79.08

Table 3-7. ADME analysis of Pyridine and Cyclopentadiene Substituted GAT228 Compounds

Compound	Mol. Wt.	QPlogBB	Donor HB	Accept HB	QPlog o/w	Rule of Five	% Human Oral Absorption	MM-GBSA (kkcal/mol)
Recommended	130 – 725	-3.0 – 1.2	0 – 6.0	2.0 – 20.0	-2.0 – 6.5	4 is Max	>80% is high	n/a
GAT1665-Cl	445.732	-0.155	1.00	2.00	6.354	1	100	-78.19
X = C_5H_6, X4 = N	446.719	-0.066	1.00	3.00	6.031	1	100.000	-73.04
2	446.719	-0.294	1.00	3.50	5.526	1	100.000	-72.44
3	446.719	-0.295	1.00	3.50	5.535	1	100.000	-71.65
4	446.719	-0.261	1.00	3.00	5.852	1	100.000	-81.44
5	447.719	-0.298	1.00	4.00	5.400	1	100.000	-73.44
6	447.719	-0.457	1.00	4.50	5.083	1	93.659	-76.87
7	447.719	-0.659	1.00	5.00	4.613	0	100.000	-73.60
8	447.719	-0.618	1.00	4.50	4.886	0	100.000	-76.68
9	451.754	0.019	1.00	2.00	6.370	1	100.000	-77.59
10	452.742	-0.220	1.00	3.50	5.552	1	100.000	-74.88
11	452.742	-0.096	1.00	3.50	5.508	1	100.000	-74.97
12	451.754	0.089	1.00	2.00	6.522	1	100.000	-78.57
13	451.754	0.078	1.00	2.00	6.530	1	100.000	-78.70
14	446.719	-0.178	1.00	3.00	5.911	1	100.000	-79.90
15	446.719	-0.238	1.00	3.00	5.818	1	100.000	-77.96
16	446.719	-0.281	1.00	3.50	5.518	1	100.000	-76.58
17	446.719	-0.237	1.00	3.00	5.773	1	100.000	-76.65
18	447.707	-0.247	1.00	4.00	5.411	1	100.000	-79.14
19	447.707	-0.388	1.00	4.00	5.187	1	94.864	-82.87
20	447.707	-0.463	1.00	4.00	5.115	1	93.413	-81.45
21	447.707	-0.453	1.00	4.50	4.991	0	100.00	-77.02
22	451.754	0.090	1.00	2.00	6.398	1	100.00	-77.34

23	451.754	0.101	1.00	2.00	6.503	1	100.00	-76.65
24	447.707	-0.604	1.00	4.50	4.839	0	100.00	-78.15
25	447.707	-0.420	1.00	4.50	5.090	1	94.480	-81.10

CHAPTER 4

Assessment of select synthetic cannabinoid receptor agonist bias and selectivity between the type 1 and type 2 cannabinoid receptor

Copyright statement

This chapter has been previously published as: Zagzoog A, Brandt AL, Black T, Kim ED, Burkart R, Patel M, et al. Assessment of select synthetic cannabinoid receptor agonist bias and selectivity between the type 1 and type 2 cannabinoid receptor. Sci Rep. 2021;11: 1–18. doi:10.1038/s41598-021-90167-w. The manuscript has been modified to meet formatting requirements.

Contribution statement

The manuscript used as the basis for this chapter was written by Ayat Zagzoog and myself – Asher Brandt with guidance from Dr. Robert B. Laprairie. *In vitro* data were collected by Ayat Zagzoog whereas *in silico* data were collected by myself. All data were analyzed by myself with technical assistance from Dr. Robert B. Laprairie.

4.1 Introduction

The availability of different synthetic cannabinoid receptor agonists (SCRAs) as new psychoactive substances (NPS) over the past decade has vastly grown.[129] SCRAs were first reported as NPS in Europe in 2008 and the first case report of acute toxicity was reported from forensic investigators in Austria and Germany in 2008.[130] Although the original intended use of SCRA was as tool compounds for studying CB1R and CB2R they became widespread throughout north American and Europe. Unfortunately, numerous cases of harm and death in the United States, Europe and Australia as well as psychological, neurological, cardiovascular, pulmonary and renal adverse effects have been reported with their use.[131] As a consequence, in 2012 the Synthetic Drug Abuse Prevention Act made 15 synthetic cannabinoids Schedule I products which are illegal to sell, buy or possess.[132] In 2016 U.S. senators Shumer and Grassley proposed legislation to add 22 additional synthetic cannabinoids to the list after 130 emergency department visits due to synthetic cannabinoids occurred in a 1-week span in New York City.[131] The federal analogs act which says that any chemical "substantially similar" to a controlled substance listed in Schedule I or II shall be treated as if it were listed in schedule 1, but only if identified for human consumption.[133] The major issue here is that its exceedingly hard for prosecutors to convince non-science-minded jurors that the chemical is "substantially similar" and that the non-science-minded sellers or purchasers knew it was. Thus, an improvement on the original Federal Analogs Act is needed.

SCRAs produce their effects by binding to the orhosteric site of CB1R which is also the same mechanism under which Δ^9-THC produces intoxication.[134] In addition to CB1R it has also been shown that cannabinoids bind to CB2R.[135] CB1R and CB2R are G_i-coupled GPCRs and thus modulate intracellular signaling through βarrestin2 and other G proteins.[136] Ligand activation of both CB1R and CB2R inhibit the production of cAMP and recruitment βarrestin2 which results in

receptor internalization, recycling or turnover.[137] Measuring these two intracellular outcomes is important in understanding which pathway is activated to a greater effect; that is, the ligand bias for G_i relative to βarrestin2, although it does not capture potential biases at other output pathways such as G_q or $G_{12/13}$.[138] In this study we aimed to quantify ligand bias between G_i and βarrestin2, affinity of SCRAs at CB1R and CB2R, as well as *in silico* studies to provide molecular determinants for the observed outcomes.

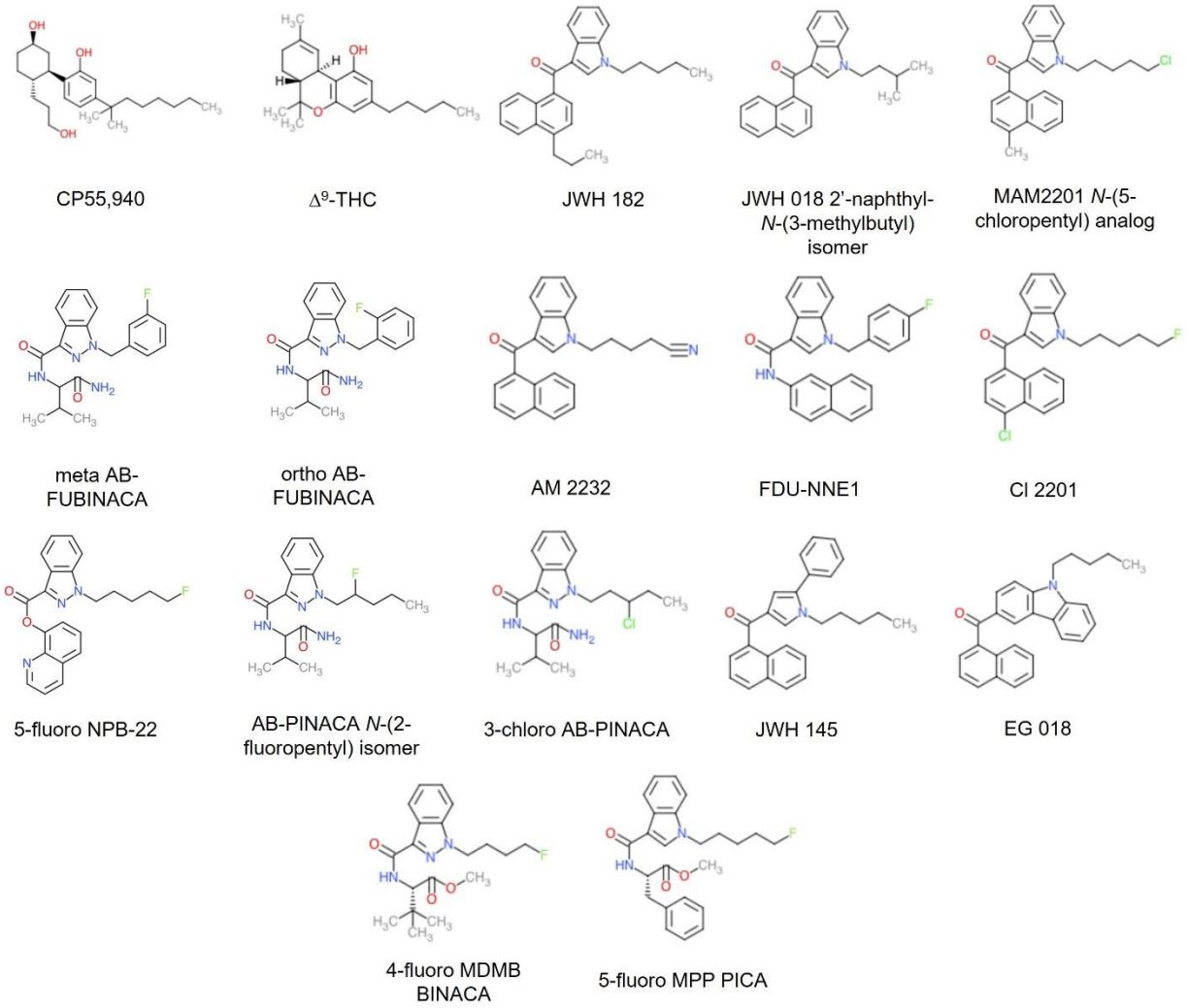

Figure 4-1. Structure of SCRAs studied

4.2 Experimental Section

4.2.1 *In vitro* evaluation

Compounds used. All compounds were purchased from Cayman Chemicals (Ann Arbor, MI) with the exception of Δ^9-tetrahydrocannabinol, which was purchased from Toronto Research Chemicals (Toronto, ON). [^{3}H]CP55,940 (174.6 Ci/mmol) was obtained from PerkinElmer (Guelph, ON). All other reagents were obtained from Sigma-Aldrich (Oakville, ON) unless specifically noted. Compounds were dissolved in DMSO (final concentration of 0.1% in assay media for all assays) and added directly to the media at the concentrations and times indicated.

Cell culture. Chinese hamster ovary (CHO)-K1 cells, either untransfected for use as controls in saturation binding studies or stably expressing human CB1R or CB2R, were cultured as described in earlier studies from our group.[95] Briefly, cells were maintained at 37°C, 5% CO_2 in F-12/DMEM containing 1 mM L-glutamine, 10% FBS, and 1% Pen/Strep as well as hygromycin B (300 µg/mL) and G418 (600 µg/mL) for CHO-K1 CB1R cells or G418 (400 µg/mL) for CHO-K1 CB2R cells.[82,95] In the case of membrane collection for radioligand binding, cells were scraped from flasks, centrifuged, and frozen at -80°C until required. HitHunter (cAMP) and PathHunter (βarrestin2) CHO-K1 cells stably-expressing CB1R or CB2R from DiscoveRx (Eurofins, Fremont, CA) were maintained at 37°C, 5% CO_2 in F-12 DMEM containing 10% FBS and 1% penicillin-streptomycin with 800 µg/mL geneticin (HitHunter) or 800 µg/mL G418 and 300 µg/mL hygromycin B (PathHunter), as described previously.[139]

[^{3}H]CP55,940 radioligand displacement assay. Saturation binding experiments were conducted with 0.1 – 100 nM [^{3}H]CP55,940 and Tris binding buffer (50 mM Tris–HCl, 50 mM Tris–base, 0.1% BSA, pH 7.4, 2 mL).[139,140] Saturation binding experiments utilized CHO-K1 cells expressing either CB1R or CB2R (total bound) and untransfected CHO-K1 cells (non-specific bound).

Specific binding curves were calculated as the difference between total and non-specific for each concentration of [^{3}H]CP55,940 used and fit to a one site total binding non-linear regression (GraphPad, Prism, v. 9.0). Competition binding experiments were conducted with 0.7 nM [^{3}H]CP55,940, SCRAs as described, and Tris binding buffer (50 mM Tris–HCl, 50 mM Tris–base, 0.1% BSA, pH 7.4, 2 mL).[139,140] Radioligand binding began with the addition of CHO-K1 cell membranes (50 µg protein per sample). Assays were performed for 120 min at 37°C and stopped by the addition of ice-cold Tris binding buffer, followed by vacuum filtration using a 24-well sampling manifold (Brandel Cell Harvester; Brandel Inc, Gaithersburg, MD, USA). Brandel GF/B filter paper was soaked with wash buffer at 4°C for at least 24 h. Each filter paper was washed 6 times with 1.2 mL aliquots of Tris-binding buffer, then air-dried overnight and submerged in 5 mL of scintillation fluid (Ultima Gold XR, PerkinElmer). Liquid scintillation spectrometry was used to quantify radioactivity. For competition binding experiments, specific binding was equal to the difference in radioactivity with or without 1 µM unlabelled CP55,940.

HitHunter cAMP assay – Cells (20,000 cells/well in low-volume 96 well plates) were incubated overnight in Opti-MEM containing 1% FBS at 37°C and 5% CO_2. Following this, Opti-MEM media was removed and replaced with cell assay buffer (DiscoveRx) and cells were co-treated at 37°C with 10 µM FSK and ligands for 90 min. cAMP antibody solution and cAMP working detection solutions were added to cells (DiscoveRx), and cells were incubated for 60 min at room temperature. cAMP solution A (DiscoveRx) was added and cells were incubated for an additional 60 min at room temperature before chemiluminescence was measured on a Cytation5 plate reader (top read, gain 200, integration time 10,000 ms).

PathHunter βarrestin2 assay. Briefly, cells (20,000 cells/well in low-volume 96 well plates) were incubated overnight in Opti-MEM containing 1% FBS at 37°C and 5% CO_2. Cells were co-treated

with ligands for 90 min at 37°C. Detection solution was added to cells (DiscoveRx), and cells were incubated for 60 min at room temperature. Chemiluminescence was measured on a Cytation5 plate reader (top read, gain 200, integration time 10,000 ms).

4.2.2 *In silico* evaluation

Molecular docking – The published cryo-EM structure PDB: 6N4B.[51] was used for the molecular modelling of CB1R. This cryo-EM structure contains the agonist MDMB-FUBINACA bound to CB1R-Ga_i. CB2R modelling utilized PBD: 6PT0[59] which contains the agonist WIN 55,212-2 bound to CB2R-Ga_i. Cannabinoids were modelled docking to GPCRs both with the G_i present to simulate the G protein-bound state or with the Ga_i removed to simulate the G protein-absent state that *may* be more conducive to βarrestin2 coupling. The G protein-absent state is limited by not having βarrestin2 within the crystal; however, no such crystal exists as of the time of writing. Each of the cannabinoids was built and optimized in Spartan '18 Parallel Suite[101] and docked via induced fit docking in Schrödinger.[102,141] To reduce atom clashing, ligand-receptor complexes were minimized using the OPLS3 force field in Prime.[102] Prime MM-GBSA was used to calculate the interaction energy between each ligand and the receptor.[102]

4.2.3 Statistical Analysis

[^{3}H]CP55,940 radioligand saturation binding data are provided as raw counts per minute (cpm) bound and fit to a one site total binding non-linear regression (GraphPad). [^{3}H]CP55,940 radioligand competition binding data are provided as % change from maximal ^{3}H bound (i.e. 100%). Data for HitHunter cAMP and PathHunter βarrestin2 data are shown as % of maximal CP55,940 response (i.e. 100%). Estimates of K_i, EC_{50}, E_{min}, and E_{max} were determined using non-linear regression with variable slope (4 parameters) (GraphPad, Prism, v. 8.0). The operational model of Black and Leff [142] was used to estimate bias (ΔΔLogR) with CP55,940 as the reference

agonist.[82,139,143] One-way analysis of variance (ANOVA), followed by Tukey's post-hoc test, was used for statistical analyses ($p < 0.05$ determined to be significant). Bartlett's test was used to confirm homogeneity of variance (GraphPad). Values are presented as the mean ± the standard error of the mean (SEM) or 95% confidence interval (CI), as indicated in tables and figure legends.

4.3 Results and Discussion

4.3.1 *In Vitro* Evaluation of CB1R

In the radioligand binding assays we observed that all ligands studied bound to and displaced [^{3}H]CP55,940 from CB1R (***Figure 4-2***). However not all ligands fully displaced [^{3}H]CP55,940 from CB1R. The highest affinity ligands which displayed affinity under 1nM were JWH-182, JWH 018 2'-naphthyl-N-(3-methylbutyl) isomer, AM 2232 and Cl 2201 (***Figure 4-2*** and ***Table 4-1***). The common scaffold between the high affinity ligands at CB1R is a naphthalene group linked to an alkyl substituted indole by a ketone (***Figure 4-1***). The lowest affinity ligands over (i.e. >100nM) were 3-chloro AB-PINACA, JWH 145, 4-fluoro MDMB-BINACA and 5-fluoro MPP-PICA. In general, non-fused aromatic rings in the naphthyl position seemed to drastically reduce binding affinity. For example, substitutions in this position that have a high degree of rotatable bonds (i.e., 4-fluoro MDMB-BINACA) tend to drastically reduce binding affinity.

Next, we looked at CB1R G protein activation by quantifying cAMP inhibition. It was observed that all 15 SCRAs studied were agonists in terms of their ability to inhibit cAMP. The SCRAs that produced the greatest E_{max} (> 90%) were CP55,940, MAM2201 N-(5-chloropentyl) analog, meta-AB-FUBINACA, AM 2232, FDU-NNEI, 5-fluoro NPB-22, 3-chloro AB-PINACA, EG 018, and 5-fluoro MPP-PICA (***Figure 4-3*** and ***Table 4-1***). Only 2 of these compounds displayed an E_{max} greater than or equal to the reference agonist CP55,940: AM 2232 and EG 018 (***Figure 4-3*** and ***Table 4-1***). In terms of potency, there were 9 compounds that displayed greater potency than

CP55,940: MAM2201 N-(5-chloropentyl) analog, meta-AB-FUBINACA, ortho-AB-FUBINACA, FDU-NNEI, Cl 2201, AB-PINACA N-(2-fluoropentyl) isomer, 3-chloro AB-PINACA, JWH 145 and 5-fluoro MPP-PICA (***Table 4-1***).

To better understand pathway selectivity, we also quantified βarrestin2 recruitment (***Figure 4-4*** and ***Table 4-1***). In terms of E_{max} there were 7 compounds that were more efficacious than the reference agonist CP55,940: JWH 182, ortho-AB-FUBINACA, 5-fluoro NPB-22, AB-PINACA N-(2-fluoropentyl) isomer, 3-chloro AB-PINACA, 4-fluoro MDMB-BINACA, and 5-fluoro MPP-PICA (***Figure 4-4*** and ***Table 4-1***). In measuring the EC_{50} at this pathway, overall, the potency was rather low with 9 of the SCRAs displaying an EC_{50} greater than 10,000 nM (***Table 4-1***). There were 5 compounds that displayed higher potency than CP55,940 which were Δ^9-THC, ortho-AB-FUBINACA, 5-fluoro NPB-22, AB-PINACA N-(2-fluoropentyl) isomer, 3-chloro AB-PINACA, and 4-fluoro MDMB-BINACA ***(Table 4-1***). Even though 4-fluoro MDMB-BINACA displayed the greatest potency in this assay the potencies measured in the cAMP assay were much greater (***Table 4-1***). Conversely, although the potencies were much greater in the cAMP assay some of the efficacies measured were much greater in the βarrestin2 assay (***Table 4-1***). With this being the case, we measured the ΔΔLogR to see which pathway is preferred relative to the reference agonist, CP55,940 (***Figure 4-5***). It was observed that Δ^9-THC, meta-AB-FUBINACA, 5-fluoro NPB-22, 5-fluoro MPP-PICA were unbiased, AB-PINACA N-(2-fluoropentyl) isomer, 3-chloro AB-PINACA, 4-Fluoro MDMB-BINACA were βarrestin2-biased and FDU-NNEI, JWH 145, EG018 were cAMP-biased (***Figure 4-5***). From these data alone it is not clear what structural features lead to pathway selectivity.

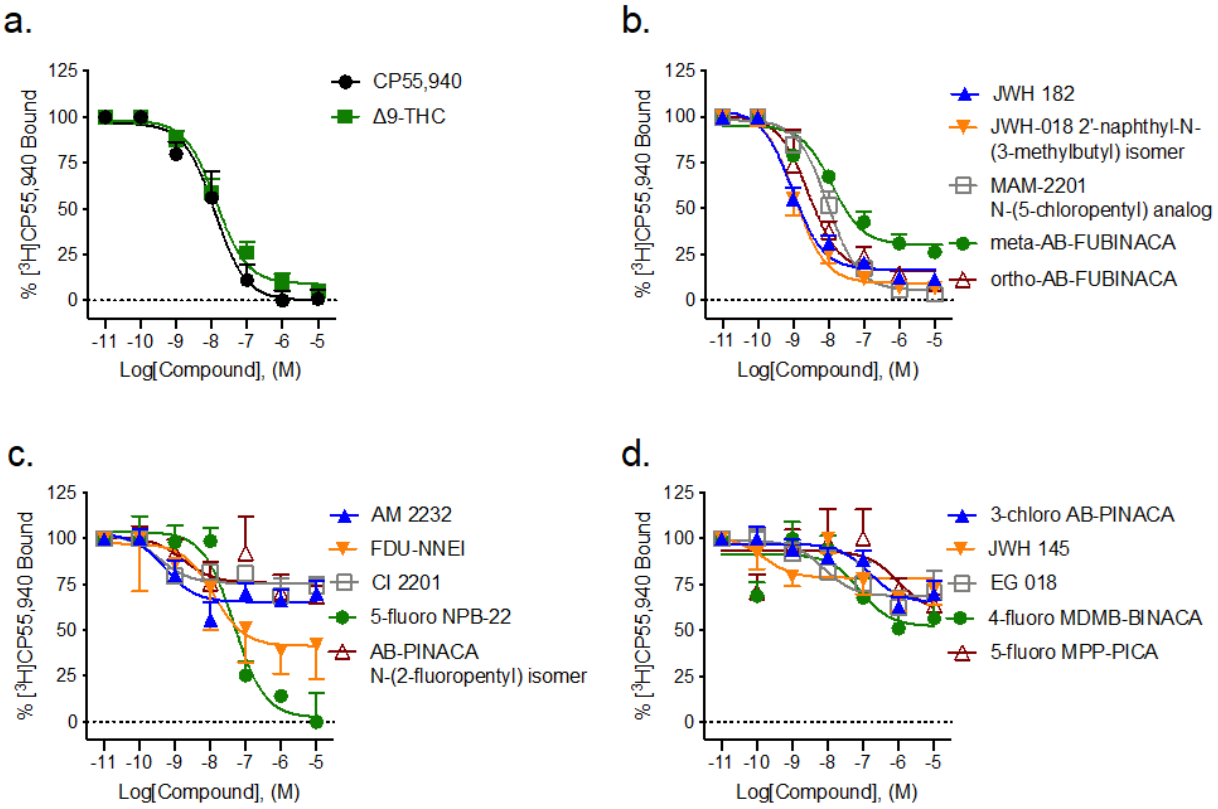

Figure 4-2. (a,b,c,d) Radioligand binding of 1 nM [^{3}H]CP55,940 to membranes from CB1R CHO-K1 cells. CB1R CHO-K1 cells were treated with 0.10 nM – 10 µM compounds in the presence 1 nM [^{3}H]CP55,940. Data are expressed as % radioligand bound. Data were fit to a nonlinear regression (4-parameter model, GraphPad v. 9.0) to determine K_D, EC_{50}, and E_{max}. Data are mean ± SEM (E_{max}) or 95% CI (K_D, EC_{50}); n ≥ 6 independent experiments. *p < 0.05 compared to CP55,940 as determined by one-way ANOVA followed by Bonferroni's post-hoc test or non-overlapping 95% CI.

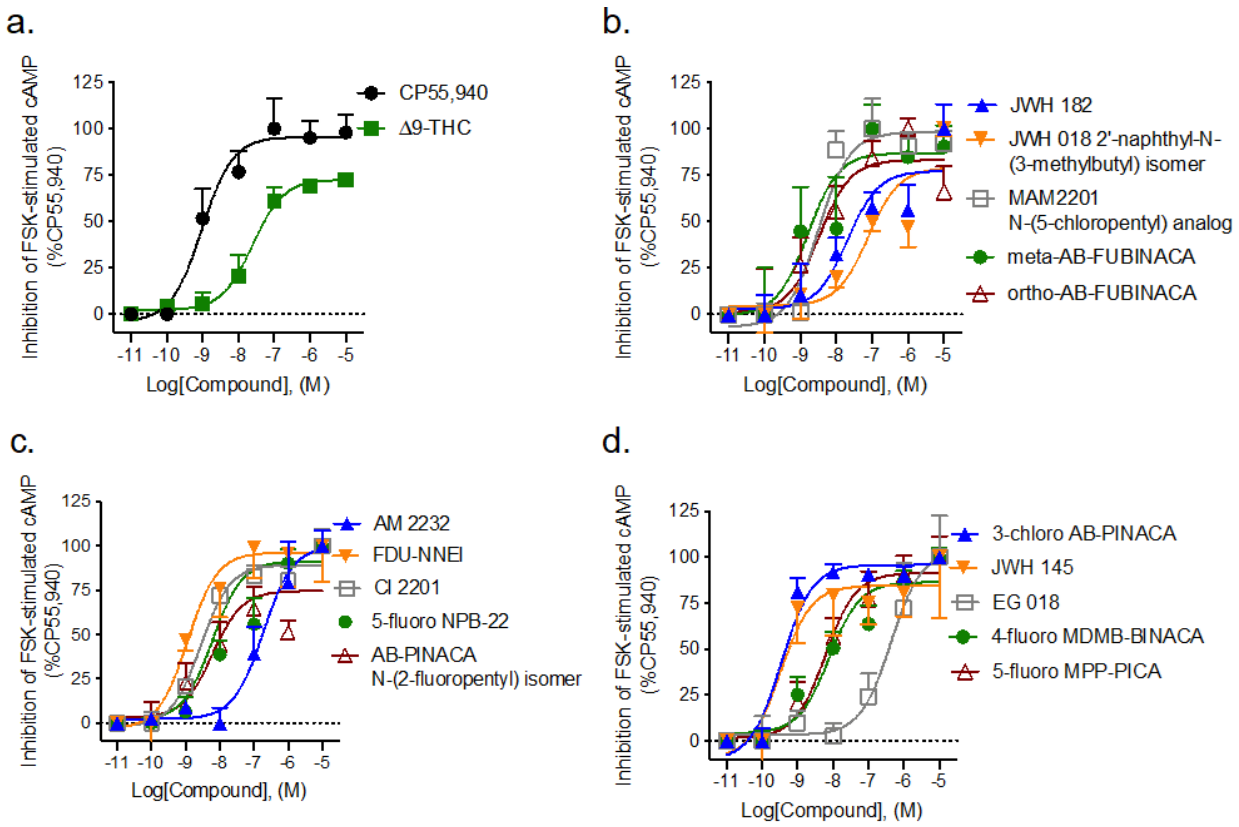

Figure 4-3. CB1R-dependent inhibition of FSK-stimulated cAMP. CB1R CHO-K1 were treated with 0.10 nM – 10 µM GAT compounds. (a,b,c.d) cAMP inhibition of GAT compounds as agonists. (a,b,d,e) Data are expressed as % CP55,940 max. Data were fit to a nonlinear regression (4-parameter model, GraphPad v. 9.0) to determine EC_{50} and E_{max}. Data are mean ± SEM (E_{max}) or 95% CI (EC_{50}); $n \geq 6$ independent experiments performed in triplicate. *$p < 0.05$ compared to CP55,940 as determined by one-way ANOVA followed by Bonferroni's post-hoc test or non-overlapping 95% CI. Concentration-response data were fit to the operational model of Black and Leff (1983) (GraphPad v. 9.0).

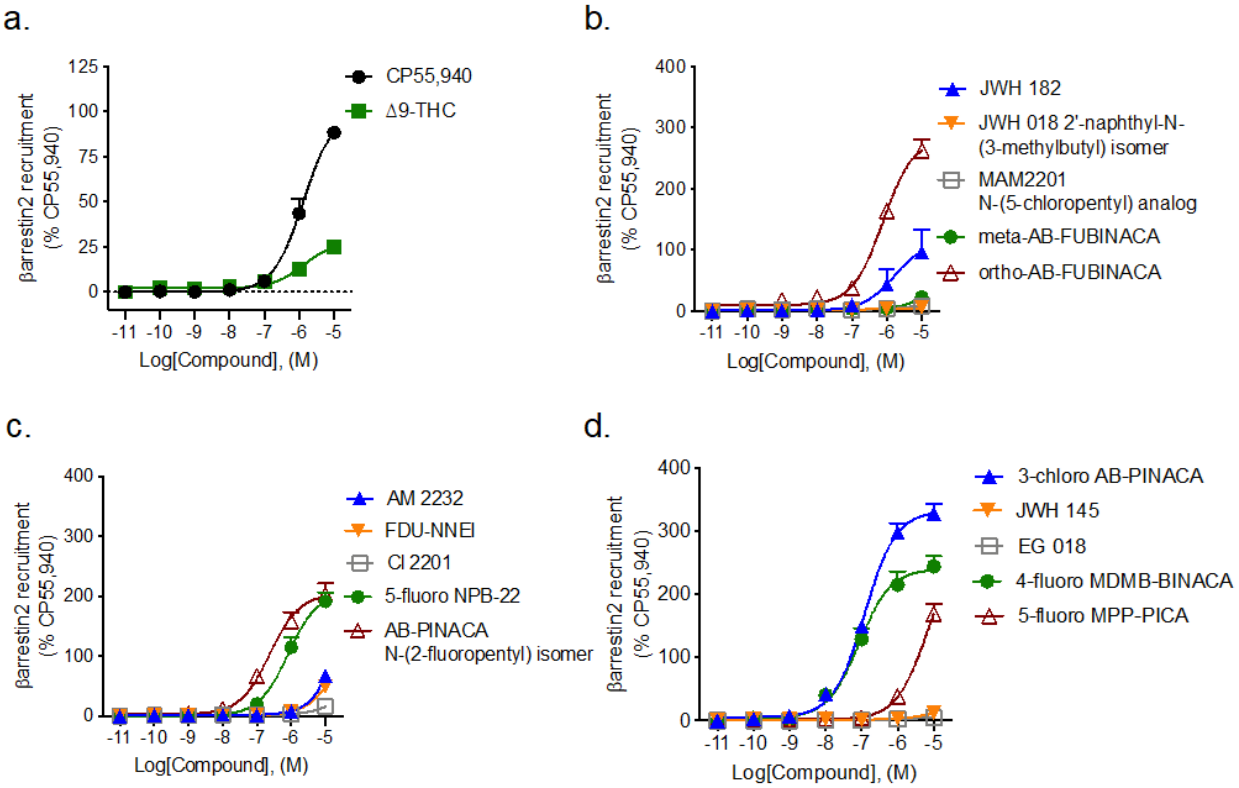

Figure 4-4. βarrestin2 recruitment to CB1R following SCRA treatment. CB1R CHO-K1 were treated with 0.10 nM – 10 µM GAT compounds. (**b,c,d,e**) βarrestin2 recruitment of GAT compounds as agonists (**a,b,c,d**). Data are expressed as % CP55,940 max. Data were fit to a nonlinear regression (4-parameter model, GraphPad v. 9.0) to determine EC_{50} and E_{max}. Data are mean ± SEM (E_{max}) or 95% CI (EC_{50}); $n \geq 6$ independent experiments performed in triplicate. *p < 0.05 compared to CP55,940 as determined by one-way ANOVA followed by Bonferroni's post-hoc test or non-overlapping 95% CI.

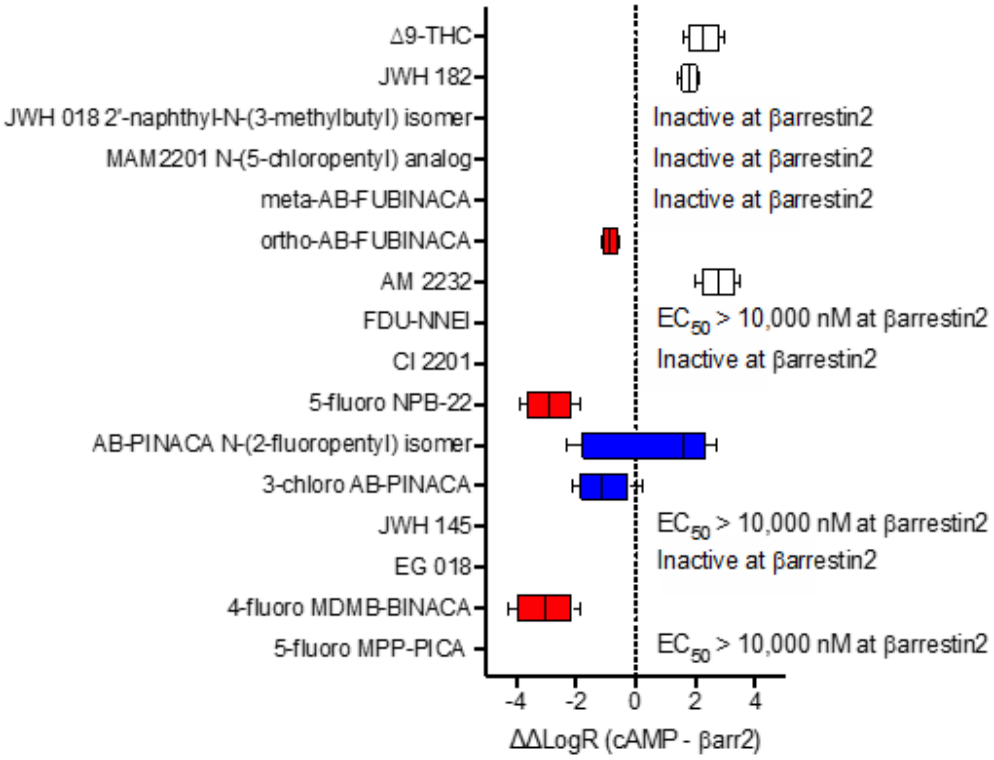

Figure 4-5. CB1R SCRA bias. Compound bias between cAMP inhibition and βarrestin2 recruitment [ΔΔLogR (cAMP - βarrestin2)] is shown here for data presented in ***Figure 4-3*** and ***Figure 4-4***. Data were fit to the operational model to calculate bias. Data are mean with 95% CI, $n \geq 6$ independent experiments performed in triplicate. Values > 0 represent cAMP bias (white), values < 0 represent βarrestin2 bias (red), and values not different from 0 are unbiased (blue) as determined by 95% CI not overlapping with 0.

4.3.2 *In Vitro* Evaluation of CB2R

The same set of experiments were performed at CB2R given that both receptors are part of the endocannabinoid system and bind the same endogenous ligands. As it will be discussed in a later section of this manuscript CB1R and CB2R have very similar sequence homology in the orthosteric binding site. There were 9 SCRAs with stronger binding affinity than the reference full agonist CP55,940; JWH 182, JWH 018 2'-naphthyl-N-(3-methylbutyl) isomer, meta-AB-FUBINACA, ortho-AB-FUBINACA, FDU-NNEI, Cl 2201, 5-fluoro NPB-22, EG 018, and 4-fluoro MDMB-BINACA. Of these SCRAs there were 3 that displayed affinity stronger than 1 nM; meta-AB-FUBINACA, ortho-AB-FUBINACA, and 4-fluoro MDMB-BINACA (***Figure 4-6*** and ***Table 4-1***). As seen in meta and ortho-AB-FUBINACA changing the chloro from the ortho to meta does increase binding affinity (***Figure 4-1***, ***Figure 4-6*** and ***Table 4-1***). A stark observation can be seen in the binding affinity difference between MAM220 N-(5-chloropnetyl) analog and Cl 2201(***Figure 4-6*** and ***Table 4-1***). When compared structurally there are 2 differences being a chloro pentyl chain (MAM2201 N-(5-chloropentyl) analog) vs a fluoro pentyl chain (Cl 2201) and a methyl-naphthyl (MAM2201 N-(5-chloropentyl) analog) vs a chloro-naphthyl (Cl 2201) and yet the affinity differs by over 4 orders of magnitude (***Figure 4-1***, ***Figure 4-6*** and ***Table 4-1***). This is likely the combinatorial effect of a chloro having a larger atomic radius than fluoro and similarly a methyl having a larger atomic radius than a chloro. However, to know with certainty the affinity of MAM2201 N-(5-chloropentyl) analog with a chloro substituent in the position of the methyl would need to be measured.

All SCRAs acted as agonists in terms of their ability to inhibit cAMP accumulation (***Figure 4-7*** and ***Table 4-1***). Seven agonists displayed greater potency than CP55,940: JWH 018 2'-naphthyl-N-(3-methylbutyl) isomer, ortho-AB-FUBINACA, AM 2232, FDU-NNEI, Cl 2201, 5-fluoro

NPB-22, and 4-fluoro MDMB-BINACA (***Figure 4-7*** and ***Table 4-1***). Of these agonists, 5 displayed potency greater than 1 nM: JWH 018 2'-naphthyl-N-(3-methylbutyl) isomer, ortho-AB-FUBINACA, FDU-NNEI and 4-fluoro MDMB-BINACA (***Figure 4-7*** and ***Table 4-1***). Interestingly if we compare ortho and meta-AB-FUBINACA, ortho (0.06 nM) displays a potency that is 90x greater than meta-AB-FUBINACA (5.4 nM). As for E_{max}, 8 SCRAs produced greater efficacy than the reference agonists CP55,940 (***Figure 4-7*** and ***Table 4-1***).

In terms of βarrestin2 recruitment, 11 SCRAs showed greater potency than the reference ligand (***Figure 4-8*** and ***Table 4-1***). Of these ligands, only 2 had potencies greater than 10 nm: AB-PINACA N-(2-fluoropentyl) isomer and 3-chloro AB-PINACA (***Figure 4-8*** and ***Table 4-1***). Given the similarities in potencies there does not seem to be a noticeable effect in changing the chloro from a 3 position (3-chloro AB-PINACA) to a fluoro in the 2 position (AB-PINACA N-(2-fluoropentyl) isomer) (***Figure 4-8*** and ***Table 4-1***). As for efficacy all of the SCRAs acted as agonists in their ability to recruit βarrestin2 (***Figure 4-8*** and ***Table 4-1***). Of these SCRAs 7 of them showed greater efficacy than the reference agonist CP55,940 including both AB-PINACA N-(2-fluoropentyl) isomer and 3-chloro AB-PINACA (***Figure 4-8*** and ***Table 4-1***).

We also evaluated pathway selectivity of the SCRAs at CBR2 (***Figure 4-9***). It was observed that ortho-AB-FUBINACA, AM2232, FDU-NNE, Cl 2201, JWH-145 and EG 018 were cAMP biased while AB-PINACA N-(2-fluoro pentyl) isomer, 3-chloro AB-PINACA and 4-fluoro MDMB-BINACA were βarrestin2 bias and lastly THC, meta-AB-FUBINACA, 5-fluoro NPB-22, 5-fluoro MPP-PICA are unbiased (***Figure 4-9)***. For the cAMP biased compounds all but ortho-AB-FUBINACA contain a naphthalene substituent whereas all βarrestin2 biased compounds contain a substituted amide or ester group (***Figure 4-1*** and ***Figure 4-9***).

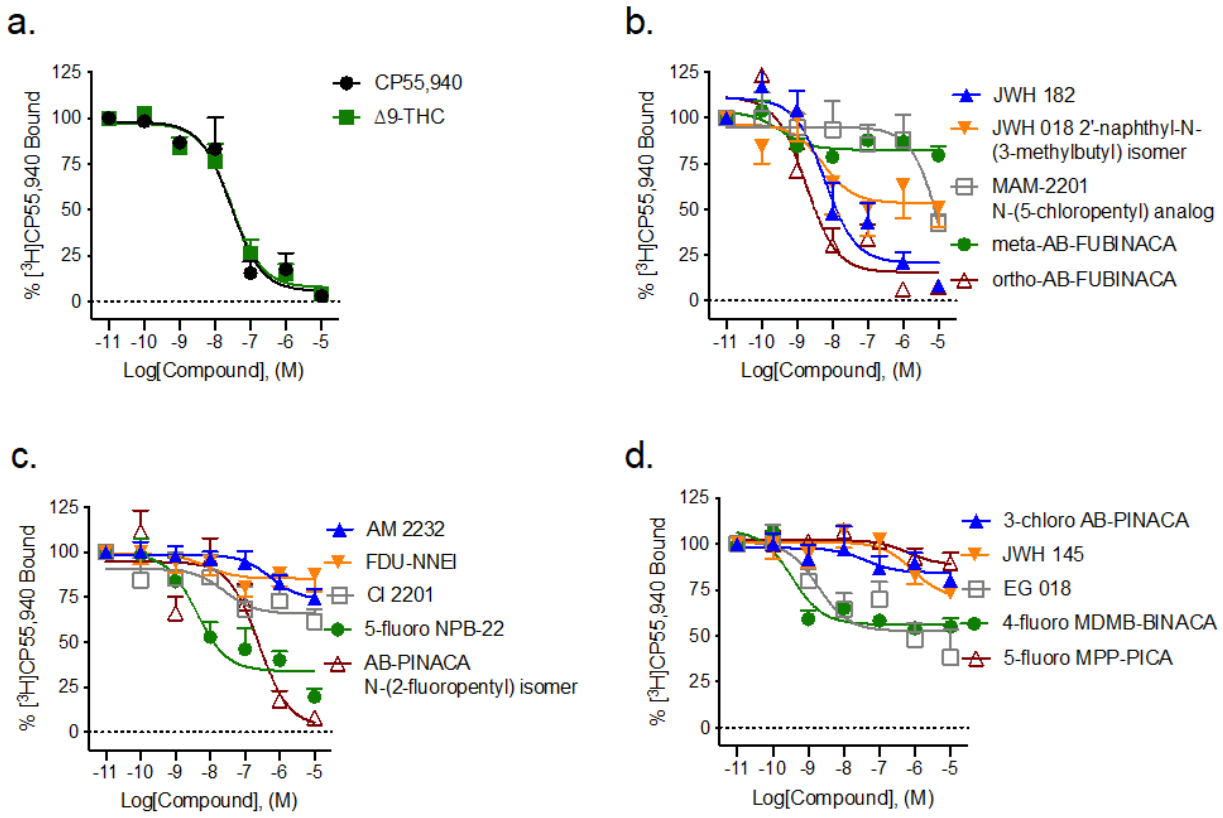

Figure 4-6. (a,b,c,d) Radioligand binding of 1 nM [^{3}H]CP55,940 to membranes from CB2R CHO-K1 cells. CB2R CHO-K1 cells were treated with 0.10 nM – 10 µM compounds in the presence 1 nM [^{3}H]CP55,940. Data are expressed as % radioligand bound or % stimulation above baseline (i.e. vehicle) levels. Data were fit to a nonlinear regression (4-parameter model, GraphPad v. 9.0) to determine K_D, EC_{50}, and E_{max}. Data are mean ± SEM (E_{max}) or 95% CI (K_D, EC_{50}); n ≥ 6 independent experiments. *p < 0.05 compared to CP55,940 as determined by one-way ANOVA followed by Bonferroni's post-hoc test or non-overlapping 95% CI.

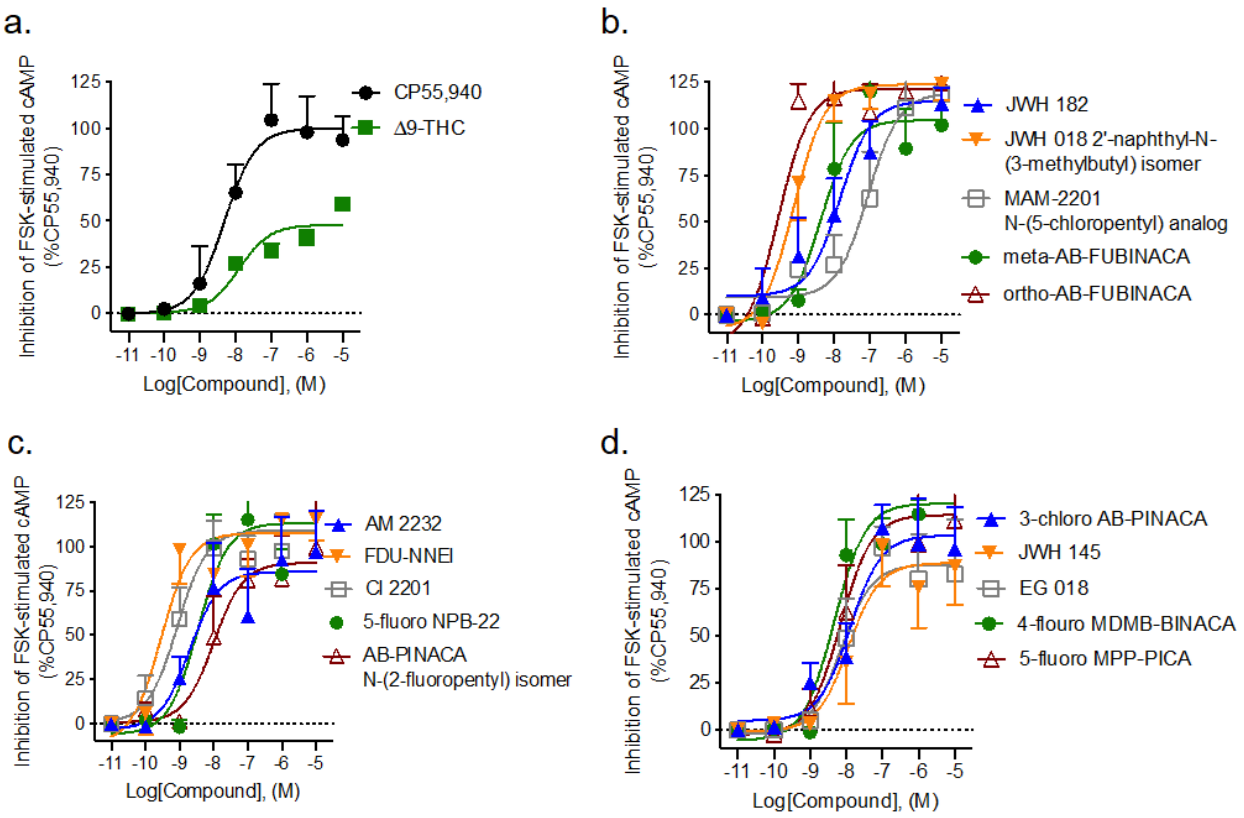

Figure 4-7. CB2R CHO-K1 were treated with 0.10 nM – 10 µM GAT compounds. (a,b,c.d) cAMP inhibition of GAT compounds as agonists. (a,b,d,e). Data are expressed as % CP55,940 max. Data were fit to a nonlinear regression (4-parameter model, GraphPad v. 9.0) to determine EC_{50} and E_{max}. Data are mean ± SEM (E_{max}) or 95% CI (EC_{50}); *n ≥ 6 independent* experiments performed in triplicate. *p < 0.05 compared to CP55,940 as determined by one-way ANOVA followed by Bonferroni's post-hoc test or non-overlapping 95% CI. Concentration-response data were fit to the operational model of Black and Leff (1983) (GraphPad v. 9.0).

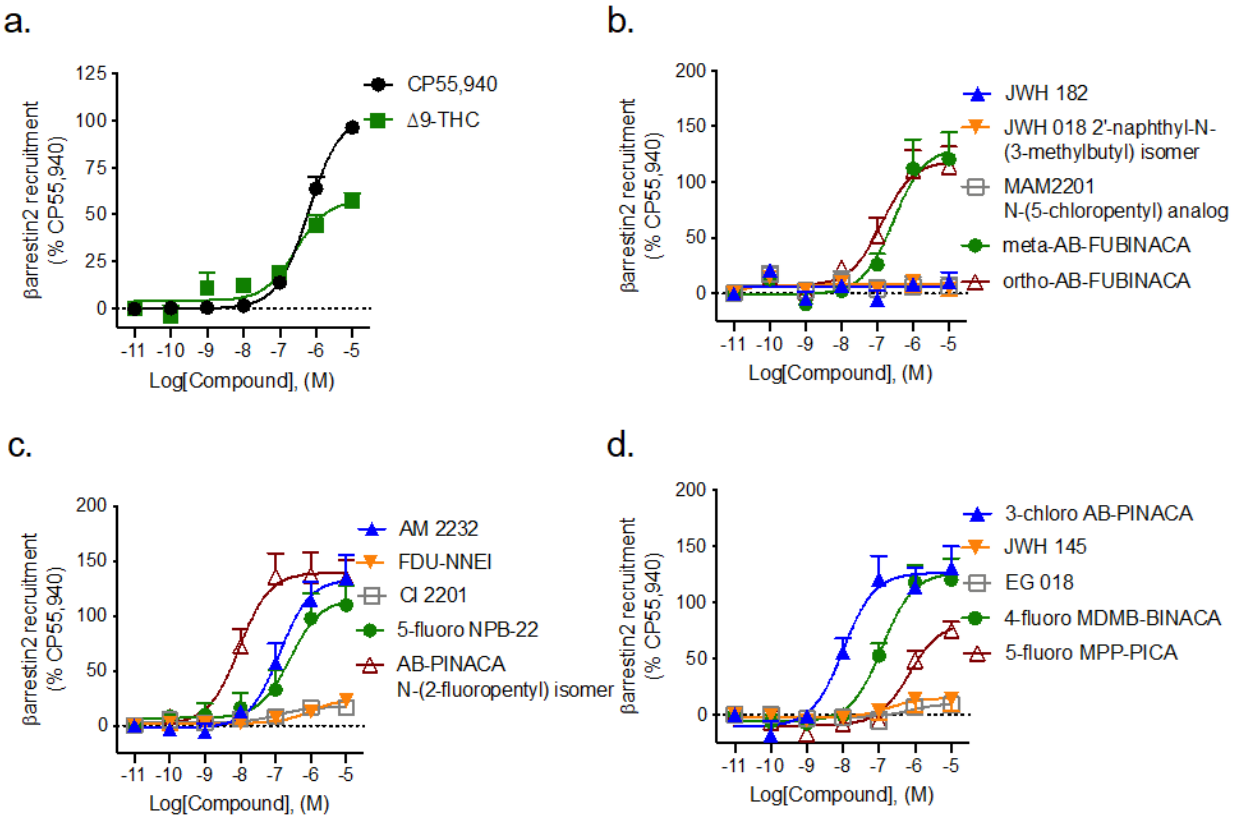

Figure 4-8. CB2R CHO-K1 were treated with 0.10 nM – 10 µM GAT compounds. (b,c,d,e) βarrestin2 recruitment of GAT compounds as agonists (a,b,c,d). Data are expressed as % CP55,940 max. Data were fit to a nonlinear regression (4-parameter model, GraphPad v. 9.0) to determine EC_{50} and E_{max}. Data are mean ± SEM (E_{max}) or 95% CI (EC_{50}); n ≥ 6 independent experiments performed in triplicate. *p < 0.05 compared to CP55,940 as determined by one-way ANOVA followed by Bonferroni's post-hoc test or non-overlapping 95% CI.

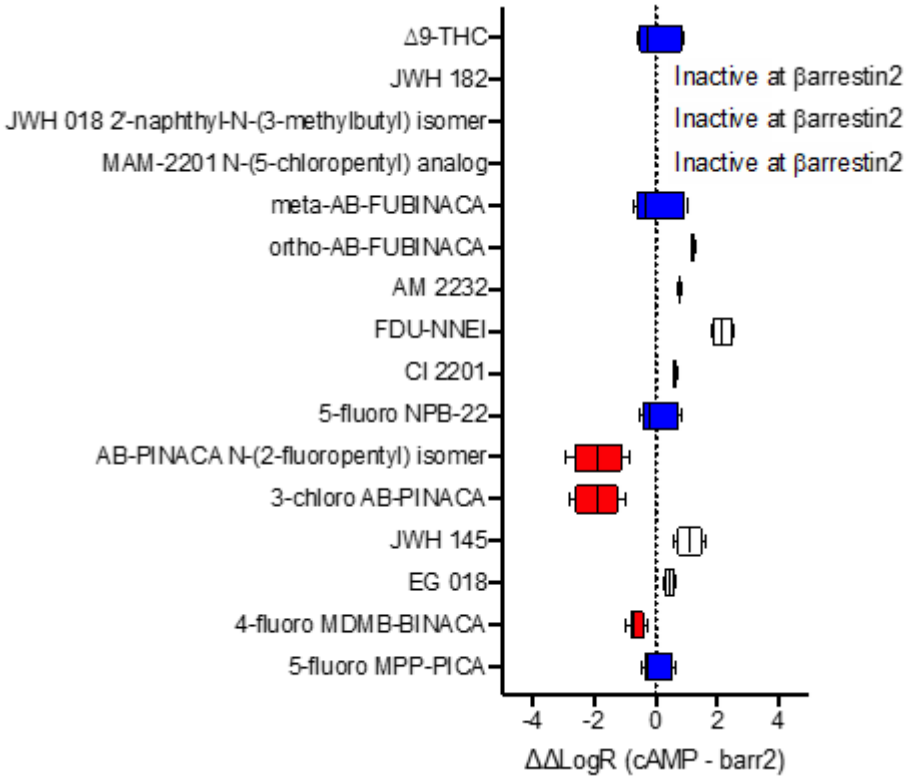

Figure 4-9. CB2R SCRA bias. Compound bias between cAMP inhibition and βarrestin2 recruitment [ΔΔLogR (cAMP - βarrestin2)] is shown here for data presented. Data were fit to the operational model to calculate bias. Data are mean with 95% CI, $n \geq 6$ independent experiments performed in triplicate. Values > 0 represent cAMP bias (white), values < 0 represent βarrestin2 bias (red), and values not different from 0 are unbiased (blue) as determined by 95% CI not overlapping with 0.

Table 4-1. Activity of SCRAs at CB1R and CB2R

Compound	CB1R						CB2R					
	[^{3}H]CP55,940		cAMP Inhibition		βarrestin2 recruitment		[^{3}H]CP55,940		cAMP Inhibition		βarrestin2 recruitment	
	K_i (nM)	E_{min} (%)	EC_{50} (nM)	E_{max} (%)	EC_{50} (nM)	E_{max} (%)	K_i (nM)	E_{min} (%)	EC_{50} (nM)	E_{max} (%)	EC_{50} (nM)	E_{max} (%)
CP55,940	13 (5.6-33)	0.0 ± 5.2	7.7 (0.13-14)	100 ± 6.2	1,500 (960-2,500)	100 ± 5.6	29 (13-67)	0.0 ± 5.6	5.0 (0.92-24)	100 ± 9.6	559 (410-761)†	100 ± 3.4
Δ^9-THC	14 (7.9-27)	9.1 ± 1.3	36 (21-63)*	72 ± 1.7*	1,400 (540-4,300)	28 ± 9.8*	31 (15-62)	65 ± 7.6*	13 (2.8-61)	48 ± 3.8*†	320 (79-730)	58 ± 1.1*†
JWH 182	0.77 (0.45-1.3)*	17 ± 2.2	24 (2.2-280)	78 ± 9.4	1,600 (720-3,100)	110 ± 9.2	6.2 (2.3 - 18)	21 ± 1.7*†	25 (3.2-210)	120 ± 11†	> 10,000[$]	13 ± 1.8*†
JWH 018 2'-naphthyl-N-(3-methylbutyl) isomer	0.93 (0.51-1.8)*	9.6 ± 2.7	98 (9.6-310)	80 ± 9.1	> 10,000	4.9 ± 0.51*	7.5 (2.6-41)	54 ± 3.5*†	0.52 (0.01-4.2)†	110 ± 9.2	> 10,000	6.1 ± 1.3*
MAM2201 N-(5-chloropentyl) analog	10 (5.9-17)	5.3 ± 3.0	2.8 (0.83-9.4)	98 ± 8.7	> 10,000	17 ± 2.7*	> 10,000[$]	40 ± 3.8*†	580 (41-1,400)*†	120 ± 25	> 10,000	5.5 ± 1.9*
meta-AB-FUBINACA	16 (7.1-37)	30 ± 2.9*	5.7 (0.64-100)	91 ± 12	> 10,000	22 ± 6.9*	0.63 (0.15-7.4)*	89 ± 6.3*†	5.4 (2.2-14)	86 ± 13	280 (93-430)[$]	130 ± 3.7*†

ortho-AB-FUBINACA	2.7 (0.77-10)	16 ± 5.4	3.6 (0.35-31)	83 ± 8.4	810 (560-1,100)	280 ± 11*	0.93 (0.04-2.4)*	17 ± 1.2	0.06 (0.001-3.1)	110 ± 6.7	140 (44-460)†	120 ± 3.1*†
AM 2232	0.31 (0.001-2.9)*	66 ± 3.6*	190 (67-700)*	100 ± 9.3	> 10,000	68 ± 1.6*	600 (430-1,100)*	73 ± 6.2*	1.7 (0.48-16)†	86 ± 1.9	130 (45-370)*	130 ± 19*†
FDU-NNEI	14 (2.2-71)	41 ± 2.8	1.0 (0.12-9.8)	96 ± 8.1	> 10,000	49 ± 8.2*	8.8 (1.8-39)	85 ± 8.1*†	0.01 (0.001-7.1)	103 ± 7.1	1,000 (390-1,300)	25 ± 1.3*†
Cl 2201	0.09 (0.001-5.4)*	76 ± 2.8*	2.6 (1.2-5.8)	89 ± 3.9	> 10,000	16 ± 1.0*	26 (7.8 - 82)	66 ± 2.5*	1.0 (0.07-8.3)	110 ± 8.4	120 (33-560)	17 ± 1.1*
5-fluoro NPB-22	47 (20-110)	2.3 ± 7.8	53 (8.2-200)	96 ± 7.0	830 (500-1,300)	210 ± 12*	4.3 (0.78-24)	34 ±8.1*†	3.2 (1.3-7.5)	110 ± 7.6	280 (65-580)	120 ± 3.7*†
AB-PINACA N-(2-fluoropentyl) isomer	1.6 (0.08-11)	76 ± 6.2*	7.3 (0.61-100)	75 ± 7.5*	240 (140-450)*	204 ± 10*	270 (97-780)*	2.8±8.1†	10 (1.8-46)	91 ± 3.2	9.4 (3.2-27)*†	140 ± 12*†
3-chloro AB-PINACA	170 (24-740)	65 ± 5.1*	0.04 (0.001-0.22)	94 ± 2.8	140 (93-200)*	340 ± 11*	52 (8.9-94)	84 ± 4.3*	19 (5.9-110)†	87 ± 15	8.8 (3.0-24)*†	130 ± 4.5*†
JWH 145	110 (21-800)	69 ± 7.6*	0.03 (0.001-1.5)	82 ± 9.3	> 10,000	27 ± 9.0*	860 (560-1,300)*	70 ± 6.1*	61 (2.7-200)†	86 ± 17	190 (37-520)	15 ± 1.7*

EG 018	8.6 (0.68-76)	68 ± 6.1*	450 (69-2,900)*	104 ± 18	> 10,000	5.2 ± 0.54*	1.9 (0.27-8.0)*	53 ± 4.0*	51 (5.2-580)	85 ± 17	770 (350-1,700)	10 ± 1.9*
4-fluoro MDMB-BINACA	99 (14-890)	52 ± 7.5*	10 (1.8-83)	87 ± 5.6	88 (49-150)*	240 ± 10*	0.41 (0.02-8.1)*	57 ± 11*	0.56 (0.05-22)	95 ± 11	120 (53-250)*	130 ± 8.2*†
5-fluoro MPP-PICA	1,200 (160-3,200)*	59 ± 18*	6.4 (1.3-30)	92 ± 6.8	> 10,000	170 ± 9.8*	540 (150-780)*	89 ± 6.3*	12 (1.5-77)	110 ± 13	630 (250-1,100)[$]	82 ± 1.9*†

4.3.3 In Silico Evaluation of CB1R and CB2R

All 15 cannabinoids studied bind to the orthosteric site of CB1R and CB2R (***Figure 4-10***). Shown in ***Figure 4-10*** is JWH 018 2'-naphthyl-N-(3-methylbutyl) isomer bound to CB1R (a) and CB2R (b). Two interactions are conserved between both CB1R and CB2R in terms of the binding of JWH 018 2'-naphthyl-N-(3-methylbutyl) isomer (***Figure 4-10***, ***Table 4-2*** and ***Table 4-3***), namely the H-bond with S7.39 and the T-shaped π- π interaction H2.65 (***Figure 4-10***, ***Table 4-2*** and ***Table 4-3***). Furthermore, the similarity in interactions of the synthetic cannabinoids (***Table 4-2*** and ***Table 4-3***) with both CB1R and CB2R suggests that the binding sites are well conserved between both receptors likely due to nearly identical amino acid sequence between these 2 GPCRs. In 9/15 cannabinoids the ketone H-bonds with $S383^{7.39}$ on CB1R while for all of the cannabinoids the ketone H-bonds to $S285^{7.39}$ on CB2R which suggests that this is the most conserved interaction (***Table 4-2*** and ***Table 4-3***).

Because the amino acid sequence and binding sites are well conserved among CB1R and CB2R the interaction energy was calculated for each cannabinoid as a predictive metric that can be used to compare the relative affinity of each cannabinoid at each receptor (***Table 4-2*** and ***Table 4-3***). This metric would predict JWH-182, JWH 018 2'-naphthyl-N-(3-methylbutyl) isomer, MAM2201 N-(5-chloropentyl) analog, Cl 2201, AB-PINACA N-(2-fluoropentyl) isomer, JWH 145 and 4-fluoro MDMB-BINACA to have higher affinity at CB1R (***Table 4-2***) while meta-AB-Fubinaca, ortho-AB-Fubinaca, AM 2232, FDU-NNE1, 5-fluoro NPB-22, 3-Chloro AB-PINACA, EG 018 and 5-fluoro MPP-PICA to have higher affinity at CB2R (**Table *4-3***). The modeling predictions except for AM 2232 agreed with experimental binding affinities measured in terms of which receptor each cannabinoid has higher affinity at when comparing CB1R to CB2R. Because the calculated interaction energy for AM 2232 is a more negative number at CB2R it would suggest

that the affinity is higher at CB2R, but our experimental binding affinity values suggests the opposite. However, in **Figure *4-12*** there is no correlation between the experimentally determined K_i values by radioligand binding and computationally determined MMGBSA values when comparing values within the same receptor. Although this model has been successful in showing correlation between non-GPCR molecular targets it has failed to do so for GPCR's.[144,145] The purpose in running this model for GPCR's is has been shown to discriminate active from inactive compounds.[145]

If we compare the highest affinity CB1R agonist (Cl 2201) to the weakest affinity CB1R agonist (JWH 145) we can understand the structural features that make a high affinity CB1R agonist. Firstly, the main structural difference between Cl 2201 and JWH 145 is that in Cl 2201 the benzene ring is fused to the pyridine vs in JWH 145 it is a branched benzene ring. Because of this the two cannabinoids only share 1 similar interaction being $F268^{ECL2}$ (***Table 4-2***). In fact, JWH 145 only has 2 electrostatic interactions with CB1R (***Table 4-2)***. However, if we compare Cl 2201 with MAM2201, which are very similar structurally, we can likely see what interactions are important for CL 2201's high affinity for CB1R. The major difference between these two structures is that MAM 2201 has a methyl coming off the naphthalene group whereas Cl 2201 has a chlorine coming off (***Figure 4-1***). The other difference is that MAM 2201 has a choro pentyl whereas Cl 2201 has a fluorine. The binding poses of these cannabinoids are identical except for the $R182^{ECL1}$ halogen bond exhibited by Cl 2201 but not by MAM2201 which is the main structural feature that gives rise to Cl 2201's high affinity at CB1R.

Lastly, in ***Table 4-4*** we looked at the most G protein-biased compound JWH 018 2'-naphthyl-N-(3-methylbutyl) isomer and the most βarrestin2-biased compound 4F-MDMB-BINACA bound to 6N4B with and without the G protein. The reason for doing so is to show that the most G protein

biased compound (JWH 018 2'-naphthyl-N-(3-methylbutyl) isomer) shows a more negative interaction energy with the G protein bound which makes sense as this compound is G protein biased. In fact, JWH 018 2'-naphthyl-N-(3-methylbutyl) isomer is 3.78 kcal/mol more stable with the G protein bound than without the G protein bound (***Table 4-4***). The same analysis was conducted for the most biased βarrestin2-baised compound 4F-MDMB-BINACA. It was found that 4F-MDMB-BINACA without the G protein bound was 10.56 kcal/mol more stable that 4F-MDMB-BINACA with the G protein bound. It should be mentioned that the ideal method of running this experiment would be to include a calculation with βarrestin2 bound to CB1R or CB2R. However, this can not be performed because there does not yet exist a CB1R or CB2R crystal structure with βarrestin2 bound.

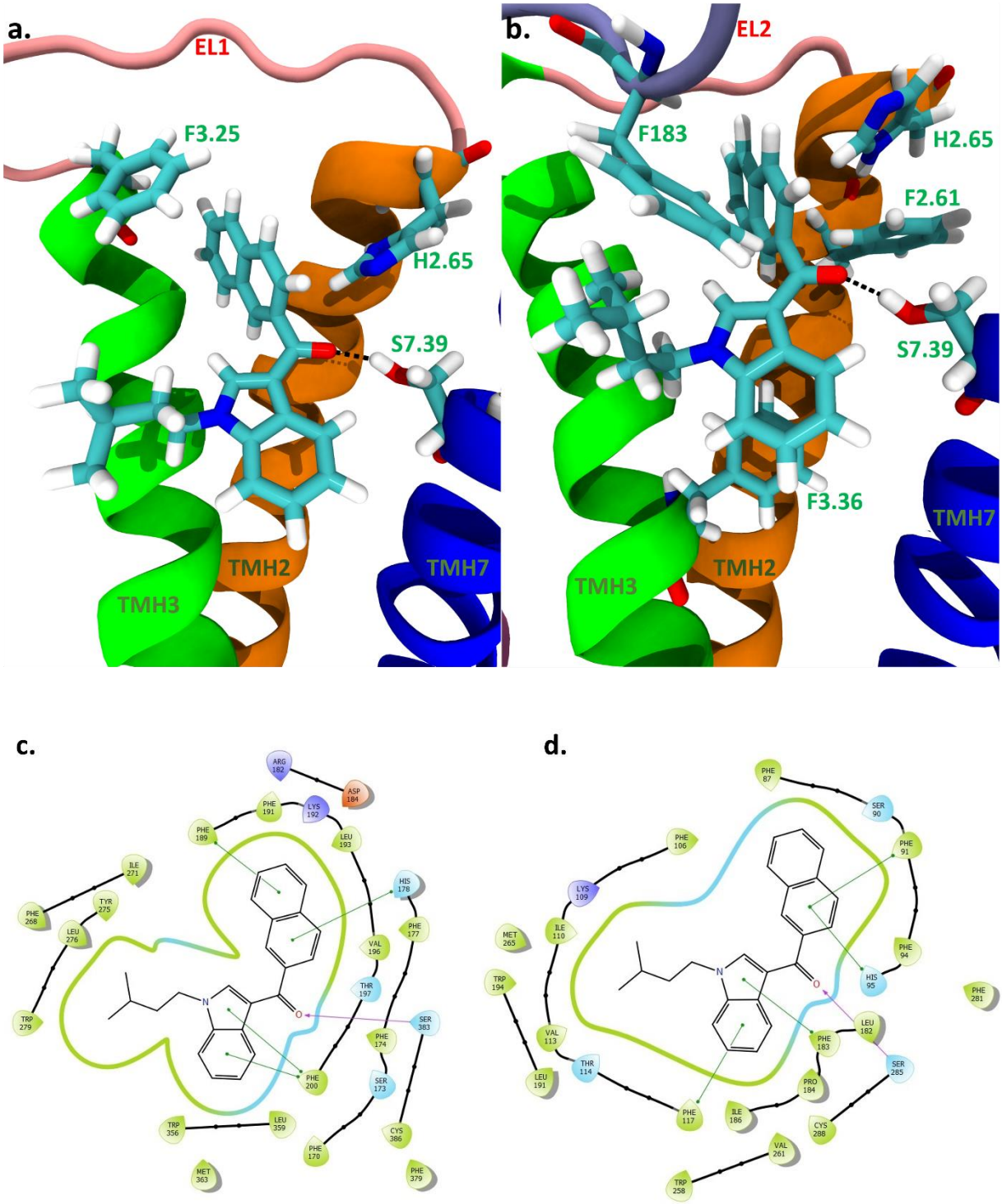

Figure 4-10. JWH 018 2'-naphthyl-N-(3-methylbutyl) isomer bound to CB1 (a) and CB2 (b) in 3D. (c) shows the interactions between JWH 018 2'-naphthyl-N-(3-methylbutyl) isomer and CB1 while (d) shows the interactions between JWH 018 2'-naphthyl-N-(3-methylbutyl) isomer and CB2

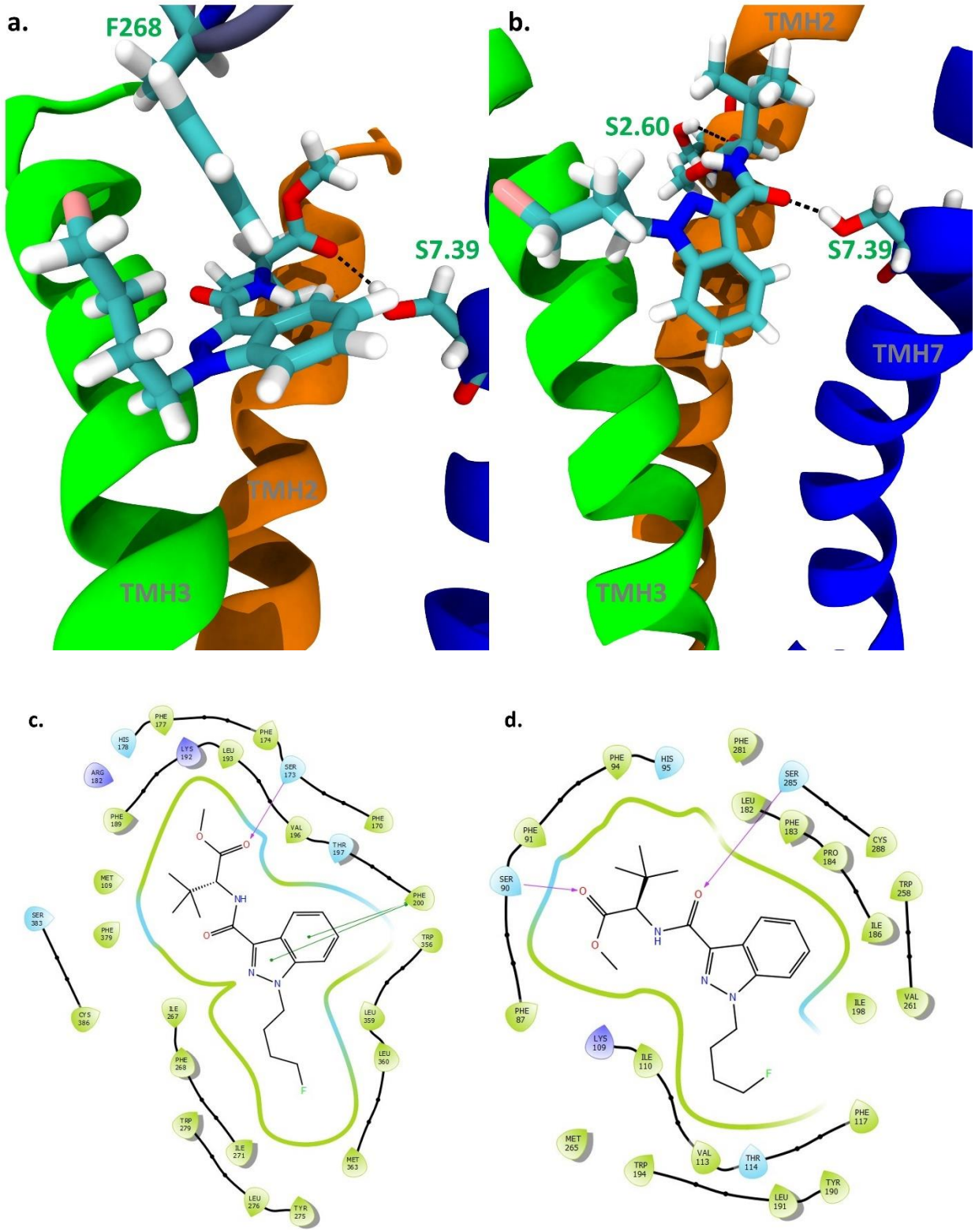

Figure 4-11. 4F-MDMB-BINACA. bound to CB1 (a) and CB2 (b) in 3D. (c) shows the interactions between 4F-MDMB-BINACA and CB1 while (d) shows the interactions between 4F-MDMB-BINACA and CB2.

Table 4-2. Summary of the interactions between the residues of the CB1R (PDB: 6N4B) and each of the synthetic cannabinoids. The right column additionally lists the interaction energy of each synthetic cannabinoid.

Compound	$F170^{2.57}$ π-π interaction	$S173^{2.60}$ H-bond	$F177^{2.64}$ π-π interaction	$H178^{2.65}$ H-bond	$H178^{2.65}$ π-π interaction	$R182^{ECL1}$ Halogen Bond	$F189^{3.25}$ π-π interaction	$F200^{3.36}$ π-π interaction	$F268^{ECL2}$ π-π interaction	$W279^{5.43}$ π-π interaction	$L376^{7.32}$ H-bond	$S383^{7.39}$ H-bond	Interaction energy (kcal/mol)
JWH-182					X			X	X	X		X	-132.75
JWH 018 2'-naphthyl-N-(3-methylbutyl) isomer					X		X					X	-118.41
MAM2201 N-(5-chloropentyl) analog			X		X			X	X			X	-128.37
meta-AB-Fubinaca										X		X	-121.84
ortho-AB-Fubinaca				X				X	X	X		X	-117.77
AM 2232	X								X		X		-113.89
FDU-NNE1			X	X			X		X	X		X	-114.64
Cl 2201			X		X	X		X	X			X	-123.69
5-fluoro NPB-22			X				X	X	X	X		X	-112.59
AB-PINACA N-(2-fluoropentyl) isomer		X	X										-116.02
3-Chloro AB-PINACA		X						X					-112.12
JWH 145									X	X			-134.03
EG 018		X	X				X		X				-126.92
4-fluoro MDMB-BINACA	X							X					-105.63
5-fluoro MPP-PICA		X						X				X	-107.13

Table 4-3. Summary of the interactions between the residues of the CB2R (PDB: 6PT0) and each of the synthetic cannabinoids. The right column additionally lists the interaction energy of each synthetic cannabinoid.

Compound	F87$^{2.57}$ H-bond	S90$^{2.60}$ H-bond	F91$^{2.61}$ π-π	F94$^{2.64}$ π-π interaction	H95$^{2.65}$ π-π interaction	T114$^{3.33}$ π-π	F117$^{3.36}$ π-π	F183^{ECL2} π-π	W194$^{5.43}$ π-π	W258$^{6.48}$ π-π	S285$^{7.39}$ H-bond	Interaction energy (kcal/mol)
JWH-182						X	X	X	X		X	-119.80
JWH 018 2'-naphthyl-N-(3-methylbutyl) isomer			X		X		X	X			X	-111.40
MAM2201 N-(5-chloropentyl) analog			X		X			X			X	-126.21
meta-AB-Fubinaca	X	X									X	-124.22
ortho-AB-Fubinaca	X	X							X		X	-118.99
AM 2232			X								X	-114.25
FDU-NNE1								X			X	-116.92
Cl 2201		X	X		X						X	-122.02
5-fluoro NPB-22			X	X						X	X	-123.90
AB-PINACA N-(2-fluoropentyl) isomer		X									X	-105.84
3-Chloro AB-PINACA	X	X					X				X	-115.84
JWH 145	X				X				X		X	-128.12
EG 018			X		X						X	-129.34
4-fluoro MDMB-BINACA								X			X	-112.01
5-fluoro MPP-PICA		X		X				X		X	X	-119.45

Table 4-4. The most G protein biased compound JWH 018 2'-naphthyl-N-(3-methylbutyl) isomer and the most biased βarrestin compound 4F-MDMB-BINACA bound to 6N4B with and without the G protein

Compound	Interaction Energy 6N4B w/o G Protein	Interaction Energy 6N4B w/G Protein	Bias
JWH 018 2'-naphthyl-N-(3-methylbutyl) isomer	-114.63	-118.41	G Protein
4F-MDMB-BINACA	-116.19	-105.63	βarrestin

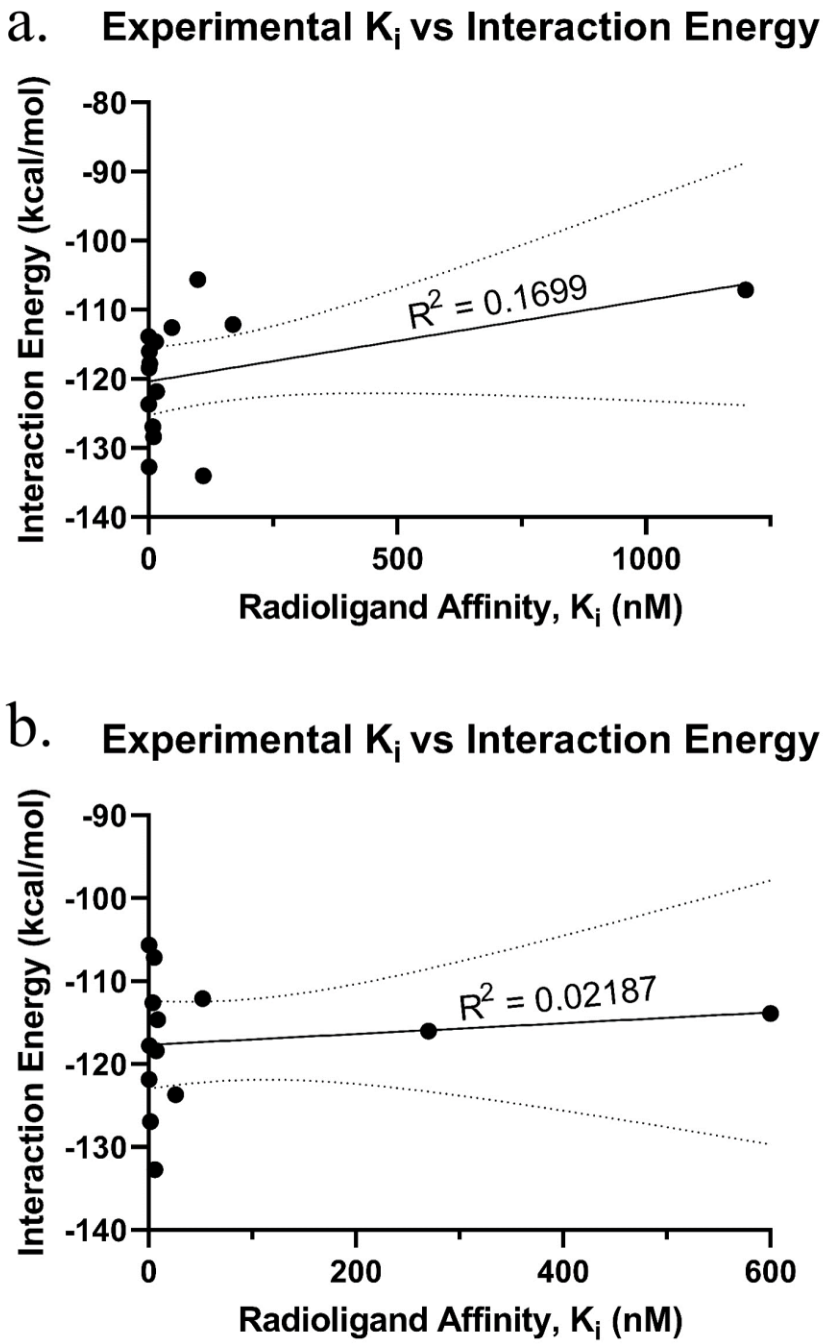

Figure 4-12. Experimentally determined K_i compared to computationally determined MM-GBSA to see if correlation exist for (a) CB1R and (b) CB2R. The dotted lines encompass the 95% confidence interval.

4.4 Conclusion

In summary it was observed that all SCRAs tested behaved as CB1R and CB2R agonists in the cAMP assay but not in the βarrestin2 assay. This suggests that for both CB1R and CB2R the ligand-receptor-G protein complex is better stabilized than the ligand-receptor- βarrestin2complex. However, a few SCRAs produced potent agonism in the βarrestin2 recruitment assay. Specifically, SCRAs with indazole cores rather than indole cores and halogen-substituted butyl or pentyl groups, such as 4-fluoro MDMD-BINACA, were the most-potent and most-efficacious agonists of βarrestin2 recruitment as CB1R and CB2R. The presence of an indole core rather than an indazole core (e.g. 5-fluoro MPP-PICA) or a halogen-substituted benzene rather than butyl or pentyl groups (e.g. meta and ortho AB-FUBINACA) abolished βarrestin2 activity; whereas moving the halogen from the terminal carbon toward the indazole core (e.g. AB-PINACA N-(2-fluoropentyl) isomer and 3-chloro AB PINACA) only reduced βarrestin2 activity. Similar studies have shown a consistent SAR between SCRA potency and efficacy and the incorporation of indazole cores and terminal halogen substitution to butyl and pentyl chains. The indazole core has been shown to have a stabilizing effect on the "twin toggle switch" ($F200^{3.36}$ and $W356^{6.48}$) that affords CB1R-$G\alpha_i$ interactions.[50,146,147]

The majority of *in silico* interactions made between SCRAs and either CB1R or CB2R are highly similar, with key homologous residues such as $Ser383^{7.39}$ (CB1R)/$Ser285^{7.39}$ (CB2R) and $His178^{2.65}$ (CB1R)/$His95^{2.65}$ (CB2R) present in our models and crystal structures of these receptors bound to SCRAs.[48,51,59] The shape and position of the binding pocket are retained and consistent for SCRAs at both CB1R and CB2R, with slight differences in amino acid interactions observed between cAMP-biased and βarrestin2-biased compounds (***Table 4-2***, ***Table 4-3***, ***Table 4-4***, ***Figure 4-10*** and ***Figure 4-11***). Perhaps most-intriguing is the observation that interaction energies differed

depending on the inclusion or exclusion of the G protein in our model. The highly βarrestin2-biased ligand 4-fluoro MDMB-BINACA incurred a 10.56 kcal/mol binding energy penalty in the presence of the G protein (***Table 4-4***). In contrast, the G protein-biased JWH 018 2'-naphthyl-N-(3-methylbutyl) isomer gained 3.78 kcal/mol in interaction energy in the presence of the G protein (***Table 4-4***). Although these static *in silico* models cannot recapitulate the dynamic interactions occurring between ligand and receptor *in vivo*, they do add support to the growing body of evidence for unique binding interactions for βarrestin2-biased ligands at the cannabinoid receptors.

Lastly this study elucidated which features of SCRAs lead to high affinity and potency SCRAs at CB1R and CB2R. For CB1R high affinity SCRAs had a naphthalene group linked to an alkyl substituted indole by a ketone (***Figure 4-1***), whereas low affinity ligands had functional groups with a high degree of rotatable bonds or non-fused aromatic rings in the naphthyl position. The highest affinity ligand Cl 2201 exhibited a halogen bond with the $R182^{ECL1}$ which is likely one of the features that leads to high affinity CB1R ligands. This could only be experimentally verified by performing site directed mutagenesis to an amino acid that can not participate in a halogen bond. It was also shown that *in silico* modelling could accurately discriminate a G protein-biased compound from a βarrestin2-biased compound.

CHAPTER 5

In Vitro and *In Silico* Evaluation of Methoxy Substituted 25H-NBOME Isomers at 5-$HT_{2A}R$

Copyright statement

Contribution statement

The manuscript used as the basis for this chapter was written by myself (*in silico* data) and Eline Pottie (*in vitro* data) with guidance from Drs. Robert B. Laprairie and Christophe Stove. *In vitro* data were collected by Eline Pottie whereas *in silico* data were collected by myself and analyses were conducted by myself and Eline Pottie with guidance from Dr. Robert Laprairie and Christophe Stove.

5.1 Introduction

Psychedelics are compounds that bind to and activate the serotonin 2a receptor (5-HT_{2A}R).[64] The term psychedelic is derived from 2 words; "psyche" which means mind and "delos" meaning manifesting.[148] This term was coined by Humphrey Osmond in 1957. There are 3 distinct known chemical scaffolds that are classified as psychedelics: (1) ergolines [compounds structurally similar to lysergic acid diethylamide (LSD) and ergotamine], (2) tryptamines (compounds structurally similar to psilocybin) and (3) phenylalkylamines (compounds similar to mescaline).[149] Within the phenethylamines, compounds can be further subdivided into 2C-X (phenethylamines), DOx (phenylisopropylamines) and 25X-NBOMe's (*N*-benzyl derivatives of 2C-X).[150] Although many of these compounds are considered controlled substances and illegal, grey market labs in Europe and Canada synthesize and sell derivatives of these compounds for those that wish to use these compounds recreationally.[151] Consequently, most 25X-NBOMe's can be acquired on the grey or illicit markets but their structure and function remain uncharacterized despite their potential to cause serious physical or psychiatric adverse events such as tachycardia, hypertension, convulsions, and dysphoria.[150] On the other hand, consideration of psychedelics as potential treatments for post traumatic stress disorder (PTSD) and depression is growing as the efficacy of LSD, psilocybin, and related chemicals is now being recognized in early stage clinical investigations.[152]

Substantial efforts have been made in the characterization of psychedelics and the receptors they bind to by the laboratories of Drs. Roth and Nichols.[29,71] Recently, structural data has been published showing both LSD and 25CN-NBOH (***Figure 5-1***) bound to 5-HT_{2A}R.[29,71] Being that 25CN-NBOH belongs to the NBOMe class, this crystal structure has vast potential to aid in the elucidation of how isomers of this compound influence the structure activity relationship (SAR)

of NBOMe compounds acting at 5-HT_{2A}R. In this study, we compared the potential of a set of 5 isomers of 25H-NBOMe to see how changing the position of the methoxy groups affects the SAR of this scaffold. Each number (24, 23, 26, 34 and 35) indicates the positions of the methoxy groups, i.e., 23H-NBOMe has a methoxy groups at the 2 and 3 position of the phenyl ring of the phenethylamine moiety of the molecule. Recently the synthesis and characterization of 25H-NBOMe has been described.[153] Functional characterization was performed by assessing the potential of these isomers to induce recruitment of cytosolic proteins to the activated 5-HT_{2A}R. To this end, we employed previously established bioassays, expressing either βarrestin2 or miniG_q with the 5-HT_{2A}R in the NanoBiT® system, in which a split nanoluciferase is functionally complemented following recruitment of the cytosolic protein to the activated 5-HT_{2A}R.[154,155] Additionally, each tested substance was docked to 5-HT_{2A}R based on adaptations of the above-mentioned published cryo-EM structure.[29]

5-HT_{2A}R is a G_q coupled GPCR which means that activation of the receptor produces an increase of intracellular Ca^{2+}.[156] G_q coupling to the receptor as well as recruitment of βarrestin2 are the most-utilized measurements for understanding biased agonism.[157] In the therapeutic context of psychedelics this is important as the βarrestin pathway is thought to be involved in hallucination in humans and head-twitch responses in rodents.[158] Further, it is both βarrestin -dependent and βarrestin–independent pathways that have been linked to psychedelic drug actions.[159] However, is it still unclear as to whether G protein or βarrestin biased compounds are favorable for the therapeutic aspect of psychedelics as this will likely be a deterministic factor for development of psychedelics.[160] It is likely the ligand bias profile will be specific for the condition treated.

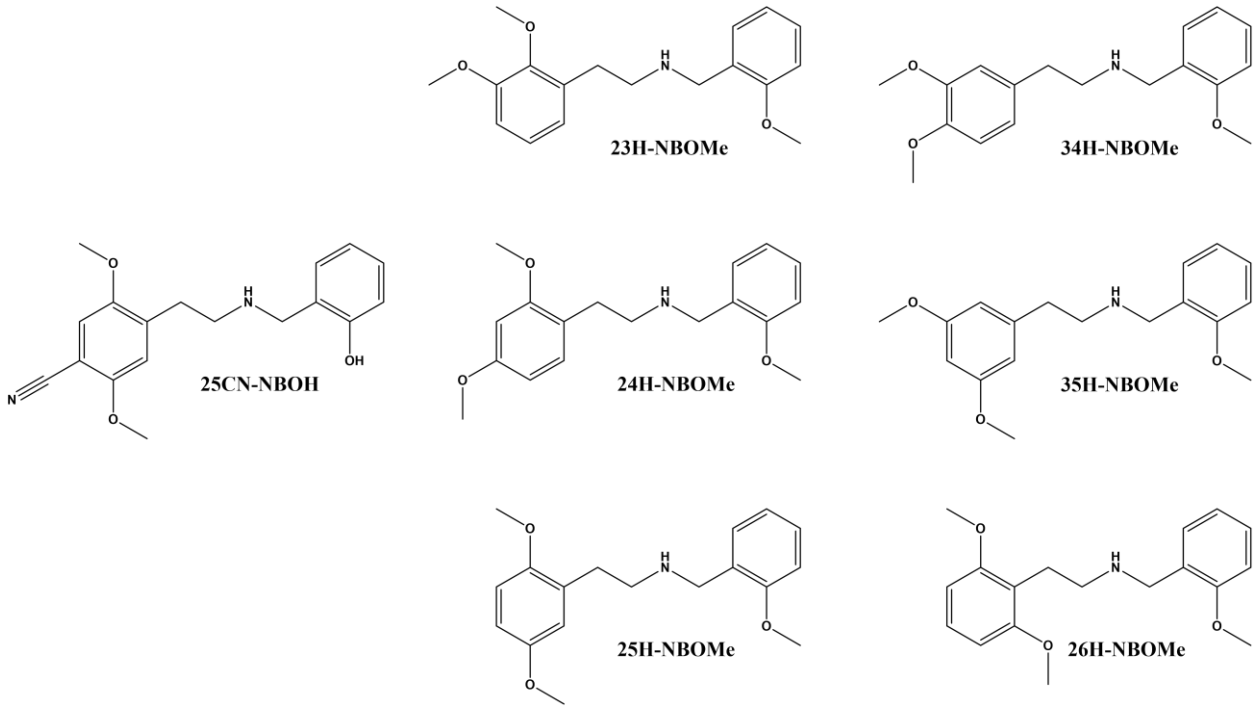

Figure 5-1. 25CN-NBOH is the co-crystallized ligand in PDB ID: 6WHA bound to 5-HT$_{2A}$R. The remaining compounds were tested in functional bioassays at 5-HT$_{2A}$R to elucidate the SAR of NBOMe Isomers

5.2 Materials and Methods

The methods described here are not the full methods. For the purposes of this dissertation, only methods which pertain to the *in vitro* and *in silico* data in ***Figure 5-2***, ***Figure 5-3***, ***Figure 5-4***, ***Table 5-1***, ***Table 5-2***, ***Table 5-3*** and ***Table 5-4*** are described. For the full methods see Pottie et al., 2021.[161]

5.2.1 Chemicals and Reagents

Dulbecco's Modified Eagle's Medium (DMEM, supplemented with GlutaMAX®), Hank's Balanced Salt Solution (HBSS) and penicillin/streptomycin (10,000 IU/mL and 10,000 µg/mL) were purchased from Thermo Fisher Scientific (Pittsburg, PA). The FuGENE® HD Transfection Reagent, Nano-Glo Live Cell reagent and the Nano-Glo LCS Dilution buffer were procured from Promega (Madison, WI). Fetal Bovine Serum (FBS), poly-D-lysine hydrobromide, methanol, and the analytical standards of LSD and serotonin were bought from Sigma-Aldrich (Overijse, Belgium). The analytical standard of 25H-NBOMe hydrochloride 2-(2,5-dimethoxyphenyl)-*N*-(2-methoxybenzyl)ethanamine was from Chiron AS (Trondheim, Norway). The positional isomers of 25H-NBOMe, depicted in ***Figure 5-1***, were synthesized as described previously, and dissolved in methanol.[162]

5.2.2 Data Processing and Analysis

The obtained time-luminescence profiles were corrected for inter-well variability and used for the calculation of the area under the curve (AUC), using either the full activation profiles of 2 h, or only the first 30 min, as described previously in more detail.[163] After subtraction of the AUC of the solvent control, the data were used for the fitting of a sigmoidal concentration-response curve through the four-parametric nonlinear regression model in GraphPad Prism software (San Diego, CA). For each separate experiment, the data were normalized to the maximal response of the

reference agonist, either LSD or serotonin, alternately set at 100% for a comparison between the obtained results. The data of all individual experiments were then pooled to determine the total EC_{50} and E_{max} values per substance.

5.2.3 Statistical Analysis

Data related to EC_{50} and E_{max} in ***Figure 5-2***, ***Table 5-1*** and ***Table 5-2*** were obtained with nonlinear regression models (4-parameter model, GraphPad Prism 9.0, San Diego, CA). Results were calculated as percent response relative to the reference agonist LSD or serotonin as percent stimulation above baseline. Significance was determined by non-overlapping 95% C.I. or by one-way ANOVA followed by Bonferroni's post-hoc test. $p < 0.05$ was considered significant. In order to calculate bias as displayed in ***Figure 5-3***, concentration-response curves were globally fit to the operational model (Eq. 2-1; Prism).[110] To best fit data, the transduction coefficient $\log(\tau/K_A)$ (*i.e.* logR), *n*, and E_{Max} were shared and $\log K_A$ was constrained between 0 and -15. Relative agonist activity compared to a reference agonist (CP55,940) was calculated as show in Eq. 2-2.[111] ΔlogR values were compared for test compounds between assays measuring inhibition of cAMP and βarrestin2 recruitment to determine bias factor (ΔΔlogR) Eq. 2-3.[112]

5.2.4 Molecular Docking

The recently published cryo-EM structure (PDW: 6WHA) of the 5-HT_{2A}R in complex with miniG_q and the psychedelic substance 25CN-NBOH was used as a starting template.[29] Each of the structures of the –NBOMe isomers and LSD and 25CN-NBOH (as controls) was built and optimized in Spartan '18 Parallel Suite (Wavefunction, Irvine, CA), and molecularly docked employing induced fit docking (Schrödinger, NY). To reduce atom clashing, ligand-receptor complexes were minimized using the OPLS3 force field in Prime (Schrödinger). Prime MMGBSA

(Schrödinger)(See section 3.1 and 3.2.3 for a more through description for MMGBSA) was used for the calculation of the amino acid interaction energy with the individual residues.

5.3 Results and Discussion

5.3.1 Pharmacological Characterization

To assess the functionality of the NBOMe positional isomers, the Nanoluciferase Binary Technology (NanoBiT®) was employed. This technique was specifically developed for the real-time monitoring of protein-protein interactions in live cells. To this end, two non-functional parts of the nanoluciferase are each fused to one of the potentially interacting proteins, in this case the 5-HT_{2A}R and a cytosolic protein. When an agonist activates the receptor, the cytosolic protein is recruited, leading to association of the split parts, which can be monitored via a luminescent readout in the presence of the enzyme's substrate.[164] A previously established bioassay to monitor the recruitment of βarrestin2, later complemented with an analogous miniG_q recruitment assay, allowing us to generate concentration-response curves.[154,155] These curves were used to compute the potency and efficacy of the compounds as compared to the reference agonist LSD which was set to 100% to serve as a positive control. Being that 5-HT_{2A}R is G_q coupled we also measured G_q activation to better elucidate the biased agonism nature of each compound. In both assays both serotonin and LSD were included as reference agonists. The data analysis was conducted using the AUC of either the first 30 min or the full 2-hour activation profile. This is because the on and off rate at which LSD associates with 5-HT_{2A}R is slow (k_{off} = 0.022 ± 0.004 min^{-1}) due to hydrophobic interaction with $L229^{ECL2}$.[71] Generally speaking, if a psychedelic interacts with $L229^{ECL2}$ both the on and off rate tend to be slower than that of a compound that does not interact with $L229^{ECL2}$. [29,71] Thus a 30-minute vs 2-hour time point can be used as a predicative measure as to if this interaction occurs or does not.

5.3.2 2-Methoxy NBOMe Compounds are more Potent than 3-Methoxy NBOMe Compounds

Table 5-1 shows differences in potency and efficacy of the methoxy substituted isomers. Being that 25H-NBOMe is the conventional NBOMe compound this was used as a comparative refence when looking at the other compounds. 25H-NBOMe yielded a low nM potency (EC_{50} = 11.4nM (6.36 - 20.4)) in the 5-HT_{2A}R βarrestin2 recruitment assay and a higher efficacy than LSD (E_{max} 164% relative to LSD). Only 1 of the isomers was slightly more potent than 25H-NBOMe: 24H-NBOMe yielded an EC_{50} value of 3.88 nM (2.33 - 6.37). The potency of 26H-NBOMe (8.70 nM (5.81 - 12.5)) is similar to that of 25H-NBOMe. The highest EC_{50} value (33.6 nM (19.8 - 57.3)) of all isomers with a 2-methoxy substituent, and hence the lowest potency, was observed for 23H-NBOMe. The least potent substances in the βarrestin2 recruitment assay appeared to be 34H-NBOMe and 35H-NBOMe, both lacking the 2-methoxy substituent. This change in the position of one of the methoxy groups drastically reduced in vitro potency yielding EC_{50} values in the higher nM range (248 nM (111 - 646) and 343 nM (187 - 645)). Although 25H-NBOMe had the highest efficacy (164%) the 95% confidence intervals of 24H-, 26H-, and 34H-NBOMe (145%, 156% and 147%) all overlap with 25H-NBOMe. Although the efficacies obtained for 23H-NBOMe (123%) and 35H-NBOMe (118%) were lower than that of 25H-NBOMe they both had higher efficacy than LSD and serotonin.

Table ***5-2*** serotonin showed the greatest efficacy (E_{max} = 305% relative to LSD). For the NBOMe isomers although 25H-NBOMe displayed the greatest efficacy the 95% confidence intervals of 24H-, 26H-, 34H- (171%, 162%, 156%) all overlap with 25H-NBOMe. While 23H-NBOMe was the only compound that showed less efficacy than LSD (89.6%), 35H-NBOMe's efficacy (107%) was only slightly greater than LSD (98.2%). In terms of potency as measured by EC_{50} LSD displayed the greatest potency (EC_{50} = 17.7 nM (10.1 - 38.6)). For the NBOMe isomers 24H-

NBOMe displayed the greatest potency (EC_{50} = 37.4 nM (20.6 - 66.4)) but the 95% confidence intervals of 25H- (EC_{50} = 86.2 nM (57.0 - 124)) and 26H-NBOMe (EC_{50} = 68.0 nM (38.6 - 115)) did overlap with 24H-NBOMe. 23H-NBOMe (EC_{50} = 236 nM (N.D.)) displayed the weakest potency of the 2-methoxy substituted NBOMe isomers. Similarly with the βarrestin2 recruitment assay in the miniG_q experiment 34H- (EC_{50} = 1321 nM (629-33780)) and 35H-NBOMe (EC_{50} = 1393 nM (N.D.)) displayed the weakest potency in terms of all the NBOMe isomers in the study.

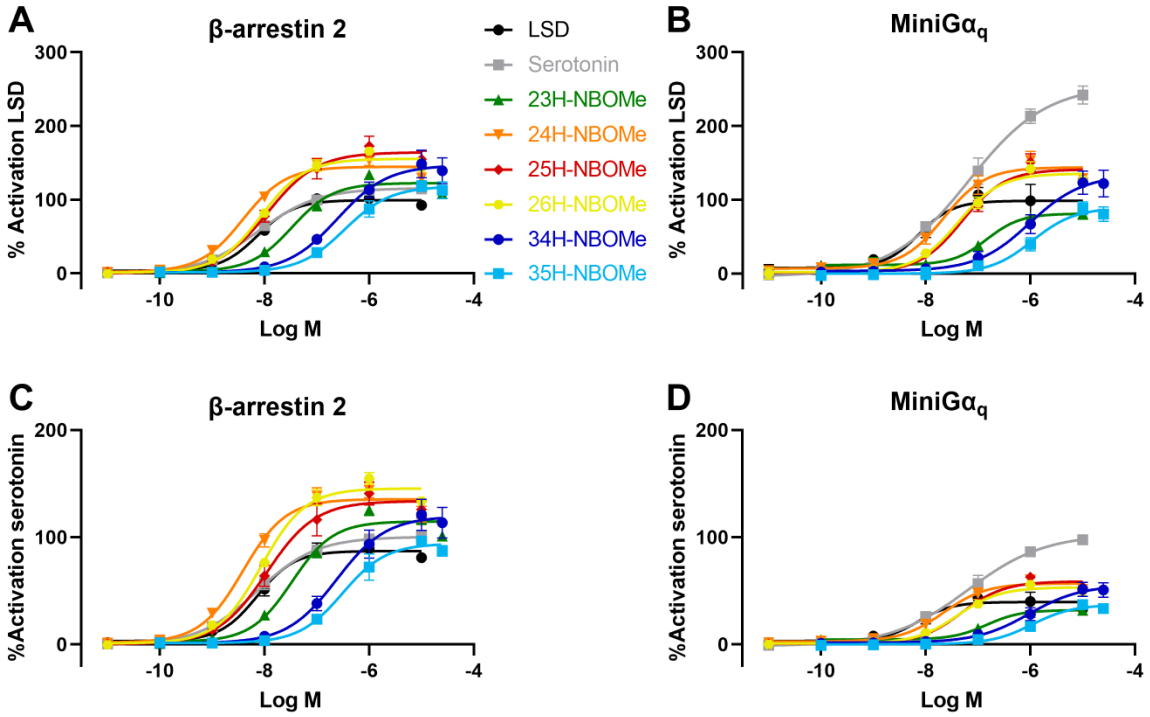

Figure 5-2. The concentration-response curves obtained by stimulation of the 5-HT$_{2A}$R followed by recruitment of (panels A and C) βarrestin2 or (panels B and D) miniG$_q$ constructs in the NanoBiT® system. Data points are given as the mean of 3 independent experiments (each performed in duplicate) ± SEM (Standard Error of the Mean). The AUC (Area Under the Curve) is normalized in each independent experiment for the maximum response (100%) of the reference agonist LSD (panels A and B) or serotonin (panels C and D).

Table 5-1. Summary of the potency (EC_{50}) and efficacy (E_{max}, where the E_{max} of either serotonin or LSD is set to 100%) values of all the tested compounds in the βarrestin2 assay, calculated using either the full 120 min activation profiles (upper half), or the first 30 min (lower half of the table). Both serotonin and LSD are highlighted in grey to indicate that they are set to 100% in each of the experiments. The structures of the compounds are provided in Figure 1. Data are from 3 independent experiments. CI: 95% confidence interval. N.D.: confidence interval not determined.

120 min activation profiles				
	Reference agonist LSD		**Reference agonist serotonin**	
Compound	**EC_{50} (nM, CI)**	**E_{max} (%, CI)**	**EC_{50} (nM, CI)**	**E_{max} (%, CI)**
LSD	7.43 (3.54 - 12.9)	100 (91 - 109)	7.29 (3.50 - 12.7)	87.1 (79.4 - 95.4)
Serotonin	7.62 (4.43 - 13.2)	116 (107 - 126)	7.24 (4.43 - 11.9)	100 (93.9 - 108)
23H-NBOMe	33.6 (19.8 - 57.3)	123 (115 - 131)	33.7 (19.7 - 57.9)	115 (107 - 123)
24H-NBOMe	3.88 (2.33 - 6.37)	145 (136 - 154)	3.89 (2.30 - 6.45)	136 (127 - 145)
25H-NBOMe	11.4 (6.36 - 20.4)	164 (151 - 180)	11.0 (5.60 - 21.5)	134 (121 - 148)
26H-NBOMe	8.70 (5.81 - 12.5)	156 (147 - 165)	8.74 (5.91 - 12.4)	146 (138 - 154)
34H-NBOMe	248 (111 - 646)	147 (129 - 182)	238 (101 - 691)	120 (104 - 152)
35H-NBOMe	343 (187 - 645)	118 (107 - 135)	310 (165 - 593)	94.1 (83.8 - 108)
30 min activation profiles				
	Reference agonist LSD		**Reference agonist serotonin**	
Compound	**EC_{50} (nM, CI)**	**E_{max} (%, CI)**	**EC_{50} (nM, CI)**	**E_{max} (%, CI)**
LSD	24.3 (N.D.)	100 (91 - 110)	23.8 (N.D.)	79.4 (72.0 - 87.3)
Serotonin	11.5 (7.13 - 18.9)	128 (119 - 139)	10.9 (7.60 - 15.8)	100 (94.8 - 106)
23H-NBOMe	74.4 (55.8 - 95.9)	133 (128 - 139)	74.5 (53.9 - 98.8)	114 (109 - 119)
24H-NBOMe	8.34 (6.11 - 11.1)	154 (147 - 161)	8.32 (5.85 - 11.5)	132 (125 - 139)
25H-NBOMe	24.3 (13.4 - 45.0)	179 (163 - 199)	22.9 (12.8 - 41.8)	130 (118 - 143)
26H-NBOMe	16.3 (13.0 - 20.8)	165 (159 - 172)	16.4 (12.4 - 22.0)	142 (135 - 149)
34H-NBOMe	488 (226 - 1707)	162 (142 - 218)	458 (191 - 2287)	118 (101 - 171)
35H-NBOMe	678 (385 - 1295)	137 (123 - 162)	625 (353 - 1148)	98.5 (88.8 - 115)

Table 5-2. Summary of the potency (EC_{50}) and efficacy (E_{max}, where the E_{max} of either serotonin or LSD is set to 100%) values of all the tested compounds in the miniG_q recruitment assay, calculated using either the full 120 min activation profiles (upper half), or the first 30 min (lower half of the table). Both serotonin and LSD are highlighted in grey to indicate that they are set to 100% in each of the experiments. Data are from 3 independent experiments. CI: 95% confidence interval. N.D.: Confidence interval not determined.

120 min activation profiles				
	Reference agonist LSD		**Reference agonist serotonin**	
Compound	**EC_{50} (nM, CI)**	**E_{max} (%, CI)**	**EC_{50} (nM, CI)**	**E_{max} (%, CI)**
LSD	7.40 (1.82 - 17.7)	100 (84 - 115)	7.23 (1.73 - 17.5)	39.6 (33.7 - 46.0)
Serotonin	66.4 (35.5 - 151)	256 (230 - 301)	63.5 (33.9 - 143)	103 (92.5 - 121)
23H-NBOMe	147 (71.8 - 436)	81.2 (70 - 102)	146 (73.8 - 408)	31.9 (27.5 - 39.6)
24H-NBOMe	22.1 (12.1 - 42.1)	144 (129 - 161)	22.2 (12.4 - 41.6)	56.9 (51.2 - 63.4)
25H-NBOMe	49.6 (27.2 - 84.8)	141 (128 - 155)	49.2 (26.6 - 85.4)	58.8 (53.3 - 64.9)
26H-NBOMe	40.9 (23.7 - 68.2)	136 (124 - 148)	40.9 (23.9 - 67.7)	53.3 (48.8 - 58.2)
34H-NBOMe	974 (N.D.)	134 (N.D.)	947 (N.D.)	55.3 (45.6 - 297)
35H-NBOMe	1097 (N.D.)	89.1 (74 - 219)	1087 (N.D.)	37.1 (30.5 - 112)
30 min activation profiles				
	Reference agonist LSD		**Reference agonist serotonin**	
Compound	**EC_{50} (nM, CI)**	**E_{max} (%, CI)**	**EC_{50} (nM, CI)**	**E_{max} (%, CI)**
LSD	17.7 (10.1 - 38.6)	98.2 (85 - 114)	16.3 (8.59 - 38.7)	31.9 (27.4 - 37.2)
Serotonin	88.5 (46.1 - 213)	305 (272 - 365)	62.2 (22.5 - 269)	87.9 (74.4 - 121)
23H-NBOMe	236 (N.D.)	89.6 (75 - 112)	191 (N.D.)	27.1 (22.6 - 33.3)
24H-NBOMe	37.4 (20.6 - 66.4)	171 (155 - 189)	35.1 (17.5 - 68.7)	54.3 (48.5 - 61.2)
25H-NBOMe	86.2 (57.0 - 124)	181 (167 - 196)	129 (69.2 - 263)	74.8 (65.6 - 88.8)
26H-NBOMe	68.0 (38.6 - 115)	162 (147 - 181)	68.3 (34.0 - 129)	51.9 (46.0 - 59.4)
34H-NBOMe	1321 (629-33780)	156 (130 - 340)	1334 (N.D.)	51.8 (N.D.)
35H-NBOMe	1393 (N.D.)	107 (94 - 163)	1296 (683–10760)	48.3 (41.0 - 83.6)

5.3.3 NBOMe compounds display biased agonism towards βarrestin2 over G_q Pathway

Previous research has shown that the *N*-benzyl substituted 25H analogues 25H-NBF, 25H-NBMD and 25H-NBOH show a preference towards the recruitment of βarrestin2 over G_q over the reference compound LSD. [155] LSD does not preferentially activate recruitment of βarrestin2 (EC50 = 6.43 nM) over Gq (7.40 nM) as seen in ***Table 5-1*** and ***Table 5-2***. Because the potencies at both these pathways are not statistically different this is suggestive of non-biased agonism (***Figure 5-3***). Conversely, serotonin displayed biased agonism towards recruitment of βarrestin2 (EC_{50} = 7.62 nM) over G_q (EC_{50} = 66.4 nM) (***Figure 5-3)***. In fact, all of the NBOMe isomers display βarrestin2 biased agonism at 5-HT_{2A}R (***Figure 5-3***). While 24H-NBOMe displays the greatest biased agonism towards βarrestin2 35H-NBOMe displays the least. However, there does not seem to be a clear distinction of how isomerization of the methoxy group affects biased agonism.

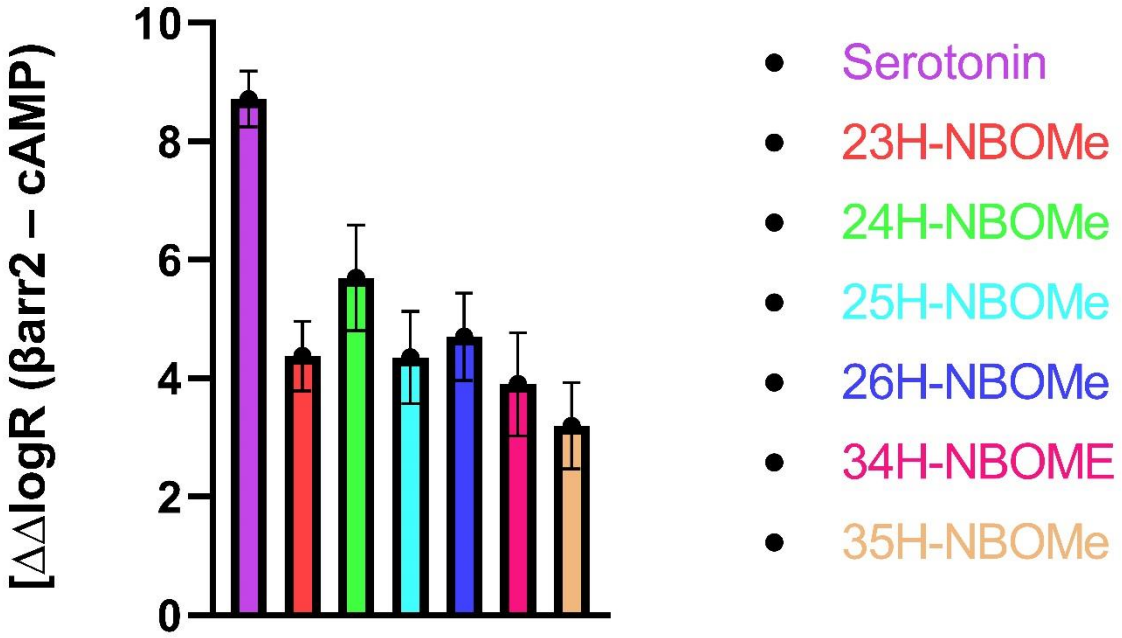

Figure 5-3. Concentration-response data were fit to the operational model of Black and Leff (1983) (GraphPad v. 9.0). Data are mean with 95% CI. *p < 0.05 compared to 0 as determined by non-overlapping 95% CI; n = 4 – 6. Agonist bias from the 2-hour time point data [ΔΔlogR (βarrestin2 – G_q)] between βarrestin2 recruitment and G_q.

5.3.4 Molecular Docking

Attempting to provide an explanation for the differences in potencies/efficacies observed for the isomers, molecular docking was performed, with a model based on adaptations of the recently published cryo-EM structure of the 5-HT_{2A}R in complex with 25CN-NBOH (PDB:6WHA).[29] ***Figure 5-4a*** shows the position of 24H-NBOMe in the orthosteric binding pocket of the receptor, in which all of the isomers bind. ***Figure 5-4c – h*** focuses on the specific interactions of the isomers, (and 25CN-NBOH in panel H) with the amino acid residues of the receptor, providing insight into the modeled interaction of specific residues with the methoxy groups. The model showed that all NBOMe isomers can be docked in the same binding pocket as 25CN-NBOH, despite the change of the hydroxyl group on the *N*-benzyl moiety into a methoxy group. This latter group specifically stabilizes the molecule through an H-bond with $S159^{3.36}$, and through hydrophobic interaction with $S159^{3.36}$, $W336^{6.48}$ and $S373^{7.46}$. The nitrogen atom is observed to form a salt bridge with $D155^{3.32}$, which has been previously defined as critical for receptor interaction, and the strength is emphasized by the interaction energies in ***Table 5-3***.[71,29] The *N*-benzyl moiety is stabilized in the binding pocket by hydrophobic interactions with $W336^{6.48}$ and $F339^{6.51}$, and both the *N*-benzyl moiety and the phenyl group of the phenethylamine function are stabilized by interaction with $F340^{6.52}$ (***Table 5-3***). The reference compound LSD interacts with $S242^{5.46}$ stronger than NBOMe compounds due to an H-bond between the indole on LSD and $S242^{5.46}$, which NBOMes cannot participate in (***Table 5-4***).

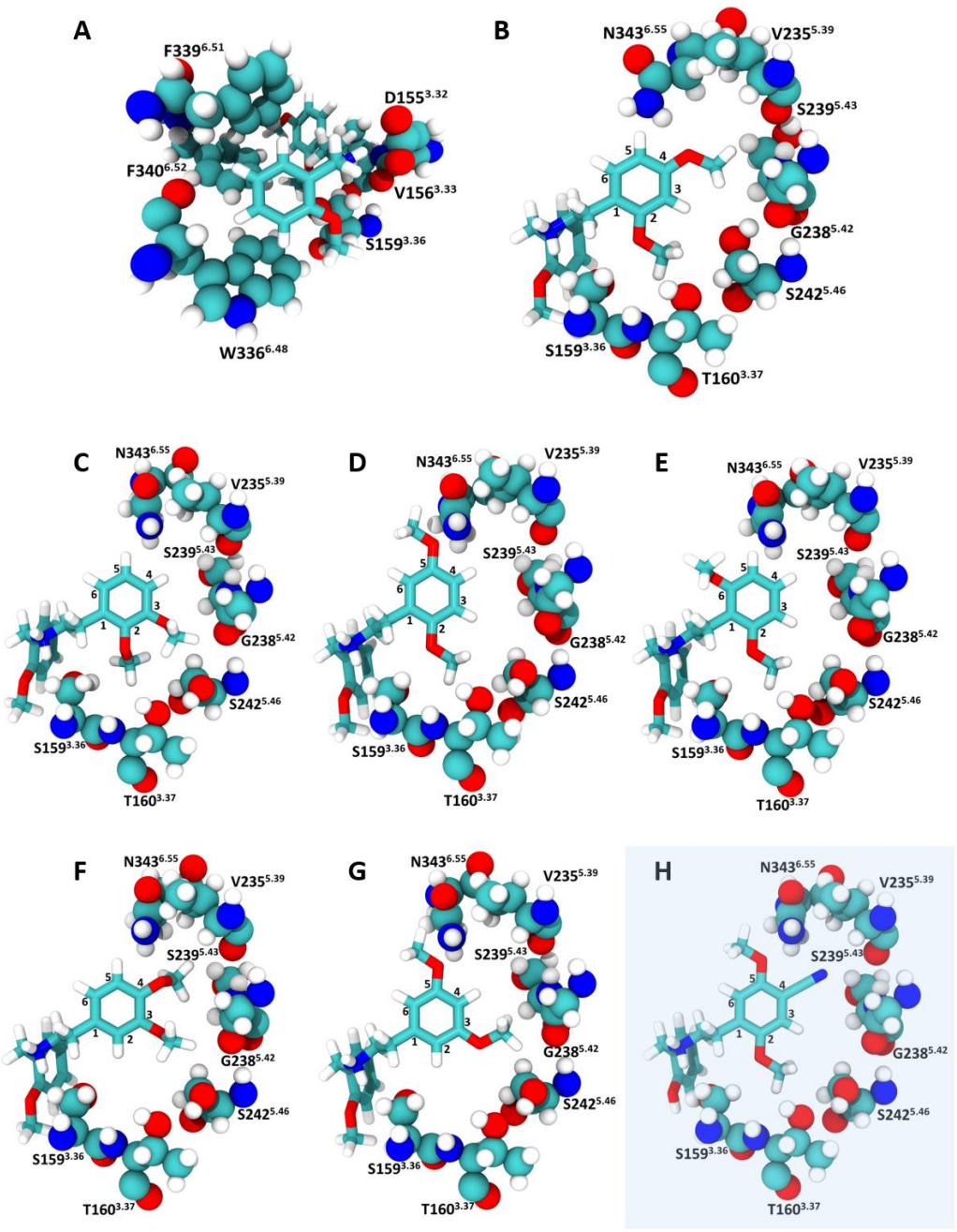

Figure 5-4. Visual representations of the NBOMe isomers and 25CN-NBOH docked into the binding pocket of the 5-HT$_{2A}$R (based on PDB: 6WHA).[29] A) 24H-NBOMe, as seen from the perspective of the N-benzyl moiety; B-H) substances bound to the 5-HT$_{2A}$R looking from the perspective of the phenyl group, with specific mentioning of the residues interacting with the methoxy groups on the phenethylamine moiety. B) 24H-NBOMe, C) 23H-NBOMe, D) 25H-NBOMe, E) 26H-NBOMe, F) 34H-NBOMe, G) 35H-NBOMe, and H) 25CN-NBOH.

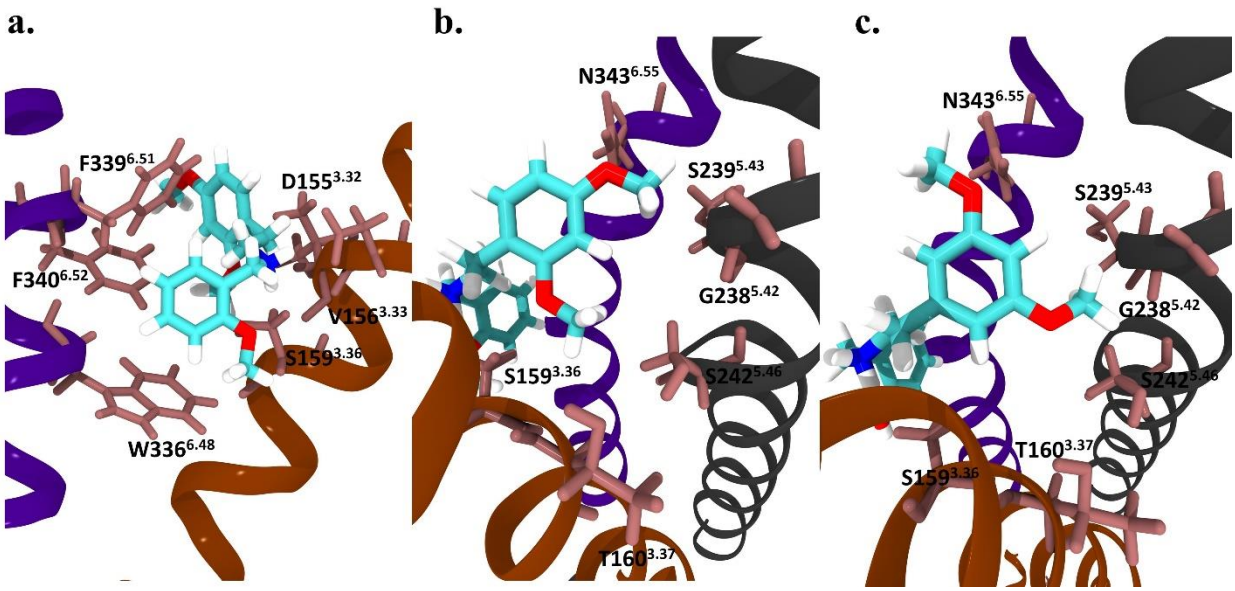

Figure 5-5. Visual representations of the NBOMe isomers docked into the binding pocket of the 5-HT$_{2A}$R with helices shown (based on PDB: 6WHA). (A) 24H-NBOMe, as seen from the perspective of the N-benzyl moiety; (B) 24H-NBOMe and (C) 35H-NBOMe bound to the 5-HT$_{2A}$R looking from the perspective of the phenyl group, with specific mentioning of the residues proposed to interact with the methoxy groups on the phenethylamine moiety.

Because of the ability of the utilized model to predict to a reasonable extent the interactions of LSD and 25CN-NBOH with the 5-HT_{2A}R, as described by Kim *et al.*[29], it was additionally used to assess the interactions with the methoxy groups of the phenethylamine moiety of the panel of NBOMe positional isomers. ***Table 5-4*** specifically focuses on the modeled interactions with these methoxy groups. A methoxy group on position 2 of the phenyl ring of the phenethylamine moiety (as is the case in 23H-, 24H-, 25H-, and 26H-NBOMe) hydrophobically interacts with $T160^{3.37}$, $S159^{3.36}$ and $V156^{3.33}$, as reflected by the weaker interaction (higher interaction energies) for substances without a methoxy group at this position. The model also proposes interactions between $G238^{5.42}$ and $S242^{5.46}$ and a methoxy group at position 3, as reflected by a weaker interaction of these residues with substances lacking a 3-methoxy group. For 25CN-NBOH, $G238^{5.42}$ interacts with the cyano group rather than with a methoxy group. The occurrence of a methoxy group at position 4 appears to be linked to a stronger interaction (lower interaction energies) with residues $S239^{5.43}$ and $V235^{5.39}$. Overall, substances containing a 5-methoxy group show a stronger interaction with residues $N343^{6.55}$ and $L229^{ECL2}$ than substances lacking that group, with the exception of 24H-NBOMe, where the 4-methoxy group may also interact with $N343^{6.55}$. However, the obtained values indicate substantially weaker interactions with these residues than those observed for LSD. Lastly, a methoxy group at position 6 contributes to the already strong interaction with $V156^{3.33}$ and $D155^{3.32}$, and weakly interacts with $L229^{ECL2}$. Based on the interactions proposed here, it is clear that there is no trivial or 'single-residue' explanation for the observed lower potencies and efficacies of 23H-, 34H- and 35H-NBOMe, suggesting a concerted impact of the interaction with several residues. Steric effects have to be considered as well when interpreting the position of the ligand in the binding pocket, as is particularly relevant for the NBOMe isomers with methoxy groups on adjacent positions (23H- and 34H-NBOMe). It must

also be taken into consideration that this model was adapted from a miniG_q bound 5-HT_{2A}R structure, and that the presence of βarrestin2 could differentially impact ligand interaction. Within the context of this study, it was not possible to generate binding data, however, such data may help to explain some of the observed differences in receptor activation by different positional isomers.

Table 5-3. Summary of the interaction energies (kcal/mol) between compounds and the 5-HT_{2A}R. as seen from the perspective of the N-benzyl moiety shown in ***Figure 5-4a***

Compound	S159$^{3.36}$	D155$^{3.32}$	V156$^{3.33}$	W336$^{6.48}$	F339$^{6.51}$	F340$^{6.52}$
LSD	-3.50	-18.5	-13.5	-2.30	-10.49	-6.39
25CN-NBOH	-9.34	-18.3	-10.7	-7.30	-8.76	-7.73
23H-NBOMe	-11.5	-19.8	-11.3	-9.06	-9.41	-8.72
24H-NBOMe	-9.86	-19.5	-11.2	-8.66	-9.35	-8.36
25H-NBOMe	-9.90	-19.3	-11.0	-8.58	-9.01	-7.54
26H-NBOMe	-9.77	-20.7	-12.9	-8.70	-9.16	-7.89
34H-NBOMe	-8.59	-20.7	-10.6	-8.62	-9.30	-8.39
35H-NBOMe	-8.72	-20.49	-10.1	-8.54	-10.27	-7.25

Table 5-4. Summary of the interaction energies (kcal/mol) involved in the interaction between the methoxy groups on the phenyl ring and nearby amino acid residues on the 5-HT_{2A}R.

Compound	T160$^{3.37}$	S159$^{3.36}$	G238$^{5.42}$	S242$^{5.46}$	S239$^{5.43}$	V235$^{5.39}$	N343$^{6.55}$	L229^{ECL2}
LSD	-1.25	-3.50	-1.54	-6.46	-4.01	-2.28	-5.02	-9.91
25CN-NBOH	-2.38	-9.34	-3.07	-1.90	-2.13	-0.68	-1.69	-2.98
23H-NBOMe	-2.77	-11.5	-2.04	-4.86	-1.29	-0.57	-0.99	-0.56
24H-NBOMe	-2.14	-9.86	-1.07	-1.74	-2.18	-3.38	-2.25	-1.13
25H-NBOMe	-2.43	-9.9	-0.82	-1.81	-0.59	-0.93	-1.61	-2.25
26H-NBOMe	-2.51	-9.77	-0.93	-1.70	-0.60	-0.58	-0.73	-1.76
34H-NBOMe	-0.47	-8.59	-2.69	-3.23	-2.29	-3.35	-0.95	-1.09
35H-NBOMe	-0.21	-8.72	-2.26	-2.57	-1.46	-1.60	-3.18	-2.46

5.4 Conclusion

In conclusion, we report on the functional characterization of a set of positional isomers of 25H-NBOMe, in which the methoxy groups are placed in different positions of the phenethylamine moiety. More specifically, the impact of the structural changes on the ability of the activated 5-HT_{2A}R to recruit cytosolic proteins was assessed. To this end, bioassays monitoring the recruitment of either βarrestin2 or miniG_q to the 5-HT_{2A}R were employed. The results show clear differences in the EC_{50} (as a measure of potency) and E_{max} (as a measure of efficacy) values of the differentially substituted isomers. Overall, the isomers with a methoxy group on position 2 were more potent than those that did not have this substituent, with 24H-NBOMe being the most potent substance tested, and 23H-NBOMe being slightly less potent than 25- and 26H-NBOMe. The two isomers lacking the 2-methoxy group, 34- and 35H-NBOMe, were substantially less potent than the others. In terms of efficacy, the differences are less apparent, with 23H- and 35H-NBOMe showing less efficacy than all other isomers, although they showed similar efficacy as LSD. The results showed that the reference agonist, the assay employed, and the method of analysis did not influence these findings. Data obtained from molecular docking of these substances into a 5-HT_{2A}R model suggest specific residues that interact with the specific methoxy groups on the phenyl moiety of the phenethylamine part of the molecule, result in the observed differential receptor activation potential of the differently-substituted isomers. As for biased agonism in general isomers with methoxy groups at the 2 positions tend to display greater ligand bias towards βarrestin2 than compounds with a methoxy in the 3 position. This is likely related to the stronger interaction between a methoxy in the 2 position and $T160^{3.37}$ whereas this interaction between the methoxy in the 3 position is significatly weaker (***Table 5-4***). When research is more conclusive which pathway is desirable for psychedelics it is studies like these that will aid in ligand design

for potential therapeutics. While the methoxy pattern on the phenylalkylamine moiety has been described extensively for *N*-unsubstituted psychedelics, this is the first report comparatively assessing the functional effects of this isomerization in their NBOMe counterparts.

CHAPTER 6

Discussion

6.1 Objectives Of This Research

The overall objective of this research was to use *in silico* computer modelling to help explain *in vitro* SAR of compounds that bind to the GPCRs CB1R, CB2R, and 5-HT_{2A}R. The research was designed to bridge the gap between *in silico* modelling and *in vitro* pharmacology. Specifically, this work demonstrates (1) how isolated enantiomers of GAT compounds display vastly different pharmacology at CB1R that may relate to their sites of binding; (2) how isomers of GAT compounds display different binding affinity at CB1R based on their chemical functional groups; (3) the relationship between functional groups of synthetic cannabinoid receptor agonists and their affinity and ligand bias at CB1R and CB2R; and (4) the relationship between functional groups of synthetic NBOMe 5-HT_{2A}R agonists and their signaling activity at 5-HT_{2A}R. Consequently, this research was successful in using *in silico*-based modelling in concert with *in vitro* pharmacological approaches to understand the activity of ligands at three GPCRs.

6.2 Summary of Research

6.2.1 GAT Compound Enantiomers and Isomers Show a Difference in Activity at CB1R

GAT591 and GAT593 were separated into their respective enantiomers GAT1664, GAT1665, GAT1666 and GAT1667. Previous research has shown that the racemic mixtures GAT591 and GAT593 displayed ago-PAM properties and thus the goal of this study was to show which enantiomer was responsible for the agonist properties and PAM properties at CB1R. In this study it was discovered that the *R*-enantiomers (GAT1665 and GAT1667) acted as ago-PAM's while the *S*-enantiomers (GAT1664 and GAT1666) showed little to no activity at CB1R. This is due to the *R*-enantiomers binding to the ago-PAM site of CB1R near the intracellular space of the receptor on the plasma membrane whereas the *S*-enantiomers bound to a PAM site on CB1R near the extracellular space. In the radioligand binding experiments it was observed that all GAT

compounds enhanced the binding of [^{3}H]CP55,940, which is consistent with expected PAM activity at GPCRs in the majority of cases published to date. From these experiments it was further observed that GAT1667 had the greatest affinity (K_D = 28 [15 – 52] nM). From a computational perspective this makes sense as ΔG (kcal/mol) for GAT1667 (ΔG = -64.55) is more negative than its isomers that binds to the same site GAT1665 (ΔG = -60.77). It was even found that this research was translatable to *in vivo* models as we found that while GAT1664 and GAT1666 showed no notable *in vivo* effects, GAT1665 and GAT1667 displayed significant cataleptic, hypothermic, and anti-nociceptive effects at 3 and 10 mg/kg i.p. compared to vehicle. GAT1664, GAT1665, GAT1666, and GAT1667 do not alter physiology in normal, otherwise healthy adult mice as agonists, but GAT1665 and GAT1667 are able to augment THC's effects as PAMs when administered once. Overall, this research shows that separated enantiomers bind distinct sites on CB1R which produce unique ligand profiles. Research such as this will help when there is a clear distinction as to which bias profile is useful for specific indications.

6.2.2 *In silico* Methods Can Be Used to Optimize Existing Compounds

In chapter 3 it was discussed how *in silico* methods can be used to improve the affinity and physiochemical characteristics of existing compounds. In the first part of the study, the effect on binding free energy (ΔG) as a function of halogen substitution on three sites (referred to as X, Y and Z) of the GAT228 was assessed for a total of 144 compounds (***Figure 3-1a***). Without any halogens the ΔG was computed to be -65.24kcal/mol for the control compound GAT228. For the fluorinated compounds a significant increase in ΔG was only observed for GAT1667 (ΔG GAT1667 = -70.88 kcal/mol) when compared to GAT228, but not GAT1665 (ΔG GAT1665 = -65.74 kcal/mol). For the chlorine derivatives a substantial decrease in ΔG was observed indicating an increase in relative binding affinity. For example, the chlorinated derivative of GAT1667

showed a ΔG of -78.19 kcal/mol which is 7.31 kcal/mol more stable than GAT1667. For both the bromine and iodine equivalent of GAT1667 the compounds did not dock to CB1R in the correct pose as shown in ***Figure 3-1b,c***. This is likely due to these halogens having large atomic radii and bond lengths, making them unsuitable as ligands for this CB1R binding site.

Next, the effect of adding a NO_2 to site 'Y' of the GAT228 scaffold was explored because there exists an arginine residue (R4.39) on CB1R close to site Y which would be expected to H-bond with the NO_2 group. It was observed that a NO_2 placed at position 2 of site Y did show a decrease in ΔG by 6.46 kcal/mol when compared to GAT228 due to the presence of a H-bond. Unfortunately, however, when the chlorines were added there was not as much space in the binding pocket which led to unfavorable steric clashing and an increase in ΔG. Thus, overall adding a NO_2 at this position was not beneficial. The effect of replacing the ring at site 'X' with a series of pyridine derivatives was also assessed and showed that the optimal position for a nitrogen in the pyridine ring was para to the R substituent ***Figure 3-4a***. This substitution was 2.25 kcal/mol more-stable than the fluorinated GAT228 control (GAT1665). Although this being the case there was not a drastic effect in terms of relative bonding affinity in changing site 'X' or 'Z' to a heterocyclic functional group.

The physiochemical properties of each compound were also assessed. Fluorinated and chlorinated GAT228 compounds broke 1 Lipinski rule while brominated and iodinated compounds broke 2. For compounds with a NO_2 group at position 2 of site 'Y' the predicted bioavailability became worse and thus this substitution was omitted. The only compound among those tested that did not break any Lipinski rules were those in which heterocycles were incorporated into the benzene rings. Because of this observation heterocycle analogs of GAT228 were considered lead compounds ***Figure 3-5***. A major limitation of this research is that *in vitro* assays would need to be

performed in order to prove the validity of this research as this was all conducted *in silico*. Recent studies have also shown that the binding site docked to in this study overlaps with n-butyl-diphenylcarboxamies which act as NAMs at CB1R [165]. This unfortunately only further complicates this research as it suggests that PAM and NAMs of CB1R do not have distinct binding sites.

6.2.3 *In silico* methods can be used to discriminate G protein from βarrestin2 biased compounds

While much of chapter 4 focused on the SAR of SCRA's at CB1R and CB2R the novel finding was that in silico methods accurately differentiated the most G protein-biased compound (JWH 018 2'-naphthyl-N-(3-methylbutyl) isomer) from the most βarrestin2-biased compound (4F-MDMB-BINACA). The most G protein-biased compound (JWH 018 2'-naphthyl-N-(3-methylbutyl) isomer) shows a more negative interaction energy with the G protein bound which makes sense as this compound is G protein biased. In fact, JWH 018 2'-naphthyl-N-(3-methylbutyl) isomer is 3.78 kcal/mol more stable with the G protein-biased bound than without the G protein bound. The most βarrestin2-biased compound (4F-MDMB-BINACA) was found to be 10.56 kcal/mol more stable than 4F-MDMB-BINACA with the G protein bound.

In a general sense it was found that the most conserved interaction was a H-bond with $S383^{7.39}$ on CB1R while for CB2R $S285^{7.39}$. The data indicate this H-bond must be present in order for activity to exist at CB1R/CB2R as discussed previously. In terms of ligand bias it was observed that Δ^9-THC, meta-AB-FUBINACA, 5-fluoro NPB-22, 5-fluoro MPP-PICA were unbiased, AB-PINACA N-(2-fluoropentyl) isomer, 3-chloro AB-PINACA, 4-Fluoro MDMB-BINACA were βarrestin2-biased and FDU-NNEI, JWH 145, EG018 were cAMP biased. However, it is not clear what structural features lead to ligand bias at the orthosteric site of CB1R and CB2R. The reason that many of these studies do not provide insights into ligand bias is because this is not the best method

of studying ligand bias. In order to expand our knowledge of ligand bias it is imperative that we begin to design studies which look at protein-protein interaction between the G protein and the intracellular helices of the GPCR where this interaction occurs and separately also looking at how the βarrestin signalling molecule interacts with CB1R.

6.2.4 2-Methoxy NBOMe Compounds are more Potent than 3-Methoxy NBOMe Compounds

25H-NBOMe yielded a low nM potency (EC_{50} = 11.4nM) in the 5-HT_{2A}R βarrestin2 recruitment assay and a higher efficacy than LSD (E_{max} 164% relative to LSD). Only one of the isomers is slightly more potent than 25H-NBOMe: 24H-NBOMe yielded an EC_{50} value of 3.88 nM. The potency of 26H-NBOMe (8.70 nM) is similar to that of 25H-NBOMe. The highest EC_{50} value (33.6 nM) of all isomers with a 2-methoxy substituent, and hence the lowest potency, was observed for 23H-NBOMe. The least potent substances in the βarrestin2 recruitment assay appeared to be 34H-NBOMe and 35H-NBOMe, both lacking the 2-methoxy substituent. This change in the position of one of the methoxy groups drastically reduced in vitro potency yielding EC_{50} values in the higher nM range (248 nM and 343 nM). In regard to the efficacy although 25H-NBOMe has the highest efficacy (164%) the 95% confidence intervals of 24H-, 26H-, and 34H-NBOMe (145%, 156% and 147%) all overlap with 25H-NBOMe. Although the efficacies obtained for 23H-NBOMe (123%) and 35H-NBOMe (118%) were lower than that of 25H-NBOMe they both were still more efficacious than LSD and serotonin.

In ***Table 5-2*** serotonin showed the greatest efficacy (E_{max} = 305% relative to LSD). For the NBOMe isomers although 25H-NBOMe displayed the greatest efficacy the 95% confidence intervals of 24H-, 26H-, 34H- (171%, 162%, 156%) all overlap with 25H-NBOMe. While 23H-NBOMe was the only compound that showed less efficacy than LSD (89.6%), 35H-NBOMe's efficacy (107%) was only slightly greater than LSD (98.2%). In terms of potency as measured by

EC_{50} LSD displayed the greatest potency (EC_{50} = 17.7 nM). For the NBOMe isomers 24H-NBOMe displayed the greatest potency (EC_{50} = 37.4 nM) but the 95% confidence intervals of 25H- (EC_{50} = 86.2 nM) and 26H-NBOMe (EC_{50} = 68.0 nM) did overlap with 24H-NBOMe. 23H-NBOMe (EC_{50} = 236 nM) displayed the weakest potency of the 2-methoxy substituted NBOMe isomers. Similarly with the βarrestin2 recruitment assay in the miniG_q experiment 34H- (EC_{50} = 1321 nM) and 35H-NBOMe (EC_{50} = 1393 nM) displayed the weakest potency in terms of all the NBOMe isomers in the study.

In terms of *in silico* molecular modelling a methoxy group on position 2 of the phenyl ring of the phenethylamine moiety (as is the case in 23H-, 24H-, 25H-, and 26H-NBOMe) hydrophobically interacts with $T160^{3.37}$, $S159^{3.36}$ and $V156^{3.33}$, as reflected by the weaker interaction (higher interaction energies) for substances without a methoxy group at this position. The model also proposes interactions between $G238^{5.42}$ and $S242^{5.46}$ and a methoxy group at position 3, as reflected by a weaker interaction of these residues with substances lacking a 3-methoxy group. This work is imperative in the psychedelic drug discovery field as it provides a framework for future compounds that will be design for specific indications. It suggests that all methoxy isomers on the phenethylamine moiety still lead to βarrestin2-biased ligands although the most βarrestin2-biased compound contains a methoxy in the 2 position. As more data accumulate as to which ligand profiles are desired for specific indications this work will aid in rational ligand design that will meet these indications.

6.3 Philosophical Considerations Surrounding this Research

6.3.1 Ambiguity of full vs partial agonist/antagonist

By definition a full agonist is a compound that induces a conformational change in the shape of the receptor it binds leading to a maximum in the measured outcome whereas a partial agonist

activates the receptor to an extent less than its maximal effect.[166] For learning purposes this definition serves its purpose but in the higher level of pharmacology the definition falls apart. The maximal effect in pharmacology is an arbitrary term that refers to the strongest measured cellular signaling outcome that has been observed to date for a given receptor and endpoint.[167] For example, if a new receptor is discovered and 20 compounds are tested at the receptor, the compound that produces the strongest effect is designated as the full agonist and anything that produces weaker effects greater than baseline are designated as partial agonists. If then a new compound is discovered that produces a stronger maximal effect, then the new compound becomes the full agonist while the one designated in the previous as a full agonist becomes a partial agonist. The terminology of partial or full only serves as a point of arbitrary point of reference, but in recent literature is often misused as an absolute. For this reason it is critically important that research published on novel agonists, allosteric ligands, and receptor systems thoroughly describe the model systems, time points, endpoints, and calculations used to arrive at determinations of affinity, potency, efficacy, and bias.[168]

6.3.2 Pharmacology in a Multidimensional System

In many branches of basic sciences including pharmacology, we measure systems as 2 dimensions. For example, we often look at dose versus response such as how different doses of a compound induce Ca^{2+} flux following GPCR activation. When a compound engages a biological system it interacts with many different systems in addition to the one being measured in an in experimental model. The measured endpoint data only provides a small representation of the compounds global effects in the biological system. This unidimensional understanding of a compounds effect may give rise to unanticipated side effects at later stages of the drug discovery process. Polypharmacological approaches have begun to bridge this gap as researchers are beginning to

screen individual compounds and multiple GPCRs to look for off target effects once the primary compounds mechanism of action has been deduced.[169,170,171] Looking ahead, what will push this field forward is the use of artificial intelligence to provide predictions for many of the unknown and off-target effects of a compound via machine learning.

6.3.3 SAR relationship is not straight forward in measuring agonism

SARs are the connection between a compounds structure and how the compound affects the measured signaling outcome. Historically, GPCR research has focused on G protein activity (e.g. an intracellular change in cAMP) or a change in βarrestin. In reality, GPCR-dependent effects are much more complicated. When a compound binds to a GPCR both the shape of the compound as well as the shape of the GPCR change. An outcome of this change in GPCR shape is the change of intracellular helical bundles on the GPCR. This change in intracellular helical bundles will cause the G protein to bind with higher or lower affinity to the intraceullar helices of the GPCR as well as changes to GPCR phosphorylation and consequent βarrestin recruitment. The unique GPCR conformation that is stabilized upon agonist binding will determine which GPCR-protein complex is best-stabilized and consequently which pathway is most-likely to be activated. From this perspective, a ligand-receptor SARs provide a limited understanding of this complex picture. A more comprehensive understanding would also incorporate how this shape change effects the affintiy of the G protein(s) and/or βarrestin to the intracellular helical bundle. The current best *in silico* approach to this is to utilize protein modelling and molecular dynamics simulations to assess conformational changes in the intracellular helices observed upon ligand docking. Using such an approach, one could dock the binding region of the interacting protein to the intracellular surface of the GPCR in the presence of a given compound to see if binding energy increases or decreases. However, this approach is limited by the current power of GPU/CPUs and the ability to accuratley

predict protein-protein interactions and folding with experimental validity.[172,173,174] The ongoing development of artificial intelligence and quantum computation may help resolve these issues. *In vitro*, multidimensional and time-sensitive reporter assays that allow for the visualization of more than 2 protein-protein interactions using multiple fluorescent-tagged proteins and/or fluorescent ligands may aid in our understanding of pluridimensional GPCR signaling and bias.[175] However, these assays are reliant upon heterelogous overexpression systems that may not translate to endogenous biological significance during drug development.[176]

6.3.4 5-HT$_{2A}$R Receptor agonists Psychedelics issue

The prevailing theory on psychedelics for quite some time now is that they elicit their effects by binding to 5-HT$_{2A}$R and acting as agonists. This was supported by work from Dr. Nichols' group that found ketanserin (5-HT2$_A$R antagonist) administered prior to a 5-HT$_{2A}$R agonist blocks the subjective effects of psychedelic compounds.[177] Independently, other research has found that following the administration of a psychedelic, glutamate levels in the medial prefrontal cortex increase, while glutamate levels in the hippocampus decrease.[178] While one could suppose that this proves 5HT$_{2A}$R is the psychedelic receptor, it is important to ask why do exogenous 5-HT$_{2A}$R agonists cause perceptual changes in reality? This is a particularly important question given that serotonin itself does not alter perception and exogeneous hallucinogenic and dissociative agents vary in their effects on perception. There are theories that attempt to explain this of which Dr. Harris' entropic brain model is the most widely accepted.[179] Put simply, the entropic brain model represents different brain regions as hubs in a network. Each hub can connect to a few other hubs but not all hubs are directly connected. Under the influence of a psychedelic, there seems to be a higher degree of interconnectivity between hubs which leads to an overall higher degree of entropy in the brain. This increased degree of entropy in human subjects is measured with fMRI.[180] A

question that could help unify the theory for how psychedelics work is how does a 5-HT_{2A}R agonist lead to the interconnectedness of these hubs? Answering such a question would be difficult as one would have to understand how to connect the dots from a compound binding to 5-HT_{2A}R (a topic in molecular pharmacology) to interconnectedness of these hubs (a topic in psychiatry). Historically, researchers are adept at taking the reductionist approach and answering a limited and specific question with strong evidence, but we often fail to answer questions that require interdisciplinary and integration and translation of data across models.

6.3.5 Will computational methods replace experimental pharmacology?

Moore's Law states that the number of transistors on a microchip doubles approximately every 2 years, though the cost of computers is halved. In the past 20 years the discipline of pharmacology has seen a widespread and growing adoption of *in silico* techniques to support *in vitro* and *in vivo* data [181]. With in this dissertation *in silico* computational modelling was able to accurately predict relative binding affinity and bias for CB1R, CB2R, and 5-HT_{2A}R. The utilization of *in silico* analysis is a product of high-resolution x-ray/cryo-EM crystal structures of GPCRs coupled with the increasing power of central processing units (CPU)/graphics processing units (GPU's). In 2020 the artificial intelligence (AI) algorithm AlphaFold v2.0 was launched. AlphaFold v2.0 uses AI to predict protein structures. While many researchers, including myself, can spot obvious issues with the predicted structures of which can be contrasted to experimentally determined structures on the protein data bank, it does bring about a future where *in silico* computational modelling is showing higher accuracy over time. Will we eventually get to a point in time where experimental pharmacology is replaced by *in silico* computational methods? Currently this is not a reality as we still need experimental pharmacology to prove the vast complex nature of *in vitro* and *in vivo* systems.

References

1. Brandt AL. Computer modeling of allosteric modulators at G protein-coupled receptors. *Allosteric Modul G Protein-Coupled Recept*. Published online 2022:31-46. doi:10.1016/b978-0-12-819771-4.00007-5

2. Goddard AD, Watts A. Regulation of G protein-coupled receptors by palmitoylation and cholesterol. *BMC Biol*. 2012;10:2-4. doi:10.1186/1741-7007-10-27

3. Alhosaini K, Azhar A, Alonazi A, Al-Zoghaibi F. GPCRs: The most promiscuous druggable receptor of the mankind. *Saudi Pharm J*. 2021;29(6):539-551. doi:10.1016/j.jsps.2021.04.015

4. Yang D, Zhou Q, Labroska V, et al. G protein-coupled receptors: structure- and function-based drug discovery. *Signal Transduct Target Ther*. 2021;6(1). doi:10.1038/s41392-020-00435-w

5. Hauser AS, Attwood MM, Rask-andersen M, Schiöth HB, Gloriam DE. Trends in GPCR drug discovery : new agents , targets and indications. *Nat Publ Gr*. 2017;16(12):829-842. doi:10.1038/nrd.2017.178

6. Sriram K, Insel PA. G Protein-Coupled Receptors as Targets for Approved Drugs : How Many Targets and How Many Drugs? 2018;(April):251-258. doi:10.1124/mol.117.111062

7. Dziedzic A, Miller E, Saluk-Bijak J, Bijak M. The gpr17 receptor—a promising goal for therapy and a potential marker of the neurodegenerative process in multiple sclerosis. *Int J Mol Sci*. 2020;21(5). doi:10.3390/ijms21051852

8. Wheatley M, Wootten D, Conner MT, et al. Lifting the lid on GPCRs: The role of

extracellular loops. *Br J Pharmacol*. 2012;165(6):1688-1703. doi:10.1111/j.1476-5381.2011.01629.x

9. Hilger D, Masureel M, Kobilka BK, Struct N, Biol M. Structure and dynamics of GPCR signaling complexes HHS Public Access Author manuscript. *Nat Struct Mol Biol*. 2018;25(1):4-12. doi:10.1038/s41594-017-0011-7.Structure

10. Blakeney JS, Reid RC, Le GT, Fairlie DP. Nonpeptidic ligands for peptide-activated G protein-coupled receptors. *Chem Rev*. 2007;107(7):2960-3041. doi:10.1021/cr050984g

11. Caron A, Reynolds RP, Castorena CM, et al. Adipocyte Gs but not Gi signaling regulates whole-body glucose homeostasis. *Mol Metab*. 2019;27(June):11-21. doi:10.1016/j.molmet.2019.06.019

12. Lazar AM, Irannejad R, Baldwin TA, et al. G protein-regulated endocytic trafficking of adenylyl cyclase type 9. *Elife*. 2020;9:1-24. doi:10.7554/eLife.58039

13. Taussig R, Tang WJ, Hepler JR, Gilman AG. Distinct patterns of bidirectional regulation of mammalian adenylyl cyclases. *J Biol Chem*. 1994;269(8):6093-6100. doi:10.1016/s0021-9258(17)37574-9

14. Khrenova MG, Kulakova AM, Nemukhin A V. Light-Induced Change of Arginine Conformation Modulates the Rate of Adenosine Triphosphate to Cyclic Adenosine Monophosphate Conversion in the Optogenetic System Containing Photoactivated Adenylyl Cyclase. *J Chem Inf Model*. 2021;61(3):1215-1225. doi:10.1021/acs.jcim.0c01308

15. Cheng X, Ma Y, Moore M, Hemmings BA, Taylor SS. Phosphorylation and activation of

cAMP-dependent protein kinase by phosphoinositide-dependent protein kinase. *Proc Natl Acad Sci U S A*. 1998;95(17):9849-9854. doi:10.1073/pnas.95.17.9849

16. Litosch I. Novel mechanisms for feedback regulation of phospholipase C-β activity. *IUBMB Life*. 2002;54(5):253-260. doi:10.1080/15216540215673

17. Sternweis PC, Smrcka A V. Regulation of phospholipase C by G proteins. *Trends Biochem Sci*. 1992;17(12):502-506. doi:10.1016/0968-0004(92)90340-F

18. Kadamur G, Ross EM. Mammalian phospholipase C. *Annu Rev Physiol*. 2013;75:127-154. doi:10.1146/annurev-physiol-030212-183750

19. Hanson CJ, Bootman MD, Roderick HL. Cell signalling: IP3 receptors channel calcium into cell death. *Curr Biol*. 2004;14(21):933-935. doi:10.1016/j.cub.2004.10.019

20. Prole DL, Taylor CW. Structure and function of ip3 receptors. *Cold Spring Harb Perspect Biol*. 2019;11(4). doi:10.1101/cshperspect.a035063

21. Zayzafoon M. Calcium/calmodulin signaling controls osteoblast growth and differentiation. *J Cell Biochem*. 2006;97(1):56-70. doi:10.1002/jcb.20675

22. Receptor O, Proteins I. Opioid receptor interacting proteins and the control of opioid signaling. 2019;19(42):734-763. doi:10.2174/1381612819421401051606 25.Opioid

23. Fong TM. *Measurement of Inverse Agonism of the Cannabinoid Receptors*. Vol 485. Elsevier Inc.; 2010. doi:10.1016/B978-0-12-381296-4.00008-7

24. Dunn HA, Stephen Ferguson SS. Regulation of CRFR1 and 5-HT2AR by PDZ Domain-Containing Proteins SAP97 and PSD-95 Recommended Citation. Published online 2014. https://ir.lib.uwo.ca/etd

25. Viñals X, Moreno E, Lanfumey L, et al. Cognitive impairment induced by delta9-tetrahydrocannabinol occurs through heteromers between cannabinoid CB1 and serotonin 5-HT2A receptors. *PLoS Biol*. 2015;13(7):1-40. doi:10.1371/journal.pbio.1002194

26. Hauser MA, Legler DF. Common and biased signaling pathways of the chemokine receptor CCR7 elicited by its ligands CCL19 and CCL21 in leukocytes. *J Leukoc Biol*. 2016;99(6):869-882. doi:10.1189/jlb.2mr0815-380r

27. Piekielna-Ciesielska J, Artali R, Azzam AAH, et al. Pharmacological characterization of μ-opioid receptor agonists with biased g protein or β-arrestin signaling, and computational study of conformational changes during receptor activation. *Molecules*. 2021;26(1). doi:10.3390/MOLECULES26010013

28. Kolb P, Kenakin T, Alexander SPH, et al. Community Guidelines for GPCR Ligand Bias: IUPHAR Review XX. *Br J Pharmacol*. 2022;(August 2021):1-24. doi:10.1111/bph.15811

29. Kim K, Che T, Panova O, et al. Structure of a Hallucinogen-Activated Gq-Coupled 5-HT2A Serotonin Receptor. *Cell*. 2020;182(6):1574-1588.e19. doi:10.1016/j.cell.2020.08.024

30. Burford NT, Traynor JR, Alt A. Positive allosteric modulators of the μ-opioid receptor: A novel approach for future pain medications. *Br J Pharmacol*. 2015;172(2):277-286. doi:10.1111/bph.12599

31. Christopoulos A. Allosteric binding sites on cell-surface receptors: Novel targets for drug discovery. *Nat Rev Drug Discov*. 2002;1(3):198-210. doi:10.1038/nrd746

32. van Aalst E, Wylie BJ. Cholesterol Is a Dose-Dependent Positive Allosteric Modulator of CCR3 Ligand Affinity and G Protein Coupling. *Front Mol Biosci*. 2021;8(August):1-14.

doi:10.3389/fmolb.2021.724603

33. Chen Y, Nong Y, Goudet C, et al. Interaction of novel positive allosteric modulators of metabotropic glutamate receptor 5 with the negative allosteric antagonist site is required for potentiation of receptor responses. *Mol Pharmacol*. 2007;71(5):1389-1398. doi:10.1124/mol.106.032425

34. Koole C, Wootten D, Simms J, et al. Allosteric ligands of the glucagon-like peptide 1 receptor (GLP-1R) differentially modulate endogenous and exogenous peptide responses in a pathway-selective manner: Implications for drug screening. *Mol Pharmacol*. 2010;78(3):456-465. doi:10.1124/mol.110.065664

35. Abdel-Magid AF. Allosteric Modulators: An Emerging Concept in Drug Discovery. *ACS Med Chem Lett*. 2015;6(2):104-107. doi:10.1021/ml5005365

36. Wood MR, Hopkins CR, Brogan JT, Je P, Lindsley CW. " Molecular Switches " on mGluR Allosteric Ligands That Modulate Modes of Pharmacology. Published online 2011:2403-2410. doi:10.1021/bi200129s

37. López-Rodríguez ML, Benhamú B, Vázquez-Villa H. *Allosteric Modulators Targeting GPCRs*.; 2019. doi:10.1016/B978-0-12-816228-6.00011-8

38. Han Y, Shang Y, Herbst JJ, Connell JO. Positive Allosteric Modulators of the δ -Opioid Receptor. *J Med Chem*. 2016;58(10):4220-4229. doi:10.1021/acs.jmedchem.5b00007.Notes

39. Kenakin T, Strachan RT. PAM-Antagonists: A Better Way to Block Pathological Receptor Signaling? *Trends Pharmacol Sci*. 2018;39(8):748-765. doi:10.1016/j.tips.2018.05.001

40. Wu Y, Tong J, Ding K, Zhou Q, Zhao S. *GPCR Allosteric Modulator Discovery*. Vol 1163.; 2019. doi:10.1007/978-981-13-8719-7_10

41. Zou S, Kumar U. Cannabinoid receptors and the endocannabinoid system: Signaling and function in the central nervous system. *Int J Mol Sci*. 2018;19(3). doi:10.3390/ijms19030833

42. Kim J, Alger BE. Reduction in endocannabinoid tone is a homeostatic mechanism for specific inhibitory synapses. *Nat Neurosci*. 2010;13(5):592-600. doi:10.1038/nn.2517

43. Navarrete F, García-Gutiérrez MS, Jurado-Barba R, et al. Endocannabinoid System Components as Potential Biomarkers in Psychiatry. *Front Psychiatry*. 2020;11(April):1-30. doi:10.3389/fpsyt.2020.00315

44. Trexler KR, Trexler KR, Virginia W. Acute and Repeated Effects of Synthetic Cannabinoid Agonism and Cannabinoid Receptor 1 Positive Allosteric Modulation and Cannabinoid Receptor 1 Positive Allosteric Modulation Department of Psychology. Published online 2019.

45. Volkow ND, Hampson AJ, Baler RD. Don't Worry, Be Happy: Endocannabinoids and Cannabis at the Intersection of Stress and Reward. *Annu Rev Pharmacol Toxicol*. 2017;57(June 2016):285-308. doi:10.1146/annurev-pharmtox-010716-104615

46. Wang X, Liu D, Shen L, et al. A Genetically Encoded F-19 NMR Probe Reveals the Allosteric Modulation Mechanism of Cannabinoid Receptor 1. *J Am Chem Soc*. 2021;143(40):16320-16325. doi:10.1021/jacs.1c06847

47. Shao Z, Yan W, Chapman K, et al. Structure of an allosteric modulator bound to the CB1

cannabinoid receptor. *Nat Chem Biol*. 2019;15(12):1199-1205. doi:10.1038/s41589-019-0387-2

48. Hua T, Vemuri K, Nikas SP, et al. Crystal structures of agonist-bound human cannabinoid receptor CB 1. *Nature*. 2017;547(7664):468-471. doi:10.1038/nature23272

49. Shao Z, Yin J, Chapman K, et al. High-resolution crystal structure of the human CB1 cannabinoid receptor. *Nature*. 2016;540(7634):602-606. doi:10.1038/nature20613

50. Hua T, Li X, Wu L, et al. Activation and Signaling Mechanism Revealed by Cannabinoid Receptor-Gi Complex Structures. *Cell*. 2020;180(4):655-665.e18. doi:10.1016/j.cell.2020.01.008

51. Krishna Kumar K, Shalev-Benami M, Robertson MJ, et al. Structure of a Signaling Cannabinoid Receptor 1-G Protein Complex. *Cell*. 2019;176(3):448-458.e12. doi:10.1016/j.cell.2018.11.040

52. Andrzejewska A, Staszak K, Kaczmarek-Ryś M, Słomski R, Hryhorowicz S. Understanding cannabinoid receptors: structure and function. *Folia Biol Oecologica*. 2018;14:1-13. doi:10.1515/fobio-2017-0004

53. Nebane NM, Kellie B, Song ZH. The effects of charge-neutralizing mutation D6.30N on the functions of CB1 and CB2 cannabinoid receptors. *FEBS Lett*. 2006;580(22):5392-5398. doi:10.1016/j.febslet.2006.09.001

54. Kapur A, Hurst DP, Fleischer D, et al. Mutation studies of Ser7.39 and Ser2.60 in the human CB1 cannabinoid receptor: Evidence for a serine-induced bend in CB1 transmembrane helix 7. *Mol Pharmacol*. 2007;71(6):1512-1524. doi:10.1124/mol.107.034645

55. Lafaye G, Karila L, Blecha L, Benyamina A. Cannabis, cannabinoids, and health. *Dialogues Clin Neurosci*. 2017;19(3):309-316. doi:10.31887/dcns.2017.19.3/glafaye

56. Marcu J, Console-Bram L, Abood ME. Current cannabinoid receptor nomenclature and pharmacological principles. *Endocannabinoid Regul Monoamines Psychiatr Neurol Disord*. Published online 2013:25-54. doi:10.1007/978-1-4614-7940-6_3

57. Brutlag A, Hommerding H. Toxicology of Marijuana, Synthetic Cannabinoids, and Cannabidiol in Dogs and Cats. *Vet Clin North Am - Small Anim Pract*. 2018;48(6):1087-1102. doi:10.1016/j.cvsm.2018.07.008

58. Yu H, Liu X, Chen B, et al. The neuroprotective effects of the cb2 agonist gw842166x in the 6-ohda mouse model of parkinson's disease. *Cells*. 2021;10(12):1-17. doi:10.3390/cells10123548

59. Xing C, Zhuang Y, Xu TH, et al. Cryo-EM Structure of the Human Cannabinoid Receptor CB2-Gi Signaling Complex. *Cell*. 2020;180(4):645-654.e13. doi:10.1016/j.cell.2020.01.007

60. Cabral GA, Griffin-Thomas LT. Emerging role of the cannabinoid receptor CB 2 in immune regulation: Therapeutic prospects for neuroinflammation. *Expert Rev Mol Med*. 2009;11(804):1-31. doi:10.1017/S1462399409000957

61. Li X, Hua T, Vemuri K, et al. Crystal Structure of the Human Cannabinoid Receptor CB2. *Cell*. 2019;176(3):459-467.e13. doi:10.1016/j.cell.2018.12.011

62. Millan MJ, Marin P, Bockaert J, Mannoury la Cour C. Signaling at G-protein-coupled serotonin receptors: recent advances and future research directions. *Trends Pharmacol Sci*.

2008;29(9):454-464. doi:10.1016/j.tips.2008.06.007

63. Chi T, Gold JA. A review of emerging therapeutic potential of psychedelic drugs in the treatment of psychiatric illnesses. *J Neurol Sci*. 2020;411(November 2019):116715. doi:10.1016/j.jns.2020.116715

64. Kelmendi B, Kaye AP, Pittenger C, Kwan AC. Psychedelics. *Curr Biol*. 2022;32(2):R63-R67. doi:10.1016/j.cub.2021.12.009

65. Pompeiano M, Palacios JM, Mengod G. Distribution of the serotonin 5-HT2 receptor family mRNAs: comparison between 5-HT2A and 5-HT2C receptors. *Mol Brain Res*. 1994;23(1-2):163-178. doi:10.1016/0169-328X(94)90223-2

66. Vollenweider FX, Vollenweider-Scherpenhuyzen MFI, Bäbler A, Vogel H, Hell D. Psilocybin induces schizophrenia-like psychosis in humans via a serotonin-2 agonist action. *Neuroreport*. 1998;9(17):3897-3902. doi:10.1097/00001756-199812010-00024

67. Halberstadt AL, Nichols DE, Vollenweider FX. *Behavioral Neurobiology of Psychedelic Drugs*. Vol 2.; 2017. http://www.springer.com/series/7854

68. Braden MR, Nichols DE. Assessment of the roles of serines 5.43(239) and 5.46(242) for binding and potency of agonist ligands at the human serotonin 5-HT2A receptor. *Mol Pharmacol*. 2007;72(5):1200-1209. doi:10.1124/mol.107.039255

69. Dong C, Ly C, Dunlap LE, et al. Psychedelic-inspired drug discovery using an engineered biosensor. *Cell*. 2021;184(10):2779-2792.e18. doi:10.1016/j.cell.2021.03.043

70. Cao D, Yu J, Wang H, et al. Structure-based discovery of nonhallucinogenic psychedelic analogs. *Science (80-)*. 2022;375(6579):403-411. doi:10.1126/science.abl8615

71. Wacker D, Wang S, McCorvy JD, et al. Crystal Structure of an LSD-Bound Human Serotonin Receptor. *Cell*. 2017;168(3):377-389.e12. doi:10.1016/j.cell.2016.12.033

72. Sliwoski G, Kothiwale S, Meiler J, Lowe EW. Computational methods in drug discovery. *Pharmacol Rev*. 2014;66(1):334-395. doi:10.1124/pr.112.007336

73. Rasmussen SGF, Choi HJ, Rosenbaum DM, et al. Crystal structure of the human β2 adrenergic G-protein-coupled receptor. *Nature*. 2007;450(7168):383-387. doi:10.1038/nature06325

74. Palczewski K, Kumasaka T, Hori T, et al. Crystal structure of rhodopsin: A G protein-coupled receptor. *Science (80-).* 2000;289(5480):739-745. doi:10.1126/science.289.5480.739

75. Singh KD, Karnik SS. Current Trends in GPCR Allostery. *J Membr Biol*. 2021;254(3):293-300. doi:10.1007/s00232-020-00167-6

76. Lu D, Immadi SS, Wu Z, Kendall DA. Translational potential of allosteric modulators targeting the cannabinoid CB 1 receptor. *Acta Pharmacol Sin*. 2019;40(3):324-335. doi:10.1038/s41401-018-0164-x

77. Alaverdashvili M, Laprairie RB, Alaverdashvili M, Laprairie RB. The future of type 1 cannabinoid receptor allosteric ligands. *Drug Metab Rev*. 2018;0(0):14-25. doi:10.1080/03602532.2018.1428341

78. Ahn KH, Mahmoud MM, Kendall DA. Allosteric modulator ORG27569 induces CB1 cannabinoid receptor high affinity agonist binding state, receptor internalization, and Gi protein-independent ERK1/2 kinase activation. *J Biol Chem*. 2012;287(15):12070-12082.

doi:10.1074/jbc.M111.316463

79. Robert B. Laprairie, Abhijit R. Kulkarni, Pushkar M. Kulkarni, Dow P. Hurst, Diane Lynch, Patricia H. Reggio, David R. Janero, Roger G. Pertwee LA, Stevenson, Melanie E. M. Kelly, Eileen M. Denovan-Wrigh and GAT. *Mapping Cannabinoid 1 Receptor Allosteric Site(s): Critical Molecular Determinant and Signaling Profile of GAT100, a Novel, Potent, and Irreversibly Binding Probe*. Vol 176.; 2016. doi:10.1021/acschemneuro.6b00041.Mapping

80. Weichert D, Gmeiner P. Covalent Molecular Probes for Class A G Protein-Coupled Receptors: Advances and Applications. *ACS Chem Biol*. 2015;10(6):1376-1386. doi:10.1021/acschembio.5b00070

81. Laprairie RB, Bagher AM, Rourke JL, et al. Positive allosteric modulation of the type 1 cannabinoid receptor reduces the signs and symptoms of Huntington's disease in the R6/2 mouse model. *Neuropharmacology*. 2019;151(May 2018):1-12. doi:10.1016/j.neuropharm.2019.03.033

82. Laprairie RB, Kulkarni PM, Deschamps JR, et al. Enantiospecific Allosteric Modulation of Cannabinoid 1 Receptor. *ACS Chem Neurosci*. 2017;8(6):1188-1203. doi:10.1021/acschemneuro.6b00310

83. Hurst DP, Garai S, Kulkarni PM, Schaffer PC, Reggio PH, Thakur GA. Identification of cb1 receptor allosteric sites using force-biased mmc simulated annealing and validation by structure-activity relationship studies. *ACS Med Chem Lett*. 2019;10(8):1216-1221. doi:10.1021/acsmedchemlett.9b00256

84. Mouslech Z, Valla V. Endocannabinoid system: An overview of its potential in current

medical practice. *Neuroendocrinol Lett*. 2009;30(2):153-179.

85. Of S, Neurobiological THE, Involved M, The IN, Eating DOF, Disorders A. Study of the neurobiological mechanisms involved in the development of eating and addictive disorders. Published online 2017.

86. Sallaberry CA, Astern L. The Endocannabinoid System, Our Universal Regulator. *J Young Investig*. 2018;34(6):48-55. doi:10.22186/jyi.34.5.48-55

87. Bissantz C, Logean A, Rognan D. High-throughput modeling of human g-protein coupled receptors: Amino acid sequence alignment, three-dimensional model building, and receptor library screening. *J Chem Inf Comput Sci*. 2004;44(3):1162-1176. doi:10.1021/ci034181a

88. Kruk-Slomka M, Banaszkiewicz I, Biala G. The Impact of CB2 Receptor Ligands on the MK-801-Induced Hyperactivity in Mice. *Neurotox Res*. 2017;31(3):410-420. doi:10.1007/s12640-017-9702-4

89. Hillard CJ. Circulating Endocannabinoids: From Whence Do They Come and Where are They Going? *Neuropsychopharmacology*. 2018;43(1):155-172. doi:10.1038/npp.2017.130

90. McDougle DR, Kambalyal A, Meling DD, Das A. Endocannabinoids anandamide and 2-arachidonoylglycerol are substrates for human CYP2J2 epoxygenase. *J Pharmacol Exp Ther*. 2014;351(3):616-627. doi:10.1124/jpet.114.216598

91. Scotter EL, Abood ME, Glass M. The endocannabinoid system as a target for the treatment of neurodegenerative disease. *Br J Pharmacol*. 2010;160(3):480-498. doi:10.1111/j.1476-5381.2010.00735.x

92. Kulkarni AR, Garai S, Janero DR, Thakur GA. *Design and Synthesis of Cannabinoid 1*

Receptor (CB1R) Allosteric Modulators : Drug Discovery Applications. Vol 593. 1st ed. Elsevier Inc.; 2017. doi:10.1016/bs.mie.2017.06.018

93. Greig IR, Baillie GL, Abdelrahman M, Trembleau L, Ross RA. Bioorganic & Medicinal Chemistry Letters Development of indole sulfonamides as cannabinoid receptor negative allosteric modulators. *Bioorg Med Chem Lett*. 2016;26(18):4403-4407. doi:10.1016/j.bmcl.2016.08.018

94. Garai S, Kulkarni PM, Schaffer PC, et al. Application of Fluorine- And Nitrogen-Walk Approaches: Defining the Structural and Functional Diversity of 2-Phenylindole Class of Cannabinoid 1 Receptor Positive Allosteric Modulators. *J Med Chem*. 2020;63(2):542-568. doi:10.1021/acs.jmedchem.9b01142

95. Garai S, Kulkarni PM, Schaffer PC, et al. Application of Fluorine- And Nitrogen-Walk Approaches: Defining the Structural and Functional Diversity of 2-Phenylindole Class of Cannabinoid 1 Receptor Positive Allosteric Modulators. *J Med Chem*. 2020;63(2). doi:10.1021/acs.jmedchem.9b01142

96. Roebuck AJ, Greba Q, Smolyakova AM, et al. Positive allosteric modulation of type 1 cannabinoid receptors reduces spike-and-wave discharges in Genetic Absence Epilepsy Rats from Strasbourg. *Neuropharmacology*. 2021;190(January):108553. doi:10.1016/j.neuropharm.2021.108553

97. Roebuck AJ, Greba Q, Onofrychuk TJ, et al. Dissociable changes in spike and wave discharges following exposure to injected cannabinoids and smoked cannabis in Genetic Absence Epilepsy Rats from Strasbourg. *Eur J Neurosci*. 2020;(December 2020):1-16. doi:10.1111/ejn.15096

98. Price MR, Baillie GL, Thomas A, et al. Allosteric modulation of the Cannabinoid CB1 receptor. *Mol Pharmacol*. 2005;68(5):1484-1495. doi:10.1124/mol.105.016162

99. Vigolo A, Ossato A, Trapella C, et al. Novel halogenated derivates of JWH-018: Behavioral and binding studies in mice. *Neuropharmacology*. 2015;95:68-82. doi:10.1016/j.neuropharm.2015.02.008

100. Kilkenny C, Browne WJ, Cuthill IC, Emerson M, Altman DG. Improving bioscience research reporting: The arrive guidelines for reporting animal research. *PLoS Biol*. 2010;8(6):6-10. doi:10.1371/journal.pbio.1000412

101. Spartan'18 Parallel Suite. Published online 2018.

102. Schrödinger Release 2018. Published online 2018.

103. Shim JY, Bertalovitz AC, Kendall DA. Identification of essential cannabinoid-binding domains: Structural insights into early dynamic events in receptor activation. *J Biol Chem*. 2011;286(38):33422-33435. doi:10.1074/jbc.M111.261651

104. Fiser A, Sali A. ModLoop: Automated modeling of loops in protein structures. *Bioinformatics*. 2003;19(18):2500-2501. doi:10.1093/bioinformatics/btg362

105. Marcu J, Shore DM, Kapur A, et al. Novel insights into CB1 cannabinoid receptor signaling: A key interaction identified between the extracellular-3 loop and transmembrane helix 2. *J Pharmacol Exp Ther*. 2013;345(2):189-197. doi:10.1124/jpet.112.201046

106. Fay JF, Farrens DL. The membrane proximal region of the cannabinoid receptor CB1 N-terminus can allosterically modulate ligand affinity. *Biochemistry*. 2013;52(46):8286-8294. doi:10.1021/bi400842k

107. Fay JF, Farrens DL. Structural dynamics and energetics underlying allosteric inactivation of the cannabinoid receptor CB1. *Proc Natl Acad Sci U S A*. 2015;112(27):8469-8474. doi:10.1073/pnas.1500895112

108. Garai S, Leo LM, Szczesniak AM, et al. Discovery of a Biased Allosteric Modulator for Cannabinoid 1 Receptor: Preclinical Anti-Glaucoma Efficacy (). *J Med Chem*. 2021;64(12):8104-8126. doi:10.1021/acs.jmedchem.1c00040

109. Song ZH, Bonner TI. A lysine residue of the cannabinoid receptor is critical for receptor recognition by several agonists but not WIN55212-2. *Mol Pharmacol*. 1996;49(5):891-896.

110. Stahl EL, Zhou L, Ehlert FJ, Bohn LM. A novel method for analyzing extremely biased agonism at G protein-coupled receptors. *Mol Pharmacol*. 2015;87(5):866-877. doi:10.1124/mol.114.096503

111. Article C. An operational model of pharmacological agonism : the effect of E /[A] curve shape on agonist dissociation constant estimation. 2010;160. doi:10.1111/j.1476-5381.2010.00855.x

112. Kenakin T, Watson C, Muniz-Medina V, Christopoulos A, Novick S. A simple method for quantifying functional selectivity and agonist bias. *ACS Chem Neurosci*. 2012;3(3):193-203. doi:10.1021/cn200111m

113. Hryhorowicz S, Kaczmarek-Ryś M, Andrzejewska A, et al. Allosteric modulation of cannabinoid receptor 1— current challenges and future opportunities. *Int J Mol Sci*. 2019;20(23):1-19. doi:10.3390/ijms20235874

114. Hillard CJ. Biochemistry and pharmacology of the endocannabinoids

arachidonylethanolamide and 2-arachidonylglycerol°. 2000;61:3-18.

115. Janero DR, Thakur GA. Expert Opinion on Drug Discovery Leveraging allostery to improve G protein- coupled receptor (GPCR) -directed therapeutics : cannabinoid receptor 1 as discovery target. *Expert Opin Drug Discov*. 2016;11(12):1223-1237. doi:10.1080/17460441.2016.1245289

116. Slivicki RA, Xu Z, Mali SS, Hohmann AG. Brain permeant and impermeant inhibitors of fatty-acid amide hydrolase suppress the development and maintenance of paclitaxel-induced neuropathic pain without producing tolerance or physical dependence in vivo and synergize with paclitaxel to reduce tumor. *Pharmacol Res*. 2019;142(August 2018):267-282. doi:10.1016/j.phrs.2019.02.002

117. Slivicki RA, Mali SS, Hohmann AG. Voluntary exercise reduces both chemotherapy-induced neuropathic nociception and deficits in hippocampal cellular proliferation in a mouse model of paclitaxel-induced peripheral neuropathy. *Neurobiol Pain*. 2019;6(May):100035. doi:10.1016/j.ynpai.2019.100035

118. Janero DR, Thakur GA. Leveraging allostery to improve G protein-coupled receptor (GPCR)-directed therapeutics: cannabinoid receptor 1 as discovery target. *Expert Opin Drug Discov*. 2016;11(12):1223-1237. doi:10.1080/17460441.2016.1245289

119. Schwartz TW, Holst B. Allosteric enhancers , allosteric agonists and ago-allosteric modulators : where do they bind and how do they act ? 2007;28(8). doi:10.1016/j.tips.2007.06.008

120. Saleh N, Hucke O, Kramer G, et al. Multiple Binding Sites Contribute to the Mechanism of Mixed Agonistic and Positive Allosteric Modulators of the Cannabinoid CB1 Receptor.

Angew Chemie. 2018;130(10):2610-2615. doi:10.1002/ange.201708764

121. Garai S, Schaffer PC, Laprairie RB, et al. Design, synthesis, and pharmacological profiling of cannabinoid 1 receptor allosteric modulators: Preclinical efficacy of C2-group GAT211 congeners for reducing intraocular pressure. *Bioorganic Med Chem*. 2021;50(July):116421. doi:10.1016/j.bmc.2021.116421

122. Zhang X, Wong SE, Lightstone FC. Toward fully automated high performance computing drug discovery: A massively parallel virtual screening pipeline for docking and molecular mechanics/generalized born surface area rescoring to improve enrichment. *J Chem Inf Model*. 2014;54(1):324-337. doi:10.1021/ci4005145

123. Ballesteros JA, Weinstein H. Integrated methods for the construction of three-dimensional models and computational probing of structure-function relations in G protein-coupled receptors. *Methods Neurosci*. 1995;25(C):366-428. doi:10.1016/S1043-9471(05)80049-7

124. Katritch V, Fenalti G, Abola EE, Roth BL, Cherezov V, Stevens RC. Allosteric sodium in class A GPCR signaling. *Trends Biochem Sci*. 2014;39(5):233-244. doi:10.1016/j.tibs.2014.03.002

125. Pattar SV, Adhoni SA, Kamanavalli CM, Kumbar SS. In silico molecular docking studies and MM/GBSA analysis of coumarin-carbonodithioate hybrid derivatives divulge the anticancer potential against breast cancer. *Beni-Suef Univ J Basic Appl Sci*. 2020;9(1). doi:10.1186/s43088-020-00059-7

126. Briegleb G. Electron Affinity of Organic Molecules. *Angew Chemie Int Ed English*. 1964;3(9):617-632. doi:10.1002/anie.196406171

127. Paladini AC, Marder M, Viola H, Wolfman C, Wasowski C, Medina JH. Flavonoids and the Central Nervous System: from Forgotten Factors to Potent Anxiolytic Compounds. *J Pharm Pharmacol*. 2010;51(5):519-526. doi:10.1211/0022357991772790

128. Vijayarani KR, Govindarajulu M, Ramesh S, et al. Enhanced Bioavailability of Boswellic Acid by Piper longum: A Computational and Pharmacokinetic Study. *Front Pharmacol*. 2020;11(December):1-8. doi:10.3389/fphar.2020.551911

129. Webb NE, Wood DM, Greene SL, et al. Change in the new psychoactive substances associated with Emergency Department acute toxicity presentations associated with the introduction of the UK 2016 Psychoactive Substances Act. *Clin Toxicol*. 2019;57(1):36-41. doi:10.1080/15563650.2018.1494277

130. Sankhla MS, Sharma A, Kumar R. Abuse of Synthetic Cannabinoids in the World of Forensic Science. 2018;2(June):1-8.

131. White CM. The Pharmacologic and Clinical Effects of Illicit Synthetic Cannabinoids. *J Clin Pharmacol*. 2017;57(3):297-304. doi:10.1002/jcph.827

132. Spaderna M, Addy PH, D'Souza DC. Spicing things up: Synthetic cannabinoids. *Psychopharmacology (Berl)*. 2013;228(4):525-540. doi:10.1007/s00213-013-3188-4

133. Rachman T. *Pathology, Toxicogenetics, and Criminalistics of Drug Abuse*.; 2018.

134. Sholler DJ, Huestis MA, Amendolara B, Vandrey R, Cooper ZD. Pharmacology , Biochemistry and Behavior Therapeutic potential and safety considerations for the clinical use of synthetic cannabinoids. *Pharmacol Biochem Behav*. 2020;199(May):173059. doi:10.1016/j.pbb.2020.173059

135. Zuccarini G, Atri ID, Cottone E, Mackie K, Shainer I. Interference with the Cannabinoid Receptor CB1R Results in Miswiring of GnRH3 and AgRP1 Axons in Zebrafish Embryos. :1-23.

136. Andersen HK, Andersen HK. Scholar Commons A Comparative Study of Cannabinoids & CB1 Receptor GI Signaling by. Published online 2020.

137. Wang W, Bian J, Sun Y, Li Z. Pharmacology & Therapeutics The new fate of internalized membrane receptors : Internalized activation. *Pharmacol Ther*. 2022;233(49):108018. doi:10.1016/j.pharmthera.2021.108018

138. Bouvier M, Bouvier M, Bouvier M, et al. Quantification of Ligand Bias for Clinically Relevant 2-Adrenergic Receptor Ligands : Implications for Drug Taxo ... Related papers Quantification of Ligand Bias for Clinically Relevant Drug Taxonomy s.

139. Zagzoog A, Mohamed KA, Kim HJJ, et al. In vitro and in vivo pharmacological activity of minor cannabinoids isolated from Cannabis sativa. *Sci Rep*. 2020;10(1):1-13. doi:10.1038/s41598-020-77175-y

140. Bolognini D, Cascio MG, Parolaro D, Pertwee RG. AM630 behaves as a protean ligand at the human cannabinoid CB 2 receptor. *Br J Pharmacol*. 2012;165(8):2561-2574. doi:10.1111/j.1476-5381.2011.01503.x

141. Miller EB, Murphy RB, Sindhikara D, et al. Reliable and Accurate Solution to the Induced Fit Docking Problem for Protein-Ligand Binding. *J Chem Theory Comput*. 2021;17(4):2630-2639. doi:10.1021/acs.jctc.1c00136

142. Black JW, Leff P. Operational models of pharmacological agonism. *Proc R Soc London* -

Biol Sci. 1983;220(1219):141-162. doi:10.1098/rspb.1983.0093

143. Laprairie RB, Bagher AM, Kelly MEM, Denovan-wright EM. Biased Type 1 Cannabinoid Receptor Signaling Influences Neuronal Viability in a Cell Culture Model of Huntington Disease s. Published online 2016:364-375.

144. Zhang X, Perez-Sanchez H, C. Lightstone F. A Comprehensive Docking and MM/GBSA Rescoring Study of Ligand Recognition upon Binding Antithrombin. *Curr Top Med Chem*. 2017;17(14):1631-1639. doi:10.2174/1568026616666161117112604

145. Weiss DR, Karpiak J, Huang XP, et al. Selectivity Challenges in Docking Screens for GPCR Targets and Antitargets. *J Med Chem*. 2018;61(15):6830-6845. doi:10.1021/acs.jmedchem.8b00718

146. Antonides LH, Cannaert A, Norman C, et al. Enantiospecific synthesis, chiral separation, and biological activity of four indazole-3-carboxamide-type synthetic cannabinoid receptor agonists and their detection in seized drug samples. *Front Chem*. 2019;7(MAY). doi:10.3389/fchem.2019.00321

147. Patel M, Manning JJ, Finlay DB, et al. Signalling profiles of a structurally diverse panel of synthetic cannabinoid receptor agonists. *Biochem Pharmacol*. 2020;175(December 2019):113871. doi:10.1016/j.bcp.2020.113871

148. Hartogsohn I. Constructing drug effects: A history of set and setting. *Drug Sci Policy Law*. 2017;3:205032451668332. doi:10.1177/2050324516683325

149. Obreshkova D, Kandilarov I, Angelova VT, Iliev YT. PHARMACO - TOXICOLOGICAL ASPECTS AND ANALYSIS OF PHENYLALKYLAMINE AND

INDOLYLALKYLAMINE. 2017;(March).

150. Dean BV, Stellpflug SJ, Burnett AM, Engebretsen KM. 2C or Not 2C: Phenethylamine Designer Drug Review. *J Med Toxicol*. 2013;9(2):172-178. doi:10.1007/s13181-013-0295-x

151. Chambers SA, Desousa JM, Huseman ED, Townsend SD. The DARK Side of Total Synthesis: Strategies and Tactics in Psychoactive Drug Production. *ACS Chem Neurosci*. 2018;9(10):2307-2330. doi:10.1021/acschemneuro.7b00528

152. Breeksema JJ, Niemeijer AR, Krediet E, Vermetten E, Schoevers RA. Psychedelic Treatments for Psychiatric Disorders: A Systematic Review and Thematic Synthesis of Patient Experiences in Qualitative Studies. *CNS Drugs*. 2020;34(9):925-946. doi:10.1007/s40263-020-00748-y

153. de Barros WA, Nunes C da S, Souza JA da CR, et al. The new psychoactive substances 25H-NBOMe and 25H-NBOH induce abnormal development in the zebrafish embryo and interact in the DNA major groove. *Curr Res Toxicol*. 2021;2(November):386-398. doi:10.1016/j.crtox.2021.11.002

154. Pottie E, Cannaert A, Van Uytfanghe K, Stove CP. Setup of a Serotonin 2A Receptor (5-HT2AR) Bioassay: Demonstration of Its Applicability to Functionally Characterize Hallucinogenic New Psychoactive Substances and an Explanation Why 5-HT2AR Bioassays Are Not Suited for Universal Activity-Based Screening . *Anal Chem*. 2019;91(24):15444-15452. doi:10.1021/acs.analchem.9b03104

155. Pottie E, Dedecker P, Stove CP. Identification of psychedelic new psychoactive substances (NPS) showing biased agonism at the 5-HT2AR through simultaneous use of β-arrestin 2

and miniGαq bioassays. *Biochem Pharmacol*. 2020;182(September). doi:10.1016/j.bcp.2020.114251

156. Fuxe K, Tarakanov A, Romero Fernandez W, et al. Diversity and bias through receptor-receptor interactions in GPCR heteroreceptor complexes. Focus on examples from dopamine D2 receptor heteromerization. *Front Endocrinol (Lausanne)*. 2014;5(MAY):1-11. doi:10.3389/fendo.2014.00071

157. Sánchez-Fernández G, Cabezudo S, García-Hoz C, Tobin AB, Mayor F, Ribas C. ERK5 activation by Gq-coupled muscarinic receptors is independent of receptor internalization and β-arrestin recruitment. *PLoS One*. 2013;8(12):1-8. doi:10.1371/journal.pone.0084174

158. Zhang G, Stackman RW. The role of serotonin 5-HT2A receptors in memory and cognition. *Front Pharmacol*. 2015;6(OCT):1-17. doi:10.3389/fphar.2015.00225

159. McClure-Begley TD, Roth BL. The promises and perils of psychedelic pharmacology for psychiatry. *Nat Rev Drug Discov*. Published online 2022. doi:10.1038/s41573-022-00421-7

160. Marder SR, Roth B, Sullivan PF, et al. Advancing drug discovery for schizophrenia. *Ann N Y Acad Sci*. 2011;1236(1):30-43. doi:10.1111/j.1749-6632.2011.06216.x

161. Pottie E, Kupriyanova O V., Brandt AL, Laprairie RB, Shevyrin VA, Stove CP. Serotonin 2A Receptor (5-HT2AR) Activation by 25H-NBOMe Positional Isomers: In Vitro Functional Evaluation and Molecular Docking. *ACS Pharmacol Transl Sci*. 2021;4(2):479-487. doi:10.1021/acsptsci.0c00189

162. Clark CR. Forensic Chemistry of Substituted N-Benzylmethoxy (N-BOMe)

Phenethylamines: Isomeric Designer Drugs Related to 25I-N-BOMe. Published online 2020.

163. Pottie E, Tosh DK, Gao ZG, Jacobson KA, Stove CP. Assessment of biased agonism at the A3 adenosine receptor using β-arrestin and miniGαi recruitment assays. *Biochem Pharmacol*. 2020;177(March):113934. doi:10.1016/j.bcp.2020.113934

164. Dixon AS, Schwinn MK, Hall MP, et al. NanoLuc Complementation Reporter Optimized for Accurate Measurement of Protein Interactions in Cells. *ACS Chem Biol*. 2016;11(2):400-408. doi:10.1021/acschembio.5b00753

165. Gado F, Ceni C, Ferrisi R, et al. CB1 receptor binding sites for NAM and PAM: A first approach for studying, new n-butyl-diphenylcarboxamides as allosteric modulators. *Eur J Pharm Sci*. 2022;169(September 2021):106088. doi:10.1016/j.ejps.2021.106088

166. Inanobe A, Furukawa H, Gouaux E. Mechanism of partial agonist action at the NR1 subunit of NMDA receptors. *Neuron*. 2005;47(1):71-84. doi:10.1016/j.neuron.2005.05.022

167. Kenakin T. Drug efficacy at G protein-coupled receptors. *Annu Rev Pharmacol Toxicol*. 2002;42(February 2002):349-379. doi:10.1146/annurev.pharmtox.42.091401.113012

168. Aghazadeh Tabrizi M, Baraldi PG, Borea PA, Varani K. Medicinal Chemistry, Pharmacology, and Potential Therapeutic Benefits of Cannabinoid CB2Receptor Agonists. *Chem Rev*. 2016;116(2):519-560. doi:10.1021/acs.chemrev.5b00411

169. Reddy AS, Zhang S. Polypharmacology: Drug discovery for the future. *Expert Rev Clin Pharmacol*. 2013;6(1):41-47. doi:10.1586/ecp.12.74

170. Peng Y, McCorvy JD, Harpsøe K, et al. 5-HT2C Receptor Structures Reveal the Structural

Basis of GPCR Polypharmacology. *Cell*. 2018;172(4):719-730.e14. doi:10.1016/j.cell.2018.01.001

171. Mccorvy JD, Butler K V, Kelly B, et al. Structure-inspired design of β-arrestin-biased ligands for aminergic GPCRs HHS Public Access Author manuscript. *Nat Chem Biol*. 2018;14(2):126-134. doi:10.1038/nchembio.2527.Structure-inspired

172. Jumper J, Evans R, Pritzel A, et al. Highly accurate protein structure prediction with AlphaFold. *Nature*. 2021;596(7873):583-589. doi:10.1038/s41586-021-03819-2

173. Bryant P, Pozzati G, Elofsson A. Improved prediction of protein-protein interactions using AlphaFold2. *Nat Commun*. 2022;13(1):1-11. doi:10.1038/s41467-022-28865-w

174. Wang L, Wang HF, Liu SR, Yan X, Song KJ. Predicting Protein-Protein Interactions from Matrix-Based Protein Sequence Using Convolution Neural Network and Feature-Selective Rotation Forest. *Sci Rep*. 2019;9(1):1-12. doi:10.1038/s41598-019-46369-4

175. Namkung Y, Le Gouill C, Lukashova V, et al. Monitoring G protein-coupled receptor and β-arrestin trafficking in live cells using enhanced bystander BRET. *Nat Commun*. 2016;7. doi:10.1038/ncomms12178

176. Zimmerman B, Beautrait A, Aguila B, et al. Differential β-arrestin - Dependent conformational signaling and cellular responses revealed by angiotensin analogs. *Sci Signal*. 2012;5(221). doi:10.1126/scisignal.2002522

177. Nichols DE, Lloyd DH, Johnson MP, Hoffman AJ. Synthesis and Serotonin Receptor Affinities of a Series of Enantiomers of α-Methyltryptamines: Evidence for the Binding Conformation of Tryptamines at Serotonin 5-HT1B Receptors. *J Med Chem*.

1988;31(7):1406-1412. doi:10.1021/jm00402a026

178. Mason NL, Kuypers KPC, Müller F, et al. Me, myself, bye: regional alterations in glutamate and the experience of ego dissolution with psilocybin. *Neuropsychopharmacology*. 2020;45(12):2003-2011. doi:10.1038/s41386-020-0718-8

179. G. Petri, P. Expert, F. Turkheimer, R. Carhart-Harris, D. Nutt PJH and FV. Homological scaffolds of brain functional networks. *J R Soc Interface*. 2014;10(4):312. doi:10.1038/nrn2618

180. Atasoy S, Roseman L, Kaelen M, Kringelbach ML, Deco G, Carhart-Harris RL. Connectome-harmonic decomposition of human brain activity reveals dynamical repertoire re-organization under LSD. *Sci Rep*. 2017;7(1):1-18. doi:10.1038/s41598-017-17546-0

181. Campbell IB, Macdonald SJF, Procopiou PA. Medicinal chemistry in drug discovery in big pharma: past, present and future. *Drug Discov Today*. 2018;23(2):219-234. doi:10.1016/j.drudis.2017.10.007